UNIVERSITÀ DEGLI STUDI DI PALERMO

PhD in Biodiversity in Agriculture and Forestry

Dipartimento di Scienze Agrarie, Alimentari e Forestali (SAAF)

Settore Scientifico Disciplinare AGR/03

Development of an effective and sustainable system to monitor fruit tree water status with precision devices

PhD Candidate

ALESSANDRO CARELLA

PhD Coordinator

PROF. RICCARDO LO BIANCO

Supervisor

PROF. RICCARDO LO BIANCO

Co-supervisor

PROF. FRANCESCO P. MARRA

XXXVI PhD Cycle

Year 2024

Table of contents

GENERAL INTRODUCTION

In recent years, sustainable water resource management has become a significant and debated issue in the agro-environmental context. Agriculture, as one of the major water-consuming sectors, plays a crucial role in water resource management. Indeed, global climate change is leading to a general temperature rising, with a consequent increase in drought phenomena. As a result, this leads to an overuse of water resources for irrigation. Therefore, understanding tree crop responses to water availability is becoming increasingly urgent, aiming to increase their water use efficiency.

In this regard, one of the primary objectives of scientific research today is to optimize the use of water resources, minimizing inputs without compromising outputs. Water resource savings alone will lead to increased profits. In recent years, deficit irrigation methods, such as regulated deficit irrigation (RDI) and partial rootzone drying (PRD), have allowed farmers to save water while increasing profit by irrigating only during specific phenological stages or with reduced volumes on alternated sides of the rootzone, inducing the plant to activate physiological mechanisms (partial stomatal closure) useful for maximizing water use efficiency. However, real-time knowledge of fruit tree water requirements with consequent automation of precise irrigation applications would allow farmers to further increase water use efficiency. In this regard, last-generation sensors allow continuous data acquisition directly from the plant, greatly increasing the level of information. The combined use of plant-based proximal sensors can provide highly precise information about its water status. Furthermore, remote sensing technologies allow strategic use of proximal sensors, taking into account the spatial variability of the orchard.

Based on these premises, the main objective of this dissertation was to develop an effective and sustainable system for monitoring the water status of fruit trees using proximal and remote sensing technologies. Firstly, the use of plant-based proximal and remote sensing technologies, as well as the combination of the two techniques, was reviewed. Subsequently, some techniques for assessing the water status of young olive trees placed in a growth chamber were tested. In the subsequent trial, fruit growth sensors (fruit gauges) were used to study responses of fruit growth from five different species (peach, mango, olive, orange, and loquat) to vapor pressure deficit. In the last trial, the combined use of proximal and remote sensing technologies was tested for estimating the water status of 'Calatina' olive trees under open field conditions.

CHAPTER 1.

Literature review: Continuous plant-based and remote sensing for determination of fruit tree water-status

Based on the **published** paper:
Carella, A., Bulacio Fischer, P. T., Massenti, R., Lo Bianco, R. (2024). Continuous Plant-Based and Remote Sensing for Determination of Fruit Tree Water Status. *Horticulturae*, *10*(5), 516. https://doi.org/10.3390/horticulturae10050516

horticulturae

MDPI

Review

Continuous plant-based and remote sensing for determination of fruit tree water-status

Alessandro Carella*, Pedro Tomas Bulacio Fischer, Roberto Massenti and Riccardo Lo Bianco

[1] Department of Agricultural, Food and Forest Sciences (SAAF), University of Palermo, 90128 Palermo, Italy
* Author to whom correspondence should be addressed

Abstract: Climate change poses significant challenges to agricultural productivity, making the efficient management of water resources essential for sustainable crop production. The assessment of plant water status is crucial for understanding plant physiological responses to water stress and optimizing water management practices in agriculture. Proximal and remote sensing techniques have emerged as powerful tools for non-destructive, efficient, and spatially extensive monitoring of plant water status. This review aims to examine the recent advancements in proximal and remote sensing methodologies utilized for assessing water status, consumption, and irrigation needs of fruit tree crops. Several proximal sensing tools have proved useful in the continuous estimates of tree water status but have strong limitations in terms of spatial variability. On the contrary, remote sensing technologies, although less precise in terms of water status estimates, can easily cover medium to large areas with drone or satellite images. The integration of proximal and remote sensing would definitely improve plant water status assessment, resulting in higher accuracy by integrating temporal and spatial scales. This paper consists of three parts: the first part covers current plant-based proximal sensing tools, the second part covers remote sensing techniques, and the third part includes a literature update on the combined use of the two methodologies.

Keywords: proximal sensors, irrigation scheduling, precision irrigation, internet of things, UAV, satellite, vegetation index

1. Introduction

The sustainable supply of water resources has become a critically important issue in the context of recent environmental and agricultural challenges. Agriculture, as one of the main water-consuming sectors, plays a crucial role in the responsible management of global water resources [2–4]. Climate change-induced temperature rises impact water availability through increased evapotranspiration and subsequent alterations in rainfall and river flows, increasing the frequency and intensity of heatwaves and drought events [5–7]. Therefore, understanding plant responses to water availability to increase their water use efficiency is becoming more and more urgent [8].

For irrigation scheduling, monitoring environmental parameters to calculate crop evapotranspiration (ET_c) has been one of the most widely used methods. It is obtained by considering reference evapotranspiration (ET_0) and crop coefficients (K_c). The ET_c can be easily estimated following the FAO-56 method described by Allen et al. (1998) [11]. Nevertheless, different studies have highlighted that this method might overestimate the irrigation needed for optimal yield and consequently diminish orchard water use efficiency [12,13], because it does not take into account the actual plant water status (PWS). In recent years, soil-based systems have been developed by using soil water potential or volumetric

Citation: To be added by editorial staff during production.

Academic Editor: Firstname Lastname

Received: date
Revised: date
Accepted: date
Published: date

water content principles [14]. This includes the use of precision instruments such as tensiometers [15,16], soil psychrometers [17,18], continuous and real-time sensors [19,20] and remote sensing techniques [21,22] capable of measuring soil moisture.

However, soil-based methods could be significantly influenced by different variables such as soil texture, and soil moisture level indirectly influences PWS rather than measuring it directly on the plant [23]. Furthermore, we should point out that the plant is the intermediate component in the soil-plant-atmosphere continuum, and its water status is directly affected by changes in leaf water content and leaf and stem water potential [10,24–26]. For these reasons, recently, the focus has shifted to the direct assessment of PWS.

Traditional systems for plant-based monitoring of PWS include measurement of stem (Ψ_{stem}) and leaf (Ψ_{leaf}) water potential using the Scholander's pressure chamber. This represents the most common method of measuring plant water potential, used as an accurate indicator of fruit trees water status [27,28]. However, assessing water potential using the pressure chamber is an invasive and labor-intensive procedure, requiring a skilled operator to consistently apply and release pressure to the chamber containing the leaf sample, and, finally, the operator must meticulously determine the pressure at which water emerges from the leaf petiole [29]. In addition, it could also be influenced by the osmotic component, i.e., a lower water potential may indicate lower hydration or a higher concentration of solutes, thus decreasing the osmotic potential and consequently the water potential [30]. Leaf relative water content (RWC) could also be considered a valid method for estimating PWS [31,32]. RWC quantifies the amount of water within leaf tissues relative to the maximum amount of water the leaf tissues can retain when fully hydrated. In addition, with respect to stem and leaf water potential, it takes into account some physiological phenomena such as osmotic adjustment. This is one of the mechanisms that plants use to maintain cell hydration. Consequently, RWC remains relatively high even under water stress conditions inducing improved cellular hydration and enhancing the ability of the plant to survive under severe water stress conditions [9,26,33]. Despite the potential reliability and relative easiness of RWC as a method for assessing PWS, similarly to water potential with the pressure chamber, it is an invasive and very time-consuming method, mainly to obtain and weigh fully saturated and dry samples [34]. An alternative conventional method to assess plant water status can be the measurement of gas exchange (e.g., stomatal conductance - g_s) since it is well known that stomatal opening and closing depends on PWS, with responses differing from crop to crop [35,36]. Similar to the previous methods, these techniques are also time-consuming and require the use of expensive instruments (e.g. porometer). Other useful approaches for PWS assessment may involve indirect estimation methods such as leaf turgor [29] and thickness [37], sap flow [38,39], stem [40,41] and fruit diameter [42]. Nonetheless, these measurements require high precision achievable with the use of sensors and other precision technologies.

In recent years, the focus has moved to two new approaches for irrigation management. The first involves the use of large-scale imagery from above using instruments such as drones (UAVs) and satellites (remote sensing). The second involves the use of plant-based ground sensors to obtain more accurate data (proximal sensing) [26]. The main advantage of ground-based sensors is that they may provide continuous and real-time PWS indications, as opposed to traditional methods. The possibility to have real-time estimates of PWS and consumption greatly facilitates the grower's decision to act at the right time with the right irrigation volume. Having precise information about the timing and volume of irrigation would allow action only when necessary, avoiding waste and thus significantly increasing water use efficiency. Consequently, there would be a positive impact on sustainability from both economic and environmental perspectives.

Last-generation sensors allow to access data directly from home via cloud, easing the farm workload. These kinds of systems belong to Internet of Things (IoT) technologies [43]. IoT mainly focuses on providing many small, interconnected devices using WSN (Wireless Sensor Network) technology [44]. With the help of WSN technologies, growers will be

able to consult weather conditions, soil conditions and plant physiological parameters collected from their farm thus obtaining an efficient decision support system (DSS) [45]. An evaluation issue may arise due to potential small errors introduced by the installation of sensors in sample plants. These errors could be associated with different variables, including soil texture, soil chemical composition, presence of pathogens, etc. Remote sensing technologies, on the other hand, by providing images of entire plot areas, allow us to have data from different types of optical sensors (RGB, multispectral, thermal, hyperspectral, etc.) to assess spatial variability in terms of health, nutrient, and water status of trees and soil [46]. The combined use of proximal and remote sensing could provide more complete and precise information on PWS since with proximal sensors we have accurate, continuous real-time data concerning individual plants, while data from UAVs or satellite may expand the information throughout the field [47]. In other words, there is a higher level of accuracy because of the possibility of integrating information at the temporal (proximal sensing) and spatial (remote sensing) scales. To do this clearly, appropriate models have to be developed, and exploiting Machine Learning techniques seems the best way to go [44,48].

On this basis, this review aims to gather state-of-the-art updates covering the use of proximal sensors, remote sensing, and the combined use of both techniques to assess the water status, consumption, and requirement of fruit tree crops. More specifically, we reviewed stem-, leaf-, and fruit-mounted sensors, the use of satellites and UAVs with multispectral, thermal, and hyperspectral sensing devices, and their combined use. In detail, the review provides an extensive overview of various proximal and remote sensors, elucidating their respective advantages, disadvantages, and practical applications. Each sensor type is carefully evaluated, offering insights into their specific capabilities and limitations when employed for assessing water status, consumption, and requirements in fruit tree crops. Following this comprehensive evaluation, the review will conclude by outlining future perspectives. Based on the insights from the analysis, the review will propose hypotheses regarding the development of efficient systems that integrate both proximal and remote sensing techniques. Ultimately, these hypotheses will foster exploration of novel approaches and methodologies for enhancing the assessment of water status, consumption, and requirements of fruit tree crops.

2. Proximal sensing

2.1. Leaf-mounted sensors

2.1.1. Leaf patch clamp pressure probe

The force exerted by water toward the cell walls of the plant cells is known as leaf turgor pressure. This force is closely dependent on the water status of various parts of the plant, most notably the leaf [49]. When the plant is well hydrated, the water inside the leaf cells tends to exert adequate pressure toward the walls. Conversely, when the plant begins to dehydrate, the cells will start losing turgor pressure and the leaf will tend to wilt [10,50]. The loss in turgor pressure is directly related to stomatal closure and decrease in transpiration rate [51]. Hence, leaf water status can be assessed by measuring the amount and rate of turgor pressure loss at solar noon (when transpiration rate is highest) and the duration required for its restoration in the afternoon [52].

Early attempts to measure cell turgor include that of Green and Stanton, in 1967, who used in *Nitella axillaris* cells a small capillary fused at the end with the other resembling the tip of a syringe needle. Such capillary contained a gas in order to act as a micromanometer [53]. A *Nitella* internodal cell is inserted into the open end. The ability of the cell to compress the gas within the capillary allows its turgor pressure to be measured directly. The first prototype of leaf turgor pressure probe was developed by Zimmermann et al. in 1969 [54]. This consisted of a pressure screw connected to a silicon membrane in turn connected

to a pressure transducer. This device allowed the instantaneous data to be taken or recorded. Although this system was widely used and improved over time [55–57], it did not allow continuous, real-time data acquisition. In 2008, Zimmermann et al. developed leaf patch clamp pressure (LPCP) probes (Figure 1), capable of continuous, non-destructive, real-time monitoring of leaf turgor pressure [29]. The sensor was validated in *Tetrastigma vonierianum* plants grown in greenhouses [29]. The probe is composed of two metal magnetic pads. One of the pads incorporates a pressure-sensing chip. These magnets are strategically positioned on both the adaxial and abaxial sides of a leaf, ensuring that the pressure chip maintains close contact with the leaf surface. The distance between the magnets above and below the clamped leaf patch can be adjusted by regulating the separation between the two magnets, depending on the thickness and rigidity of the leaf. The sensors are connected by wire into a radio transmitter that sends the output directly to a gateway located in the field. After that, they are transmitted to a server via a general packet radio service (GPRS) system. The data can be accessed via a cloud platform.

The sensor output (P_p) varies with the distance between the two magnets and is inversely proportional to turgor pressure (P_c). For example, as P_c decreases in response to daytime stomatal opening, the P_p gradually increases. Conversely, when stomata close at night, causing an increase in P_c, P_p gradually decreases [9,58]. Nevertheless, in olive (*Olea europaea* L.) it has been observed that as water stress increases, P_p values tend to drop causing a semi-inversion of the curve under moderate stress situations, and a complete inversion at severe stress conditions [58–61]. Moreover, the output signal may vary with the tree height [29]. In addition, leaving the probe in the same leaf for too long could cause depigmentation of the sensor area due to a loss of chlorophyll, causing altered measurements as a result [26]. Specifically, data from the electrical output of the sensor were coupled with actual leaf turgor pressure data determined by the method developed by Zimmermann et al. in 1969 (described previously) [54]. Validation process was carried out over a wide range of turgor pressure (0-100 kPa), thus considering a full hydration status of the plant up to severe water stress. In the following years, LPCP sensors have been tested in various horticultural crops, such as in grapevine (*Vitis vinifera* L.) [62], grapefruit (*Citrus x paradisi* Macfad.) [62,63], nectarine (*Prunus persica* L.) [64,65], persimmon (*Dyospiros kaki* L.) [66,67], clementine (*Citrus clementina* Tanaka) [66] and olive [58–61,68–70]. In olive, it has been extensively tested with excellent results indicating great reliability of the sensor for both ecophysiological studies and irrigation scheduling. Sghaier et al. [71] utilized these probes to study the effect of three irrigation levels on water relations of young 'Koroneiki' and 'Picholine' olive trees, demonstrating the suitability of the sensor to monitor plant physiological and biological mechanisms [71]. In 2016, Padilla-Díaz et al. established an irrigation plan using such sensors to monitor the PWS in a hedgerow 'Arbequina' olive orchard. In details, the authors found that the relation between the output trend and the tree water stress levels is robust for olive trees of different age under a wide range of growing conditions [60]. To identify actual water stress thresholds, recent studies have suggested monitoring other plant organs as well by combining the use of LPCP probes with other sensors and instruments. Rodriguez-Dominguez studied the sensitivity of olive leaf turgor to air vapor pressure deficit (VPD), finding strong relationships. Moreover, the authors normalized the P_p data with the VPD values in order to predict diurnal max stomatal conductance ($g_{s,\,max}$) measured with an open flow gas exchange system (IRGA Li-6400, LI-COR) in olive trees grown in a hedgerow orchard. The sensors were proved to be highly reliable to predict $g_{s,\,max}$. In nectarine, Scalisi et al., tested the combined use of LPCP probes and fruit gauges, demonstrating the suitability of a dual-organ sensing approach for improved prediction of tree water status [64]. In 2020, Scalisi also confirmed the effectiveness of these two sensors when used together for detecting plant water stress in two olive cultivars ('Nocellara del Belice' and 'Olivo di Mandanici'). In the same trial, the authors also demonstrated the suitability of the probes to predict stomatal conductance and stem water potential [68].

Barriga et al. have developed a new expert system based on machine learning (ML) techniques together with an IoT infrastructure based on continuous measurements of leaf turgor pressure providing very important information for irrigation scheduling [72]. The study shows that the ML models and the developed algorithm are valid for sweet orange (*Citrus sinensis* (L.) Osbeck cv. Navelina), while subsequent studies should test these models on other orange varieties and other citrus species, like lemon or tangerines (Barriga et al., 2022). Another model was proposed by Palomo et al. based on ML techniques to classify olive (*Olea europaea* L.) trees cv Arbequina into three distinct levels of water stress by analyzing data daily trends [73].

Figure 1. LPCP probe mounted in an olive leaf.

2.1.2. Leaf water meter

A recent non-invasive leaf-mounted sensor developed and commercially available to assess plant water status is the leaf water meter (LWM). This optical sensor was developed in 2022 by Brunetti et al. [74] and is based on the photon attenuation during the passage of the light at specific wavelengths (about 1450 nm) through the leaf, the signal intensity of which is related to leaf water content. LWM is composed of three plastic wires connected to a controller equipped with additional sensors (soil moisture sensor, temperature, relative humidity, and PPFD) and a LoRa module to transmit data via radio frequencies. The main sensor consists of a plastic clamp with a pair of LEDs and photodiodes inside, to be placed in the abaxial and adaxial part of the leaf, respectively. The two pairs (LEDs and photodiodes) operate at two specific wavelengths, producing an electrical (analog) signal that correlates with leaf water content. Specifically, one LED is set at 1450 nm (SWIR) and the other at 890 nm (NIR). The first is directly related to water status assessment [75,76], while the second is mainly linked to dry matter [74]. Also in this case, the data are transmitted (through a LoRa module) to a gateway located in the field that sends the data directly to an Internet server. The data are accessible in a cloud. The acquired data express the leaf dehydration level (DL). These need to be normalized by the feature scaling method (min-max normalization) to have comparable data between sensors.

This sensor was first tested by Brunetti et al. in 2022 in woody crops with different morphology and biological characteristics (*Citrus limon* L., *Olea europaea* L., *Acer platanoides* L., and *Arbutus unedo* L.). A strong correlation was found between DL and both Ψ_{stem} and especially leaf RWC ($R^2 = 0.73$ and $R^2 = 0.84$, respectively). The significance of estimating RWC lies in the ability to bypass leaf osmotic regulation phenomena, providing more accurate data regarding the plant actual hydration status [33]. Hence, the results of the first

test demonstrated that LWM can be a reliable and non-destructive alternative sensor for continuous and real-time assessment of leaf water status in woody crops. Nevertheless, no other study employing the LWM has been conducted to date that confirms the sensor's reliability. Therefore, its official validation on other economically significant fruit tree species (e.g., apple, pear, peach, grapevine, etc.) under various agro-environmental conditions is still pending.

2.1.3. Leaf thickness sensors

The relationship between leaf thickness and plant water status has been known for a long time. Basically, changes in leaf thickness are the result of water exchanges between the plant or the atmosphere and the leaf [77]. Leaf thickness undergoes changes not only due to oscillations in leaf water content, but also in response to various physiological and environmental mechanisms [78]. For instance, leaf thickness exhibits diurnal-nocturnal cycles: in well irrigated plants, leaf thickness remains relatively constant during nighttime, decreasing throughout the day, until reaching the minimum peak at solar noon [77,79]. Furthermore, leaf thickness shows a negative correlation with VPD and light [80,81]. Thus, environmental factors influence leaf thickness changes by affecting the transpiration process [82,83].

The first studies were carried out in 1922 by Bachmann [84], followed by Meidner (1952) [77]. The latter was the first to use a gear micrometer to measure changes in leaf thickness continuously. He also observed a strong correlation between leaf thickness and leaf water content. In 1987, Búrquez used a spring-loaded gear-wheel micrometer in different herbaceous crops finding strong correlations between leaf thickness and RWC (R^2 = 0.96-0.99) [81]. However, these instruments were found to be impractical and unable to make automatic and continuous measurements. In subsequent years other less bulky and more accurate devices were developed, mainly based on the principle of a differential transformer, i.e. linear variable displacement transducers (LVDTs) [85–87]. Seelig et al. designed an efficient irrigation scheduling method on cowpea using a miniaturized leaf thickness sensor consisting of electrical distance transducers [79]. Sharon and Bravdo conducted a comparison of irrigation scheduling methods, including continuous leaf thickness monitoring and four conventional drip irrigation regimes based on schedules and water depletion [87]. The results showed that the sensor-based drip irrigation treatment achieved the highest yield and exhibited the greatest water use efficiency for 'Oroblanco' grapefruit.

In 2017, Afzal et al. integrated leaf capacitance and leaf thickness measurements into a single sensor to investigate whether the combination of the two measurements can be used as an indicator of PWS [83]. In detail, the sensor consists of a clamp with two sensing units, one capable of measuring leaf thickness and the other capacitance. Thickness is measured by a pair of magnets, and based on their distance, measurements of leaf thickness (which depends on leaf turgor) can be obtained. A PCB is connected to the sensors via wires, and through a transmission module, it sends data to an internet-connected central unit. In summary, it is a kind of combination of LPCP probes and LMCS. The device was tested on tomato plants. From initial results, it was observed that changes in leaf thickness reflect the leaf transpiration rate. While capacitance is strongly related to light period and photosynthesis. Thus, capacitance can be a reliable indirect measure of PWS through the water-photosynthesis relationship. Despite its reliability and simplicity, there are no studies on this sensor applied in fruit crops. Indeed, variations in leaf thickness and capacitance may differ from one species to another and environmental variables may strongly influence sensor data. Hence, further studies are needed to validate the sensor.. Currently, the sensor is not commercially available.

2.1.4. Leaf-mounted capacitance sensor (LMCS)

In 2023, Talheimer developed the leaf-mounted capacitance sensor (LMCS) (Figure 2) [88]. This is a very low-cost sensor that is able to continuously measure a signal that follows the patterns of leaf transpiration and solar irradiance. The sensor is based on the approach of sensing leaf transpiration flow by forcing water vapor to condense in the leaf blade whose temperature is below the atmospheric dew point [89]. The condensation process is driven by a declining temperature gradient, resulting from the decreasing temperature across the sunlit leaf and the underneath sensor plate. The sensor is based on a capacitive principle and incorporates a photodiode as a light sensor. Simultaneously and continuously measuring incident light and leaf transpiration enables a qualitative assessment of the PWS. This estimation involves comparing the pattern of plant transpiration with the fluctuation in solar irradiance, which acts as its main driving force [90]. The sensor consists of a circular printed circuit board (PCB) and a photodiode. The circular PCB represents a capacitance sensor that can provide different outputs (in pF) depending on the vapor deposition in the lower leaf lamina. For this reason, the circular PCB has to be placed in contact with the lower leaf blade (Figure 2B). The sensors are then connected to a battery-powered Arduino-based microcontroller. Capacitance and irradiance data are transmitted via LoRaWan to an Internet-connected gateway. Thus, the data can be accessed via a cloud. An additional strength of the device is its low cost due to its simple components. The principle of capacitance used to estimate leaf transpiration was studied by Afzal et al. in 2017 [91].

The sensor was first tested in 2023 in several perennial species: grapevine, persimmon, walnut (*Junglans regia* L.), olive, and apple (*Malus domestica* Borkh.). For instance, grapevine leaves revealed a signal indicating severe water stress under drought conditions, and a restoration of conditions (curve rise) after rainfall events and irrigation. Carella et al. (unpublished data) correlated the capacitance output of LMCS with VPD data in fig (*Ficus carica* L.), finding a similar relationship to that between Transpiration and VPD already well documented in the literature. Specifically, the relationship follows a hysteretic pattern due to the lag time of stomatal response [92–94]. In details, capacitance increases more and more slowly as VPD increases, until it reaches an asymptote where capacitance becomes stable. In contrast, an inverse pattern was observed in the afternoon, in which as VPD decreases, capacitance decreases more and more rapidly, until an asymptote is reached, indicating a transpiration stop. Clauser tested the LMC sensor in apple (cv Rosy Glow Pink Lady®) relating it to other technologies that measured soil moisture [95]. The results showed that this sensor allows for monitoring tree water status to define whether the lack of soil moisture is really a problem for the plant.

Since there are no other trials that use LMCS, further validation studies of the sensor, e.g. by appropriate Machine Learning techniques, are needed to predict leaf transpiration and to evaluate the performance of the sensor under different climatic and physiological conditions of the tree. Furthermore, additional field testing will be essential to validate the sensor's long-term reliability and determine the most effective methods for integrating it into smart irrigation strategies across various crops and environmental conditions, with specific attention to crop performance and water use.

Figure 2. LMCS sensors mounted in fig (A), olive (B) and orange (C) leaves.

2.1.5. Continuous thermal sensing

Temperature is closely related to the PWS, since the physical principle behind changes in canopy temperature depends on transpiration flow. Indeed, the closure of stomata caused by water deficit causes a reduction in leaf transpiration, consequently leading to an increase in leaf temperature [96]. Unfortunately, relying exclusively on leaf temperature (T_c) may have several limitations due to the significant impact of environmental variables, including wind speed, radiation, air humidity, and air temperature [97]. Therefore, it becomes imperative to normalize the data with other parameters (e.g., air temperature or a constantly heated thermocouple) or calculate vegetation indices to acquire thermal data that can be readily associated with plant physiological information, such as crop water stress index (CWSI) [98,99]. Thermal sensors can be classified into contact and non-contact sensors. Among contact sensors, the most widely used are thermal resistance sensors and the better-known thermocouples. Non-contact ones, on the other hand, are based on temperature measurement by infrared sensors or thermal imaging cameras [99].

A thermal resistance sensor is a temperature sensor consisting of a known resistance that varies with temperature, such as platinum resistance temperature measurement [99]. A thermal resistance sensor (LT-1T) was used to validate a system based on estimating plant water status using thermal images [100,101]. In 2012, Atherton et al. [102] developed a microsensor able to continuously and real-time monitor leaf temperature, in order to estimate leaf water content. The device is composed of a thin-film resistive heater and two thin-film thermocouple (TFTC) temperature sensors molded on a 10 μm thick polyimide substrate. The sensor measures the leaf thermal resistance. The resistive heater generates a thermal gradient that changes in response to the overall thermal resistance of any sample in contact with the device. The resulting thermal gradient is measured as a temperature difference (ΔT) between the two TFTC sensors. The results achieved showed a strong positive linear correlation between ΔT and leaf RWC. Despite its reliability and potential, the sensor has never been tested in horticultural crops or commercialized. Additional studies are necessary to establish specific thresholds for detecting water stress, to improve the sensitivity of the sensor and minimize its impact on plant health, possibly through design refinement or parameter adjustment. In addition, the effectiveness of the sensor under different environmental conditions needs to be thoroughly investigated to ensure reliable operation in various agricultural settings. In this regard, a thermocouple works as a transducer that converts thermal energy into electrical energy, and it is constructed by connecting wires made from different metals to create a junction. When the temperature at the junction changes, voltage is generated. The fundamental principle behind the thermocouple is the Seebeck effect, which states that if dissimilar metals are joined at a point, they produce a small measurable voltage when the temperature at the connection point

changes [103,104]. The magnitude of the voltage is determined by the extent of the temperature change and the characteristics of the metals. To date, thermocouples are used in validation operations of other techniques for estimating PWS by thermal sensing. For instance, Pou et al. utilized thermocouple for the validation of thermal indices for water status assessment in grapevine [105]. Costa et al. developed models to estimate water and heat fluxes in grapevine using leaf-mounted thermocouples and thermal imaging techniques [106].

In 2017, Dhillon et al. developed a continuous leaf monitoring system to assess plant water status by combining low-cost thermal infrared thermometers and environmental sensors [107]. The authors found a negative linear relationship between ΔT (T_{leaf} - T_{air}) and stem water potential. Moreover, the combination of sensors provided the data to accurately calculate the CWSI. The method was successfully tested in almond (*Prunus amygdalus* Batsch) and walnut (*Juglans regia* L.) [108]. Despite the demonstrated accuracy of measurements, for a definitive validation of the system, studies on different crops and evaluation of the system performance under different conditions are needed to fully assess its potential as an irrigation scheduling tool.

2.1.6. Further new sensors (microsensors)

The emerging wearable electronics industry has shown promising results in various applications although it is in its early stages in agriculture. The flexibility of the wearable sensors allows their easy positioning close to specific plant organs and portions, facilitating continuous and accurate monitoring. This capability helps in early plant stress detection and reduces plant productivity loss [109,110].

In addition to those already described other interesting leaf-mounted sensors for PWS estimation have been developed in the past two years. In 2024, Peng et al. built a wearable and capacitive sensor for real-time and precise monitoring of leaf water content. It was tested in golden pothos (*Epipremnum aureum* Lindl. and Andre) leaves [111]. The microsensor consisted of two wearable electrodes. The leaf has to be placed between the two electrodes. Due to the excellent flexibility of the electrodes, the device can be used in a multitude of leaf types. The authors found that the leaf capacitance value is positively correlated with the leaf moisture content, and the results were similar to those found with conventional rigid electrodes [91,112]. Despite the results achieved and the high potential of the sensor, several problems remain to be solved. For example, attention needs to be paid to leaf integrity when monitoring physiological information, which could be influenced by wearable electrodes. In addition, as the sensor has been tested for only a few days, it will be necessary to test it under open-field conditions and evaluate the timing of measurement reliability. Im et al. built a flexible polyimide (PI)-based sensor, also based on the capacitance principle [113]. This microsensor proved useful for estimating the transpiration flux of tobacco plants grown in growth chamber conditions. Also in this case, although the sensor has demonstrated accuracy of growth chamber measurements and is lightweight, it still requires testing under open field conditions, particularly on fruit trees, to assess its consistency and durability.

2.2. Stem-mounted sensors

2.2.1. Stem dendrometers

The plant water status can also be estimated by measuring diameter changes in different organs such as stem, branches, and fruits [26]. Regarding the stem diameter variations (SDV), C3 plants follow a precise mechanism depending on the transpiration flow. In the early morning, as transpiration begins, the xylem water potential starts to decrease [114]. This tension extends from the foliage to the other organs of the plant, leading to the loss of water stored overnight [115]. Consequently, the plant responds to atmospheric water

demand at a time when root uptake is not fully active, acquiring water from other organs such as fruits, branches and trunk and causing daily fluctuations of their diameter [116,117]. In trees, the trunk's contribution to water transfer is significant [118]. Thus, a reduction in diameter occurs due to this transpiration water withdrawal from xylem and phloem vessels [119]. During the evening and night, the water potential is restored, and the trunk returns to its volume or increases, depending on the amount of carbohydrates gained during the day [120]. The fluctuations amplitude depends on the elastic properties of the tissues [117], the difference in osmotic pressure between the bark and xylem [121], the diffusive properties of water in the phloem [122], and the growth rate of the trunk [117].

From measuring changes in stem diameter, several SDV-derived indicators can be taken into account to assess PWS, e.g. the trend of maximum and minimum daily growth, daily growth, stem growth rate (SGR) and maximum daily shrinkage (MDS) [9,123]. The two last indicators are the most widely used [114].

The first prototype dendrometer (dendrograph) was built in 1883 by Böhmerle [124]. The use of automated dendrometers, on the other hand, has occurred since the second half of the 20th century [9,125,126]. Nowadays, the most commonly used dendrometers are optical types (infrared distance sensor [127]), electronic point dendrometers [128,129] or strain gauges with linear variable differential transformers (LVDTs). The majority of authors have used LVDTs-type sensors, mainly because they are easy-to-use and low-cost [9].

Naor and Cohen utilized LVDTs dendrometers to study the sensitivity and variability of maximum daily shrinkage, midday stem water potential, and daily transpiration rate in response to withholding irrigation from field-grown drip-irrigated 'Golden delicious' apple trees [130]. The authors observed that both MDS and Ψ_{stem} exhibit higher sensitivity to variations in soil water availability compared to the daily transpiration rate (determined using a 'Class A' evaporation pan). Moreover, MDS was more responsive than Ψ_{stem} to changes in soil water availability. This may be explained by the non-linear relationship between Ψ_{stem} and MDS [130,131]. However, they found that MDS showed a higher variability than Ψ_{stem}. In particular, MDS variability increased with water stress. Therefore, the authors concluded that more measures than just Ψ_{stem} and MDS need to be integrated. Additionally, establishing an irrigation scheduling threshold based on MDS measurements is likely to be more complex because thresholds may vary from one apple commercial plot to another due to changes in parameters influencing trunk bark thickness, such as tree age and rootstock. More recently, Wheeler et al. utilized stem dendrometers to determine tree water status of high-density apple orchards [132]. They aimed to enhance precision of irrigation scheduling by correlating continuous data obtained from stem dendrometers with Ψ_{stem} and atmospheric evaporative demand. On the other hand, in peach trees (*Prunus persica* L.), Conejero et al. showed that using dendrometers alone and calculating MDS is sufficient for irrigation scheduling [133]. These results were confirmed by Mirás-Avalos et al. [134] and De la Rosa [135] in 2017 and 2016. In almond, on the other hand, stem growth rate (SGR) was found to be more reliable than MDS for assessing water status [136]. In pear (*Pyrus communis* L.), MDS was found to be a good indicator of water stress, due to the quick response to environmental conditions [137]. On the contrary, Blanco and Kalcsits found that despite MDS detected water stress earlier, it did not increase in the same proportion as Ψ_{stem} when it was lower than − 1.4 MPa [138]. In a table olive orchard, Corell et al. showed that both TGR and MDS were found to be reliable indicators to detect mild water stress, even though less than Ψ_{stem} [139]. In cherry (*Prunus avium* L.), MDS was less precise than Ψ_{stem} but more sensitive and responsive to detect water stress, making it useful in situations where even a slight water deficit could impact vegetative growth, fruit development, and yield [140]. In grapevine, MDS and TGR were found unsuitable to predict water stress after veraison [141]. Finally, it can be stated that while the measurement of trunk diameter to assess PWS can prove reliable depending on crop, phenological stage and water stress level and is easy to apply, it does not provide comprehensive information regarding leaf and fruit water status [9,26].

476
477 2.2.2. Microtensiometers

478 Stem water potential (Ψ_{stem}) is considered one of the main indicators for assessing plant
479 water status. However, as indicated previously, the most reliable method to measure Ψ_{stem}
480 has been the pressure chamber method, which is labor-intensive and time consuming.
481 Fortunately, in recent years, devices that can measure Ψ_{stem} continuously and real-time
482 are being developed. Recently, people at Cornell University together with the FloraPulse
483 (FloraPulse Co., Davis, CA, USA, www.florapulse.com) company developed an electro-
484 mechanical system-based microtensiometer embedded in the trunk and capable of meas-
485 uring water potential continuously. This sensor was first described by Pagay et al. in 2014
486 [142]. In 2019, Black et al. published a detailed description of the sensor with its physical
487 principle, also adding improvements [143]. The sensor is based on the tensiometer princi-
488 ple, i.e., an instrument able to monitor the water potential of an external matrix (xylem)
489 by balancing an internal volume of water, where the hydrostatic pressure is considered
490 the negative counterpart of the external water potential [144,145]. Briefly, the microtensi-
491 ometer combines two common sensing circuits: a strain gauge and a thermometer. The
492 thermometer is made of a serpentine thin film platinum resistance (PRT), which changes
493 its resistance with temperature. The strain gauge consists of four polycrystalline silicon
494 resistors (piezoresistors) in a Wheatstone bridge placed on a diaphragm, and its re-
495 sistances vary with strain. Below the strain gauge, a 3-μm deep cavity is etched with a
496 diaphragm and a water reservoir [143]. Also in this case, data can be transmitted either
497 via a wireless system, or can be downloaded from a datalogger. The sensor is capable of
498 continuously monitoring trunk water potential (Ψ_{trunk}), thus providing another tree water
499 status indicator [142,146]. Although in early studies it was thought that the sensor directly
500 measured Ψ_{stem}, Pagay et al. showed that in grapevine, there were differences between
501 Ψ_{stem} measured with the pressure chamber and Ψ_{trunk} [144]. Specifically, Ψ_{trunk} was gener-
502 ally higher than Ψ_{stem} measured at the same time. The authors deduced that this difference
503 is mainly due to hydraulic resistances between the trunk and leaves. Zucchini et al. also
504 noticed this difference between Ψ_{trunk} and Ψ_{stem} on olive trees [147]. In particular, they
505 observed that in 32 out of 33 measurements, the Ψ_{stem} data obtained using the pressure
506 chamber were lower than the Ψ_{trunk}, with a maximum difference of 1.15 MPa. On the other
507 hand, in almond [146] and nectarine [148] Ψ_{trunk} and Ψ_{stem} were found to be quite similar.
508 Due to such differences, new thresholds of water stress need to be established using Ψ_{trunk}.
509 The microtensiometer was first field tested on two grapevine cultivars, Shiraz and Caber-
510 net Sauvignon [144]. The author characterized the seasonal and diurnal dynamics of Ψ_{trunk}
511 and compared these values with Ψ_{stem} and Ψ_{leaf} measured with the pressure chamber. He
512 found that Ψ_{trunk} correlated better with Ψ_{stem} than with Ψ_{leaf}. Moreover, he showed that the
513 relationship between Ψ_{trunk} and Ψ_{stem} is stronger under low VPD than under high VPD
514 conditions. In details, under high VPD conditions, Ψ_{trunk} consistently declined below Ψ_{stem}
515 around mid-afternoon, followed by a recovery observed by early evening. The author
516 concluded that the microtensiometer provided good measurement reliability and several
517 studies will be needed to establish irrigation thresholds.
518 Blanco and Kalcsits tested the microtensiometer in pear by relating Ψ_{trunk} and Ψ_{stem} meas-
519 ured with pressure chamber and found strong correlations, concluding that microtensi-
520 ometers provide an accurate continuous method for measuring water potential in trees
521 throughout the growing season, even under diverse environmental conditions and varia-
522 tions in soil water content [149]. In 2023, Blanco and Kalcsits again published the results
523 of 2-years of monitoring a pear orchard [138]. The authors found a strong correlation be-
524 tween Ψ_{stem} and Ψ_{trunk} ($R^2 = 0.88$), and variations in trunk diameter (measured with a LVDT
525 dendrometer) followed changes in Ψ_{trunk} mainly at the beginning of the irrigation season.
526 Once again, the sensor demonstrated high reliability for continuous PWS assessment.
527 Kisekka et al. compared and evaluated data recorded on almond leaves with the Scholan-
528 der chamber, microtensiometers and osmotic cells for continuous measurement of Ψ_{stem}

[150]. The excellent results confirmed the potential of these sensors in facilitating irrigation scheduling.

Nieto et al. studied the relationship between Ψ_{trunk} and fruit growth rate and managed to determine irrigation thresholds in apple trees [151]. In detail, through logistic regression analysis between Ψ_{trunk} and fruit growth rate (in terms of fruit weight), the authors identified the critical value of approximately -0.97 MPa which corresponded to irrigation intervention threshold in that ecosystem. Satisfactory results about the suitability of microtensiometers to assess PWS were also obtained in nectarine [148] and almond [146,152] orchards.

Despite its reliability, usefulness of the data, and ease of installation, the sensor still needs to be validated at wider ranges of plant hydration given that so far it has been tested down to about -3.5 MPa (as also indicated on the FloraPulse website). Indeed, in species such as olive, especially in areas characterized by water scarcity, it is important to have a reliable sensor also at Ψ_{stem} values below -3.5 MPa [69,153]. Also, at least for strict determinations of tree water status, a 20-30-minute time lag of the microtensiometer readings compared to actual Ψ_{stem} values has been observed, which must be taken into account, especially when daily curves are being studied. Additionally, there are still no studies where the microtensiometer has been employed for more than two consecutive years. Finally, the high cost of the sensor may represent a limiting factor for many growers and agricultural areas.

2.2.3. Sap flow sensors

The transpiration flow is closely dependent on PWS, as the latter influences stomatal opening and thus gas exchange between the plant and the atmosphere. Nevertheless, in parallel with PWS, transpiration (and thus sap flow) can be affected by environmental factors (VPD) [154]. Transpiration rates of whole trees can be assessed by sap flow methods that quantify the rate at which sap rises through the stems [155]. Such methods are collected on the dedicated working group web page of the International Society for Horticultural Science (ISHS) (https://www.ishs.org/sap-flow/ishs-working-group-sap-flow-online-resources), and recently Noun et al. published a review on plant-based methodologies and approaches for estimating plant water status of horticulture crops in which there is an exhaustive update on methods for measuring sap flow [10]. In addition, there is SAPFLUXNET (https://sapfluxnet.creaf.cat/), a global database maintained by the Centre for Ecological Research and Forestry Applications (CREAF) (Barcelona, Spain), which aims to advance scientific understanding of the ecological factors that determine plant transpiration and drought response worldwide [156]. One of the main advantages of sap flow sensors is that they are easily automated for continuous measurements [10].

Sap flow can be defined in terms of sap flow rate (g or L h^{-1} or equivalent) or sap flux density (sap flow rate per sapwood area) [157]. Flo et al. split the methods in four groups depending on their physical principle [157]: (1) dissipation [158,159], (2) pulse [88,160–166], (3) field [167] and (4) balance [38,168]. Such methods are briefly described in the following table (Table 1):

579 **Table 1.** A list of the main techniques for measuring sap flow, with briefs descriptions.

580

Method		Brief description	Reference
1) Dissipation		It measures heat dissipation from a heated probe inserted in the sapwood compared to a non-heated reference probe	
Thermal dissipation	TD	The upper probe is constantly heated, and the measured temperature difference decreases with increasing sap flow density	[158]
Transient thermal dissipation	TTD	It works under transient conditions by introducing a relatively short heating and cooling cycle	[159]
2) Pulse		It applies heat intermittently and monitor changes in sapwood temperature induced by thermal convection and conduction	
Compensation heat pulse	CHP	A heater probe is inserted into the xylem between two temperature sensors. By measuring the time, it takes for the heat pulse to travel via convection to the midpoint, the velocity of the pulse is determined	[160]
Heat ratio	HR	It employs a brief heat pulse to trace water movement, and by analyzing the heat ratio between two symmetrical temperature sensors, the magnitude and direction of water flow can be determined	[161]
Cohen's heat pulse	T-max	It uses a single temperature sensor located downstream of the heater probe. The sap flow rate is calculated from the time it takes the downstream temperature sensor to register the maximum temperature rise	[162]
Calibrated average gradient	CAG	Useful for calculating low sap velocities from sap flow records obtained with the standard CHP method, but the temperature differences between the readings of the two temperature probes are averaged (ΔT_a) over a certain period of time.	[163]
Sapflow+	SF+	It uses a four-needle sensor to measure heat velocity in the entire density range of natural sap flow and allows simultaneous estimation of stem water content	[164]
Single probe heat pulse	SPHP	It uses a single-probe sensor based on the fundamental conduction−convection principles of heat transport in sapwood	[165]
Dual heat pulse	Dual	It combines two heat-pulse methods: The HR, effective for low and reverse flows, and CHP, suitable for moderate to high flows, within a single set of sensor probes	[166]
Ratio heat pulse	T_mRatio	It uses the ratio of temperature maxima on downstream and side probes	[88]
3) Field		It measures the shape variations of a continuous heat field within the sapwood by utilizing tangential and axial probes	
Heat field deformation	HFD	It uses a sensor composed of one needle-like heater inserted in the sapwood and three temperature sensors placed above, below and at the side of the heater	[167]
4) Balance		It measures the energy balance through a heated wood section	
Stem heat balance	SHB	It involves employing a sensor with a flexible heater, typically several centimeters wide, encircling the stem and protected by layers of insulating and weather-resistant materials	[38]
Trunk heat balance	THB	It consists of three to five stainless steel metal plates inserted in parallel into the sapwood, spaced two centimeters apart, covering the entire sapwood depth. This configuration allows for the integration of sap flow across the sapwood.	[168]

581

Sap flow sensors based on the principle of thermal dissipation have been widely used in the literature [156]. Their popularity likely stems from their reliability, simplicity, ease of construction for handmade probes, and cost-effectiveness [169]. In 1985, Granier developed a thermal sensor consisting of two needle-shaped probes inserted radially into the sapwood [158]. One of these probes is heated at constant power, while the other serves as a temperature reference. In details, a thermocouple (copper-constantan) is placed in the middle of the heating resistor, and an aluminum sheath covers the entire system to equalize the temperature. The second probe, positioned in the trunk below the previous one, contains an identical thermocouple mounted in opposition to that of the heating element. The system then permits measurement of the temperature difference (ΔT) between the two probes [170]. The author also found experimentally that the volumetric sap flow density ($cm^3\ cm^{-2}\ s^{-1}$) is related to temperature (T) by the following relationship (calibrated for different woody crops):

$$u = 0.119 \cdot K^{1.231} \quad (1)$$

In which:

$$K = \frac{\Delta T_{max} - \Delta T}{\Delta T} \quad (2)$$

Where ΔT_{max} represents the maximum temperature value (when u = 0, i.e. during the night) and ΔT is the temperature difference between the two probes. In addition, the total sap flow ($cm^3\ s^{-1}$) can be calculated from the sap flow density using the formula:

$$F = u \cdot A_{sw} \quad (3)$$

In which A_{sw} is the cross-sectional area of the sapwood (cm^2) [170].

The latter estimate (F) can be used for appropriate precision irrigation management since it is possible to estimate the actual volume of water transpired by the tree in the unit of time. The sensor was initially validated on forest species [158,170], but over the years it has been widely used in fruit crops. However, considering the high sensitivity of sap flow to weather conditions, sap flow sensors often require calibration in the field [171] and therefore it is highly recommended to use them in conjunction with other sensors, such as LPCP probes and/or fruit gauges [9,26]. This need for constant calibration., [25]. Fuchs et al. performed recalibration and comparison tests between TD and HFD methods [172]. The results showed that TD probes tend to underestimate flux density by 23-45% with Granier's original calibration. The accuracy improves by performing species-specific recalibration. In contrast, HFD sensors overestimate flux by up to 11%. Under low and medium sap flow conditions, the HFD method underestimates the flux by 0.8%, thus demonstrating high accuracy. The authors concluded that both HFD and TDP sensors require new species-specific calibration to improve measurement accuracy. Furthermore, sap flow systems are currently not affordable for a significant portion of the agricultural community.

Despite these issues, sap flow has been used as an indicator for water stress in several cases. On apple trees, Nadezhdina used a sap flow index estimated by the heat pulse velocity (HPV) method that proved sensitive to water stress, with a strong correlation with pre-dawn Ψ_{leaf} (R^2 = 0.96) [167]. Hernandez-Santana et al. [173] correlated sap flow data with gas exchange in olive trees. They found that stomatal conductance (g_s) and net pho-

tosynthesis (An) can be readily estimated from sap flow. Ferrara et al. used sap flow meters with the thermal dissipation method to evaluate the influence of water deficit on water use efficiency and water productivity in olive trees (cv. Arbosana) cultivated in an adult super-high-density orchard [174]. In orange *(Citrus sinensis* Osbeck*)*, Cohen's heat pulse (T_{max}) sap flow was successfully used to identify water stress conditions [175]. In cherry, the joint use of sap flow sensors and dendrometers (MDS) represented a suitable system for irrigation scheduling [176]. Marino et al. included continuous TD probes in a multiple plant-based sensing system to detect mild water stress in olive [58]. The authors concluded that sap flow probes are not as useful as LPCPs and fruit gauges for detecting water stress in olive because they are strongly influenced by VPD. However, they can provide a useful quantitative indication of transpired water.

2.2.4. Thermocouple psychrometer

An additional non-invasive method to monitor the water status of the plant through water potential is using thermocouple psychrometers. These instruments allow to determine the Ψ_{leaf} or Ψ_{stem}. The principle is based on the Seebeck effect which consists of a complete electrical circuit formed by two dissimilar metals forming a thermocouple. If the measuring and reference junctions of the circuit are at different temperatures, a voltage difference, which depends on the temperature difference between the junctions, will be generated by a flowing current [98]. In thermocouple psychrometry, the relative humidity of the air around the sensing junction is crucial because it affects the temperature difference between the wet sensing junction and the dry reference junction [177]. To directly calculate the water potential from the measurements, the instrument needs to be empirically calibrated using solutions of known water potential [178]. This method started to be used around the 50s. Initially psychrometry was only used in the laboratory because it required accurate temperature control. Over time, advancements in new projects and electronic instrumentation have provided the capability to perform on-site measurements quickly and non-destructively. There are currently three types of psychrometers: non equilibrium, isopiestic and dew point psychrometers [179]. Nowadays, the most used psychrometer is the PSY1 Stem Psychrometer built by Dixon and Tyree and currently produced by ICT International (Armidale, NSW, Australia) [180]. The PSY1 Stem Psychrometer consists of two soldered chromel-constantan thermocouples connected in series inside a chrome-plated brass chamber that forms a large thermal insulating mass. Inside the chamber, one thermocouple is in contact with the stem sample and the other simultaneously measures the chamber air temperature and, after a Peltier cooling pulse, the wet bulb depression. A third copper-constantan soldered thermocouple is located inside the sample chamber body to measure the temperature of the instrument for temperature compensation purposes. The use of PSY1 Stem Psychrometer has proven to be reliable for monitoring the water potential, after validation with other techniques, including the Scholander pressure chamber [181,182]. Kokkotos et al. used the PSY1 Stem Psychrometer to evaluate the variation of water potential in response to alternate fruit bearing [183]. In this study, the instrument was calibrated with a NaCl solution, and the water potential data was acquired every 30 minutes. In another study carried out in olive [184], water potential measurements were taken every 20 minutes, and the purpose was to evaluate how hydraulic conductance changes in plants under water deficit. The PSY1 Stem Psychrometer was also used on grapevine to evaluate plant response to a 6-week drought experiment [185]. In conclusion, the use of the PSY1 Stem Psychrometer has proved to be a very valid method for the continuous measurement of stem water potential [186]. Despite the sensor reliability, the main disadvantages can be related to the need for calibration with standard solutions, difficult installation, and high cost [186].

2.2.5. TreeTalker®

The TreeTalker® is a continuous real time system that was developed by Valentini et al. (Figure 3) to measure water transport in trees, radial trunk growth, spectral characteristics of leaves and microclimatic parameters using artificial intelligence [127, 187]. The instrument consists of a microcontroller with an ATMega 328 processor chip connected with different sensors designed for the measurement of plant physiological variables. The TreeTalker® includes a reference and a heated probe (Murata Electronics, Nagaokakyo, Kyoto, Japan) to measure sap flow rate through the Heat Pulse method; a capacitive sensor to measure trunk moisture content; a 12-spectral-band spectrometer (AS7262 for visible and AS7263 for near infrared band – AMS, Premstaetten, Austria) centered at the wavelengths of 450, 500, 550, 570, 600, 610, 650, 680, 730,760, 810 and 860 nm to measure multispectral signature of light transmitted through the canopy; a MMA8451Q thermohygrometer (Silicon labs, Austin, TX, US) to measure air temperature and relative humidity; an infrared distance sensor (SHARP, Osaka, Japan) to measure tree trunk radial growth; a Si7006 accelerometer (NXP/Freescale, Austin, TX, US) to measure accelerations along a 3D coordinate system used to detect tree movements. The TreeTalker® has been mainly used in forestry but could potentially be used in fruit trees [188–190]. This device could be valuable for assessing both plant water status and consumption. Specifically, integrated sapflow probes can provide data on transpired water, while the infrared resistance sensor, capacitive trunk moisture sensor, and spectroradiometer can offer a good indication of PWS. Such comprehensive information can be of great advantage for irrigation management. On the contrary, it requires a validation with PWS main references (RWC, Ψ_{stem}). To date, no experimental trials with TreeTalker® on assessing plant water status and consumption and irrigation management of fruit trees have been conducted.

Figure 3. TreeTalker® mounted on an olive trunk.

2.3. Fruit-mounted sensors

2.3.1. Fruit gauges

Fruit growth parameters can be a reliable indicator of PWS [191]. The total volume of the fruit is determined by the balance of water inflow and outflow through the phloem and xylem, along with atmospheric exchanges that occur through the exocarp [26]. Such water flows into and out of the fruit are determined from the water potential gradient differences between the plant and the fruit [191,192]. Similar to what happens in the trunk, water exchanges cause diametric fluctuations during the day. Furthermore, due to the composition of fruit tissues (relatively high-water content compared to wood tissues), they

exhibit greater sensitivity in diametric variation to changes in water potential gradients compared to the trunk. This increased sensitivity allows for timely measurements, which are useful in preventing adverse effects on fruit growth and final yields. Daily diametric fluctuations are due to the imbalance between inflow and outflow. Indeed, during the midday hours fruit transpiration rate is higher than xylem inflow (outflow> inflow) causing fruit shrinkage [193]. During the evening and night, water potential is restored, and the fruit returns to its original volume or expands thanks to the accumulation of carbohydrates during the day [193–195].

Since the second half of the 1900s, several studies have reported the use of devices to monitor fruit diameter [196–200]. Most of the sensors developed are LVDTs (strain gauges) connected to a plunger that makes direct contact with the peel, usually mounted in a metal frame [199]. The first rudimentary LVDT device for continuous monitoring of fruit diameter was designed by Tukey in 1964 [196]. In 1984, Higgs and Jones devised an accurate system for continuous measuring of fruit diametric fluctuations [197]. In 1998, Link improved the sensor by making it more flexible and suitable for greater thickness ranges [200]. Despite the accuracy and reliability of these sensors, they were relatively expensive and, considering the number of sensors to be used in the field, non-sustainable for a farm [26]. In 2007, Morandi et al. constructed a low-cost sensor consisting of a linear potentiometer connected to a plunger that must be kept in contact with the peel and a stainless-steel frame (Figure 5) [199]. The gauge is adjustable and can be used with fruits of various sizes, from olive [68] to mango (*Mangifera indica* L.) [193]. To date, it is the most widely used type of fruit gauge in studies of fruit growth dynamics in response to external factors, including changes in PWS [65,69,201–203]. In 2016, Thalheimer built a fruit diameter monitoring sensor with low-cost optoelectronic components with a flexible two-color tape for movement detection by the optoelectronic sensor [198]. However, this sensor may prove useful for monitoring the active growth of the fruit, but it does not seem suitable for assessing PWS because it is only able to detect fruit enlargements and it does not react to shrinkage. The latest sensor built for monitoring fruit growth was presented by Peppi et al. in 2023 [204]. It is part of a low-cost multi-channel sensor-node architecture capable of transmitting data with a low-power LoRa transmission system. The sensor structure consists of two solid arms bound together at one end with a bolt. The plier is held in place by a spring, while a reference voltage-supplied potentiometer is located within the fulcrum of the plier and rigidly connected to one of the two arms of the clamp. This seems to be a more stable sensor on the fruit and more suitable for IoT systems. However, it still needs to be validated in fruit crops.

Fruit gauges have been abundantly used to understand the physiological dynamics of fruit water exchanges, i.e., to study the relative contribution of xylem, phloem, and transpiration flows to fruit growth and understand the water relationships between fruit, plant, and environment at different fruit development stages. These mechanisms were studied in peach [194], apricot (*Prunus armeniaca* L.) [205], kiwifruit (*Actinidia deliciosa* Chev.) [206], sweet cherry [207] and pear [208]. Carella et al. used fruit gauges to test the effect of vapor pressure deficit (VPD) on fruit relative growth rate (RGR), by comparing data of peach, mango, loquat (*Eriobotrya japonica* Lindl.), olive and orange [209].

Several studies have investigated the suitability of continuous monitoring of fruit growth to promptly detect when the fruit starts to be affected by water deficit in order to establish the moment to apply irrigation water. Boini et al. [210] monitored fruit growth to detect the onset of water stress in 'Imperal Gala' apples by correlating various growth parameters (fruit net daily growth, midday AGR, maximum AGR, minimum AGR and fruit daily shrinkage) with Ψ_{stem}. Results showed that fruit daily growth rate (g day^{-1}) is the index that better correlates with Ψ_{stem}, thus having the potential to be used as a reference in apple irrigation scheduling. In addition, the authors were able to define the threshold indicating the onset of moderate water stress in terms of fruit daily growth rate (1.2 to 1.3 g day^{-1}). Khosravi et al. carried out a three-year study using fruit gauges to assess abnormalities in the fruit growth of 'Frantoio' olive trees due to several factors including tree water status.

The purpose of the study was also to find the best way to analyze data with different statistical models [211]. Marino et al. used fruit gauges in conjunction with sap flow probes and leaf turgor pressure sensors (LPCP probes) [58]. The authors showed that the joint use of these three sensors can provide a comprehensive indication of olive trees water status. For instance, the two olive cultivars studied showed different response behavior to water deficit: one manifested it in pronounced changes in leaf turgor and fruit RGR, the other significantly reducing sap flow and reaching very low values of leaf turgor pressure. In nectarine, Scalisi et al. demonstrated the suitability of a dual-organ sensing approach by using fruit gauges with LPCP probes to determine irrigation timing by assessing which organ and sensor exhibited the strongest correlation with Ψ_{stem} [64]. Ultimately, it was found that a combination of both approaches proved most effective in determining irrigation timing. In 2020, Scalisi et al. replicated the experiment with olive trees and similarly concluded that a combination of leaf and fruit sensing proved most effective in determining irrigation timing [68].

Although monitoring fruit diameter may be important to identify when fruits are adversely affected by water deficit (fruit is the strongest sink organ), this data alone may not be enough for a complete information, as its growth dynamics may be influenced by other factors like crop load and mainly phenological stage [64]. In most stone fruits, water exchanges between the fruit and the plant or the atmosphere are at their lowest during pit hardening, while transpiration rate peaks during cell enlargement [212]. Having information from multiple organs simultaneously, such as leaves and xylem, can be valuable for assessing the physiological behavior of the entire plant system across the stages of fruit development. Therefore, it would be necessary to use this sensor in combination with others, for example, sap flow and LPCP sensors, as previously showed.

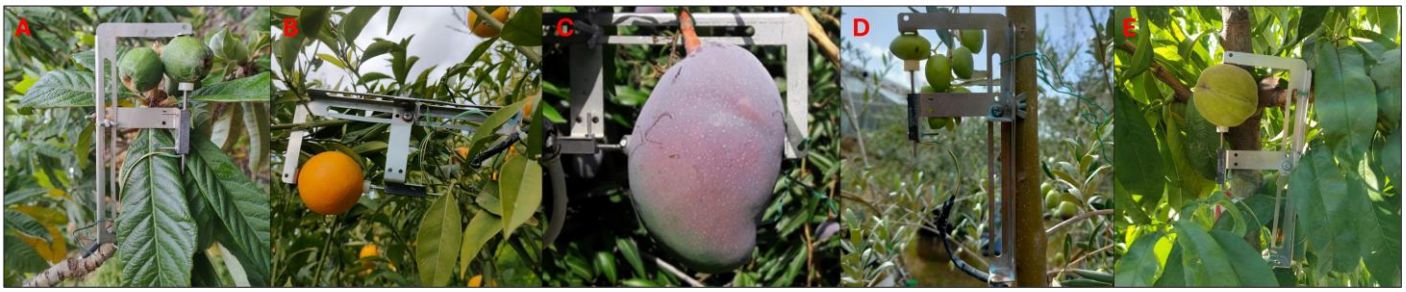

Figure 3. LVDT fruit gauges mounted in loquat (A), orange (B), mango (C), olive (D), and peach (E) fruit.

3. Remote sensing

Investigating the spatial and temporal variability of the field is one of the primary goals of precision irrigation. Ground-based measurements, although reliable, continuous in time, and accurate, provide a spot indication of the whole-field water status. Remote sensing techniques, although generally unable to monitor variability over time, are meant to overcome this spatial limitation of proximal measurements [45,213,214]. Remote sensors are capable of acquiring images containing information of different types and covering a wide area. In order to understand what type of sensor to use, one must be clear about the variable to be analyzed. Generally, remote sensors that are able of measuring reflected or transmitted by crops are used. This is because different components of the canopy structure are capable to reflect energy at different wavelengths depending on the molecules in the tissues. The spectral bands used in precision farming include ultraviolet (UV; 300-400 nm), visible (VIS; 400-700 nm), near infrared (NIR; 700-1400 nm), shortwave infrared (SWIR; 1400-3000 nm) and thermal infrared (TIR; 3000-25000 nm), [46,215]. These spectral

bands allow the calculation of vegetation indices (VI) useful to assess plant physiological parameters, e.g. normalized difference vegetation index (NDVI), crop water stress index (CWSI), normalized difference red edge index (NDRE), normalized difference water index (NDWI), etc. In this regard, remote sensors include optical cameras that are distinguished by various factors such as type of operation to carry out, type of acquisition, and number of spectral bands [46]. In precision irrigation, thermal, multispectral, and hyperspectral sensors can provide accurate PWS information [6]. The main platforms used in remote sensing are satellites and Unmanned Aircraft Systems (UAS, drones). Generally, satellites can provide a large amount of information since they can cover huge areas, but with a relatively low resolution [216]. Drones, on the other hand, manage to cope the resolution problem since they can fly at closer distances (40-120 m above the ground) [217–220]. Nevertheless, with the growing prevalence of free satellite data sources such as MODIS, Landsat, Sentinel, and Gaofen, commercial satellite imagery resolutions continue to improve both spatially (WorldView) and temporally (Planet). This improvement is attributed to cost reductions in small satellite systems [221,222].

The following paragraphs briefly describe the main remote sensing techniques for assessing field water status (FWS) in woody fruit crops by using thermal, multispectral, and hyperspectral sensors.

3.1. Thermal sensing

Plant temperature has been a longstanding indicator of water availability [96]. In the last three decades, thermal infrared (TIR) cameras have proven to be effective tools for estimating leaf and canopy temperature (T_c), which has been recognized as a rapid, reliable and non-destructive indicator of transpiration and PWS [223,224]. Plants tend to regulate their temperature by transpiring through the stomata, thereby balancing the energy fluxes within and outside the canopy [6,225]. When the plant undergoes stress the transpiration rate decreases, leading to an increase of T_c. This increase in T_c may serve as an indicator for detecting plant water stress [46,225]. However, T_c alone may not be sufficient, as it is influenced by various factors, mainly air temperature (T_{air}). Several Authors have often decided to normalize canopy temperature with air temperature ($T_c - T_{air}$) before correlating it with the main indicators of PWS (Ψ_{stem}, RWC, g_s, etc...) [66,226,227]. In 1981, Jackson et al. [96] developed the crop water stress index (CWSI), derived from the energy balance equation. In details, the complete formula for CWSI is the following [98]:

$$CWSI = \frac{(T_c - T_{air}) - (T_c - T_{air})_{LL}}{(T_c - T_{air})_{UL} - (T_c - T_{air})_{LL}} \quad (4)$$

Where $(T_c - T_{air})_{LL}$ is the lower limit of the difference between T_c and T_{air}, corresponding to a fully transpiring canopy. $(T_c - T_{air})_{UL}$ is the upper limit, corresponding to a non-transpiring canopy. $(T_c - T_{air})_{LL}$ is also defined as non-water stress baseline (NWSB), established through the relationship between $T_c - T_{air}$ and VPD. Whereas, $(T_c - T_{air})_{UL}$ corresponds to of the relationship between $T_c - T_{air}$ and VPD of a non-transpiring canopy. Conventionally $(T_c - T_{air})_{UL}$ is obtained from the intercept of the equation used to calculate NWSB corrected for air temperature, according to the methodology proposed by Idso et al. in 1981 [98,228]. In 1999, Jones simplified the equation as follows [229]:

$$CWSI = \frac{T_c - T_{wet}}{T_{dry} - T_{wet}} \quad (5)$$

In which T_c is the actual canopy temperature obtained by thermal photo, and T_{dry} and T_{wet} are the references representing the non-transpiring leaf (or canopy) temperature and a fully transpiring leaf (or canopy) temperature, respectively. CWSI ranges from 0 (fully

hydrated plant) to 1 (fully stressed plant). One of the most debated issues concerns the methodology to establish T_{dry} and T_{wet} references. To date, several methods have been studied. One may involve a theoretical (or analytical) approach, determining the CWSI and references via the balance equation at the canopy surface. However, this method requires the use of several environmental parameters (for more details see Jackson et al. [230] and Agam et al. [231]). An alternative approach involves the use of a wet artificial reference surface (WARS) [232,233] as T_{wet}, while T_{dry} can be estimated empirically as T_{air} + 5 °C [234]. Nevertheless, the accuracy of this method could be significantly affected by the material of the WARS, which should have similar leaf emissivity [6,235]. Apolo-Apolo et al. built a paper-based hemispheric surfaces that were placed in a 3D-printed plastic structure that continuously allows water storage [236]. Another common approach involves using leaves sprayed with water and detergent 30 seconds before measuring the leaf temperature as wet references. For the dry reference, the leaf is covered with petroleum jelly at least 30 minutes before the measurement to artificially close stomata and inhibit transpiration [225]. Finally, a frequently used approach in recent studies involves extrapolating the temperature of the pure canopy from the entire thermal image through image analysis, aiming to obtain the temperature distribution histogram of the pure canopy. T_{wet} corresponded to the average temperature of the 0.5% values on the left side of the histogram, whereas T_{dry} to the average temperature of the 0.5% values on the right side [237–241]. The latter approach has proven reliable in different species such as nectarines [237], grapevine [242], plums (*Prunus domestica* L.) [243] and olive [241].

Image analysis is necessary to extract temperature values. The main methods for canopy extraction consist of selecting a region of interest (ROI), temperature threshold, and binary mask [244]. ROI containing a single leaf or an area of leaves is identified in the thermal image either through manual or automatic delineation of an area mainly covered by leaves within the central portion of the thermal image [105]. ROI selection is rarely used for canopy segmentation in thermal imaging obtained by UAVs. This is largely due to the presence of significant ground background pixels in UAV-obtained thermal images, which makes it difficult to accurately isolate the canopy pixels. Temperature thresholding consists of distinguishing the soil and canopy pixels using a bimodal histogram showing two temperature peaks attributed to the soil and canopy [245]. Thus, Temperature thresholding can be easily determined from the temperature frequency histogram of thermal imaging. Although most pure canopy pixels can be extracted, the temperature threshold has shown a lack of suitability for distinguishing canopies under severe water stress, because the T_c is higher than that of well-watered canopies and is likely to be improperly discarded as soil pixels [244]. This could lead to subsequent errors in the calculation of mean canopy temperature and CWSI. Finally, for the binary mask technique, it is necessary to capture thermal and RGB images simultaneously. The binary mask is created by interactively determining the threshold values for the color components in the visible (RGB) images. The visible images are then processed to segment the canopy pixels according to color characteristics [246]. Afterwards, the segmented RGB image and the thermal image are perfectly overlaid to determine the temperature of the selected areas. Great care must be taken at this stage since a slight misalignment of the images will cause the soil background to be included in the thermal image, leading to errors in the calculation of the average canopy temperature (a problem that can be solved by a temperature thresholding operation).

In practice, CWSI from remote sensing has proved useful for estimating PWS in terms of both water potential (Ψ_{stem} and Ψ_{leaf}) and gas exchange (g_s) in woody fruit crops. Strong correlations have been shown in multiple crops, such as grapevine [105,238,247], olive [231,248–250], almond [251], plum [243], peach [237,245,252], apple [253], cherry [223], pear [227] and citrus [228,254,255] among all. In 2023, Mortazavi et al. developed a predictive model for Ψ_{stem} in almond and pistachio using vegetation indices obtained from aerial images through a Machine Learning approach [256]. Employing the Random Forest

(RF) algorithm, which demonstrated higher accuracy (88% for pistachio, 89% for almond), they found that CWSI played a more significant role in predicting Ψ_{stem} in both crops.

Thermal imaging techniques can be applied with images from both unmanned aerial vehicles (UAVs) and satellites. Although thermal satellite imagery is mainly used to study climate change, due to the ease of access to low-resolution imagery, Landsat and Sentinel-2 have been quite used in agriculture for CWSI calculation [257]. Jamshidi et al. [254] used both Landsat and Sentinel-2 data to assess CWSI in citrus. The authors found strong correlations by comparing CWSI calculated from satellites data and *in-situ* CWSI obtained from UAVs thermal imagery.

In summary, remote thermal sensing has proven to be a reliable method on medium to large scales for assessing the water status of fruit trees. However, despite the strong and significant relationships between thermal indices and direct ground-based measurements, there are varying ranges of CWSI values depending primarily on the methodology applied for calculating the different indices. Furthermore, it would be beneficial to develop models not only for individual species but also for different cultivars.

3.2. Multispectral sensing

Reflectance data in the different bands can provide direct or indirect indications of PWS. The reflectance spectrum of water can be identified in the infrared region as there are overtone bands of OH-bond at about 760, 970, 1450 and 1940 nm (regions of the NIR and SWIR, respectively) [258,259]. Multispectral cameras are sensors that can commonly provide data in 5 or 6 spectral regions, usually included in the VIS, rededge, and NIR bands. Since multispectral cameras mounted in drones or satellites generally do not go beyond NIR, crop water status is often assessed by indices that provide an indirect estimate [260]. Chlorophyll or nitrogen content may prove useful indirect indicators of PWS. Therefore, indices have been developed that are calculated in the reflectance band of these molecules, i.e., in the VIS, rededge and NIR regions [221,261]. The index that has been most widely used in fruit crops is NDVI, calculated by considering rededge and NIR reflectance [262]:

$$NDVI = \frac{NIR - RED}{NIR + RED} \quad (5)$$

When biotic or abiotic stress phenomena begin to occur, the reflectance of the NIR tends to decrease. In contrast, the reflectance of RED increases. NDVI values range from -1 to +1. Negative values are referred to soil properties, and positive to vegetation [263]. Numerous works have investigated about NDVI to assess PWS. For instance, Ballester et al. [264] examined the effectiveness of multiple xanthophyll, chlorophyll, and structure-sensitive spectral indices from UAVs for identifying water stress within a commercial orchard that included five different species (apricot, almond, peach, orange, and lemon). The authors showed that NDVI and photochemical reflectance index (PRI; a further VI calculated in the VIS region) were the indices that best correlated with Ψ_{stem} (R^2 = 0.61 and 0.65, respectively). Whereas, analyzing within single species, peach and 'Garrigue' almond were found to be the most suitable species for the prediction of both Ψ_{stem} and g_s from NDVI data (R^2 = 0.72 and 0.74 for Ψ_{stem} and R^2 = 0.75 and 0.71 for g_s respectively). In olive, Caruso et al. [265] demonstrated that NDVI can be a reliable indicator of tree water stress. In grapevine, several works confirm that NDVI can be a good indicator of PWS [266–269]. Other vegetation indices commonly used for PWS assessment, and which have been shown to be reliable are green normalized difference vegetation index (GNDVI), modified soil adjusted vegetation index (MSAVI), optimized soil adjusted vegetation index (OSAVI), green index (GI), normalized differenced RedEdge index (NDRE), enhanced vegetation index (EVI), simple ratio index (SR), water index (WI) [6,268,270-273]. Zúñiga Espinoza successfully used the green normalized difference vegetation index (GNDVI; a further VI calculated as the ratio between the difference of NIR

and Green bands and the sum of NIR and Green bands) for estimating g_s in grapevine [261]. Stagakis found strong relationships between PRI and Ψ_{stem} in orange [274]. In 2023, Fasiolo et al. introduced a novel method to assess the effects of different water regimes on water potential, vegetation indices, and canopy geometric data in grapevine [275]. This approach combined geometric measurements gathered by a mobile robot with multispectral data obtained from a UAV, as well as traditional measurements like Ψ_{stem} and Ψ_{pd} (pre-dawn stem water potential). In detail, sixty vegetation indices were accurately calculated using the projected area of the vineyard point cloud as a mask. Among them, 3 vegetation indices were identified that correlated best with the Ψ_{stem}: green difference vegetation index (GDVI; $R^2 = 0.90$), perpendicular vegetation index (PVI; $R^2 = 0.90$) and triangular greenness index (TGI; $R^2 = 0.87$). In addition, they observed that canopy volume and area projected onto the ground were affected by water status, as were measurements of Ψ_{stem} and Ψ_{pd}. Their scientific contribution involved integrating multispectral data from UAVs with ground-based data from a robot, enabling the extraction of spectral information exclusively from plants while excluding non-canopy surfaces.

Also in 2023, Longo-Minnolo et al. developed a new combined approach based on the use of multispectral imagery from UAVs and statistical models to determine the water status of an orange orchard (cv. Tarocco Sciara) during different phenological stages, compared with the traditional Ψ_{stem} [276]. The results first indicate that significant correlations with Ψ_{stem} were found for 9 of the 14 calculated vegetation indices: atmospherically resistant vegetation Index (ARVI), EVI, MSAVI, NDRE, NDVI, OSAVI, renormalized difference vegetation index (RDVI), soil adjusted vegetation index (SAVI) and SR. Second, the use of statistical methods such as stepwise linear regression and principal component regression (PCR) with all bands and vegetation indices allows for more reliable Ψ_{stem} estimates. Both methods have comparable performance, with PCR showing slightly lower errors.

Satellite multispectral imaging provides different information with respect to drones. Satellites can provide images at a wider multispectral range. Sentinel-2 [277,278] and Landsat 8 [279], for example, are capable to obtain information on the spectral bands of VIS, NIR, SWIR and thermal infrared (TIR) [6]. Other satellites used for the water status of fruit crops are Landsat 7 [280], WorldView-2 [281,282] and MODIS [283]. In pear, Van Beek [281] successfully estimated Ψ_{stem} through WorldView-2 multispectral imagery. In recent years, the Planet [284] platform has been developed, which uses a wide network of satellites (including PlanetScope, SkySat and RapidEye, Landsat 8 and Sentinel-2) to collect images and data from around the world. These satellites constantly capture information about the Earth's surface, giving users access to recent and historical images [285]. For example, Helman et al. used planet satellite images to monitor grapevine Ψ_{stem} [285]. In olive, Garofalo et al. [286] developed a machine learning algorithm to predict Ψ_{stem} using Planet.

Since the spectral bands of water are the NIR and SWIR, with the use of satellites, indices can be calculated for direct estimation of PWS, such as the moisture stress index (MSI) [283] and the better-known normalized difference water index (NDWI) [287]. For instance, Rodríguez-Fernández found strong relationships between Ψ_{stem} and NDWI ($R^2 = 0.67$) in grapevine [288]. Also in olive, NDWI proved to be a reliable predictor of water potential [270].

Multispectral methods may prove useful for PWS assessment, albeit often indirectly (especially with sensors lacking the SWIR band). Moreover, it could be argued that handling this extensive amount of data and conducting image analysis requires specialized skills. Knowledge of GIS-based software for geographic data visualization, management and analysis is crucial. Furthermore, the acquisition and management of these tools can be expensive, particularly when working with high-resolution imagery. This limitation may restrict access to such technologies for certain growers. Environmental conditions could also significantly affect the measurements. Reflection and refraction of sunlight on the Earth's surface can vary depending on environmental conditions, such as the presence of fog, clouds, atmospheric dust, or humidity. These phenomena can affect the quantity and

quality of the reflected light recorded by multispectral sensors, compromising the accuracy of the measurements [6]. Nevertheless, optimistic future prospects for multispectral remote sensing in PWS monitoring exist. The growing accessibility of this system, refinement of vegetation indices, and advancements in artificial intelligence may lead to the development of new models and ready-to-use systems for an efficient irrigation management.

3.3. Hyperspectral

In recent years a rapid advancement in spectroscopic and imaging technologies has occurred. In this regard, hyperspectral remote sensing imaging (HRS) has emerged as an efficient nondestructive technique to monitor several plant physiological parameters [289,290]. Multispectral imaging involves capturing spectral signals in specific bands, covering a wide spectral range from tens to hundreds of nanometers. Hyperspectral imaging, on the other hand, captures spectral signals in a sequence of continuous channels with a narrow spectral bandwidth, usually less than 10 nm. This capability allows hyperspectral imaging to capture detailed spectral features of targets that might be overlooked by multispectral imaging [291,292]. Besides cameras, spectrometers are also used in HRS. A spectrometer analyzes the spectral signatures of ground features in the sensor's field of view by examining the spectral characteristics of light radiation and separating the incoming energy into various wavelengths. Unlike optical, multispectral, and hyperspectral cameras that capture multiple bands of the electromagnetic spectrum and offer continuous gridded pixel area coverage, a spectrometer provides coverage in single pixel footprints determined by its field of view. Nevertheless, its high spectral resolution makes it a viable alternative to multispectral sensors [293]. Both hyperspectral cameras and spectrometers are mounted on UAVs during remote sensing measurements. In addition, hyperspectral sensors are also mounted on some satellites. However, few studies have been carried out with satellite remote sensing. Moreover, compared to the large number of satellite-mounted multispectral sensors, there are fewer with hyperspectral sensors. These include EO-1 Hyperion (the most widely used in agriculture), Tian-Gong-1, PRISMA, and PROBA-CHRIS [235,292]. For future perspective, the European Space Agency (ESA) is developing the Copernicus Hyperspectral Imaging Mission for the Environment (CHIME). This will carry a unique infrared spectrometer in the visible and shortwave to provide routine hyperspectral observations to support new and improved services for sustainable management of agriculture and biodiversity, as well as characterization of soil properties. The mission will complement Copernicus Sentinel-2 for applications such as land cover mapping (https://www.esa.int/ESA_Multimedia/Missions/CHIME/(result_type)/images) [294].

Various vegetation indices based mainly on NIR and SWIR bands (950-970, 1150-1260, 1450, 1950, and 2250 nm) can be determined from the hyperspectral sensors, such as NDWI, water index (WI) and water band index (WBI) among all [6,295,296]. Specifically, NDWI is calculated as the ratio between the difference in reflectance at approximately 860 nm and the reflectance at approximately 1240 nm bands, divided by their sum. Meanwhile, WI is determined by the ratio of reflectance at 970 nm the reflectance at 900 nm. Finally, WBI is calculated as the ratio of reflectance at 900 nm to the reflectance at 970 nm. In addition, despite its recognizable higher precision, hyperspectral TIR remote sensing has still received little attention to date [235,297].

Hyperspectral sensors have been used in several studies for PWS assessment. In citrus, Zarco-Tejada, with a UAV-mounted micro-hyperspectral imager, was able to estimate g_s and Ψ_{stem} by vegetation indices calculated in the VIS-NIR band (NDVI, TCARI, PRI, etc…) and chlorophyll fluorescence indices [298]. Several works on PWS estimation by hyperspectral images have been carried out on grapevine [269,295,299]. Matese et al. conducted the first evaluation of a UAV hyperspectral dataset on the entire vine ecosystem, using

narrowband VIS and multivariate PLS regressions [300]. This study included assessments of water status, vegetative parameters (such as total and lateral leaf area, pruning weight), as well as pomological and quality parameters. In 2023, Vasquez et al. used a Machine Learning approach to predict grapevine Ψ_{stem} from UAV-based hyperspectral imagery in the NIR-SWIR at different phenological stages [301]. Again, an RF model was used to model the data and 10-fold cross-validation for evaluation. The authors were able to develop a predictive model of the Ψ_{stem} with RMSE = 0.12 MPa. Exhaustive results were also found on apple [302], cherry [303], and almond [304] trees.

An important consideration about hyperspectral sensing in general is the relatively high cost. Currently, due to their technological complexity, hyperspectral sensors are less affordable than multispectral sensors. Additionally, a higher level of expertise is required to handle and interpret hyperspectral data [292].

4. Combined approaches of proximal and remote sensing

The joint use of proximal and remote sensing technologies could provide a more comprehensive information on orchard water status and facilitate the acquisition of irrigation needs in terms of timing and volumes. Field water availability may depend on several factors, e.g. soil texture [305] and chemical and physical properties [306], leaf area [307], presence of cover crops [308], field microclimate [309], etc.

Data from remote sensing could provide useful insights into spatial variability by allowing an adequate field mapping. In this way, it would be possible to strategically place proximal sensors according to the distinct zones of the field. In addition, during the irrigation season, continuous acquisition of data from proximal sensors could expand throughout the orchard by developing appropriate predictive models from vegetation indices obtained via UAVs or satellites. The result would be the expansion of information in time and space. For these reasons, the combination of the two approaches (proximal and remote) may prove to be an efficient and sustainable system for irrigation scheduling, greatly increasing water saving. Yet, as of now, affording a comprehensive system that integrates data from both proximal and remote sensors remains economically challenging for a significant portion of the agricultural community. For this reason, new low-cost sensors are continually being developed and validated, in part due to the simplicity of setting up affordable electronic systems and in part to the advancement of validation techniques such as machine learning. Furthermore, the UAV industry is making rapid progress producing miniaturized and cost-effective devices. Similarly, the accessibility and affordability of various satellite platforms could facilitate the retrieval of remote data.

To date, there is not a large number of studies combining remote and proximal sensing. Caruso et al. evaluated the combined use of multispectral data from UAV with data from soil electrical conductivity sensors in order to identify homogeneous zone in a high-density irrigated olive orchard [265]. The authors found that the impact of various irrigation strategies on tree performance and water use efficiency (WUE) is location-dependent within the orchard, and tree vigor emerges as a primary factor influencing the ultimate fruit yield when soil water availability is optimal. Matese et al. combined ground-based infrared thermography and thermal imaging from UAV [310]. The results showed that CWSI values obtained from both remote and proximal sensors serve as useful indicators for evaluating the spatial variability of crop water status in Mediterranean vineyards. In almond, Gonzalez-Dugo et al. related the actual transpiration measured with heat-pulse sap flow probes with the CWSI, calculated using an empirical Non-Water Stress Baseline [311]. The relationship obtained between CWSI and relative transpiration was high (R^2 = 0.69), demonstrating the effectiveness of the combined use of sap flow probes with airborne thermal imaging. To further confirmation, a relationship between CWSI and transpiration calculated from sap flow output was also found on 'Tonda Romana' hazelnut

(*Corylus avellana* L.) by Pasqualotto et al. [312]. No further coupling studies were found between remote sensing techniques and the proximal sensors mentioned above.

5. Conclusions

The management of irrigation water in orchards has become a crucial issue. Today, thanks to the techniques mentioned in this review, it is possible to develop an efficient and sustainable irrigation plan. As shown above, several types of sensors can prove useful in estimating PWS, but the future challenge lies in being able to find the appropriate combination for crop type, soil, and climate. The integration of remote and plant-based proximal sensing techniques can effectively provide large-scale (time and space) information for efficient monitoring of orchard water availability. However, few studies have investigated the combination of both techniques.

Developing appropriate protocols for efficient and sustainable irrigation management remains a primary research goal. Artificial intelligence may be an effective tool for the integration of different sensors, leading to new machine learning algorithms that can easily make system automation possible. Another challenge lies in the choice of sensors to be combined. An efficient and sustainable precision irrigation system should incorporate sensors that not only provide qualitative information about irrigation timing, but also offer quantitative data on plant water usage. One hypothesis is to combine sensors that provide direct information on water status (e.g., microtensiometers, psychrometers) with sensors that can monitor the response of various plant organs to different hydration levels (e.g., leaf turgor sensors and fruit gauges), and finally, those that can provide information on actual water consumption (e.g., sap flow sensors, leaf transpiration sensors).

Furthermore, integrating proximal systems with remote sensing can offer comprehensive information for more precise and efficient irrigation management, thereby minimizing water waste, meeting plant requirements, and maintaining good yields. Moreover, such accurate information would more easily enable an increasingly punctual irrigation system within the orchard, which could lead to significant water savings by increasing profits and positively impacting environmental sustainability. In addition to system precision, economic factors must also be considered. Nowadays, thanks to the more affordable prices of electronic components along with continuously evolving artificial intelligence tools, obtaining sensors and models that overcome the high costs associated with precision systems may become possible. Therefore, improving existing systems that have high potential but also high costs (e.g., microtensiometers, sap flow sensors) and making them accessible to a wide range of producers could be an immediate challenge. Regarding remote sensing systems, prices of drones and satellite imagery are progressively decreasing, and such expenses can represent an investment to significantly increase profits.

This review provides updates on both proximal and remote sensing methodologies, encompassing established techniques like LPCP probes, fruit gauges, and sapflow probes to emerging technologies like microtensiometers, as well as potentially reliable and user-friendly options such as LWM and LMCP. In particular, the affordability of the latter is emphasized, as it would make it easily accessible to farmers. It is crucial to note the ongoing evolution of remote sensing methodologies, facilitated by the growing accessibility of instruments like UAVs, satellite platforms, and nanotechnologies. The final challenge launched by this review is to encourage researchers to investigate these techniques further and develop appropriate protocols that could make these methodologies increasingly accurate, reliable, and low-cost.

Author Contributions: Conceptualization, A.C. and R.L.B; methodology, A.C.; investigation, A.C.; resources, A.C., P.T.B.F., R.L.B. and R.M.; data curation, A.C. and R.L.B.; writing—original draft preparation, A.C., P.T.B.F., R.M. and R.L.B.; writing—review and editing, A.C., P.T.B.F., R.L.B. and

R.M.; visualization, A.C., R.M. and P.T.B.F.; supervision, R.L.B. and R.M.; funding acquisition, R.L.B. and R.M. All authors have read and agreed to the published version of the manuscript.

Funding: The present study was funded by the projects: Ecosistema dell'innovazione Sicilian MicronanoTech Research and Innovation Center -SAMOTHRACE. Fondo Finalizzato alla Ricerca di Ateneo FFR_D13_008811. European Project H2020-MSCA-RISE-2020 - ref. 101007702.

Data Availability Statement: Not applicable.

Conflicts of Interest: The authors declare no conflict of interest.

References

1. Mirdashtvan, M.; Najafinejad, A.; Malekian, A.; Sa'doddin, A. Sustainable Water Supply and Demand Management in Semi-Arid Regions: Optimizing Water Resources Allocation Based on RCPs Scenarios. *Water Resour. Manag.* **2021**, *35*, 5307–5324.
2. Velasco-Muñoz, J.F.; Aznar-Sánchez, J.A.; Belmonte-Ureña, L.J.; Román-Sánchez, I.M. Sustainable Water Use in Agriculture: A Review of Worldwide Research. *Sustainability* **2018**, *10*, 1084.
3. Gosling, S.N.; Arnell, N.W. A Global Assessment of the Impact of Climate Change on Water Scarcity. *Clim. Change* **2016**, *134*, 371–385.
4. Del Pozo, A.; Brunel-Saldias, N.; Engler, A.; Ortega-Farias, S.; Acevedo-Opazo, C.; Lobos, G.A.; Jara-Rojas, R.; Molina-Montenegro, M.A. Climate Change Impacts and Adaptation Strategies of Agriculture in Mediterranean-Climate Regions (MCRs). *Sustainability* **2019**, *11*, 2769.
5. Webb, L.; Whiting, J.; Watt, A.; Hill, T.; Wigg, F.; Dunn, G.; Needs, S.; Barlow, E. Managing Grapevines through Severe Heat: A Survey of Growers after the 2009 Summer Heatwave in South-Eastern Australia. *J. Wine Res.* **2010**, *21*, 147–165.
6. Gautam, D.; Pagay, V. A Review of Current and Potential Applications of Remote Sensing to Study the Water Status of Horticultural Crops. *Agronomy* **2020**, *10*, 140.
7. Hristov, J.; Barreiro-Hurle, J.; Salputra, G.; Blanco, M.; Witzke, P. Reuse of Treated Water in European Agriculture: Potential to Address Water Scarcity under Climate Change. *Agric. Water Manag.* **2021**, *251*, 106872.
8. Allen, C.D.; Macalady, A.K.; Chenchouni, H.; Bachelet, D.; McDowell, N.; Vennetier, M.; Kitzberger, T.; Rigling, A.; Breshears, D.D.; Hogg, E.T. A Global Overview of Drought and Heat-Induced Tree Mortality Reveals Emerging Climate Change Risks for Forests. *For. Ecol. Manag.* **2010**, *259*, 660–684.
9. Fernández, J.E. Plant-Based Methods for Irrigation Scheduling of Woody Crops. *Horticulturae* **2017**, *3*, 35.
10. Noun, G.; Lo Cascio, M.; Spano, D.; Marras, S.; Sirca, C. Plant-Based Methodologies and Approaches for Estimating Plant Water Status of Mediterranean Tree Species: A Semi-Systematic Review. *Agronomy* **2022**, *12*, 2127.
11. Allen, R.G.; Pereira, L.S.; Raes, D.; Smith, M. Crop Evapotranspiration-Guidelines for Computing Crop Water Requirements-FAO Irrigation and Drainage Paper 56. *Fao Rome* **1998**, *300*, D05109.
12. Cammalleri, C.; Ciraolo, G.; Minacapilli, M.; Rallo, G. Evapotranspiration from an Olive Orchard Using Remote Sensing-Based Dual Crop Coefficient Approach. *Water Resour. Manag.* **2013**, *27*, 4877–4895.
13. Allen, R.G.; Pereira, L.S. Estimating Crop Coefficients from Fraction of Ground Cover and Height. *Irrig. Sci.* **2009**, *28*, 17–34.
14. Jones, H.G. Monitoring Plant and Soil Water Status: Established and Novel Methods Revisited and Their Relevance to Studies of Drought Tolerance. *J. Exp. Bot.* **2007**, *58*, 119–130, doi:10.1093/jxb/erl118.
15. Paramasivam, S.; Alva, A.; Fares, A. An Evaluation of Soil Water Status Using Tensiometers in a Sandy Soil Profile under Citrus Production1. *Soil Sci.* **2000**, *165*, 343–353.
16. Coolong, T.; Snyder, J.; Warner, R.; Strang, J.; Surendran, S. The Relationship between Soil Water Potential, Environmental Factors, and Plant Moisture Status for Poblano Pepper Grown Using Tensiometer-Scheduled Irrigation. *Int. J. Veg. Sci.* **2012**, *18*, 137–152.
17. So, H. Water Potential Gradients and Resistances of a Soil-Root System Measured with the Root and Soil Psychrometer. In *The Soil–Root Interface*; Elsevier, **1979**; pp. 99–113.
18. Savage, M.J.; Ritchie, J.T.; Bland, W.L.; Dugas, W.A. Lower Limit of Soil Water Availability. *Agron. J.* **1996**, *88*, 644–651.
19. Payero, J.O.; Qiao, X.; Khalilian, A.; Mirzakhani-Nafchi, A.; Davis, R. Evaluating the Effect of Soil Texture on the Response of Three Types of Sensors Used to Monitor Soil Water Status. *J. Water Resour. Prot.* **2017**, *9*, 566.
20. Intrigliolo, D.S.; Castel, J.R. Continuous Measurement of Plant and Soil Water Status for Irrigation Scheduling in Plum. *Irrig. Sci.* **2004**, *23*, 93–102.
21. Ines, A.V.; Das, N.N.; Hansen, J.W.; Njoku, E.G. Assimilation of Remotely Sensed Soil Moisture and Vegetation with a Crop Simulation Model for Maize Yield Prediction. *Remote Sens. Environ.* **2013**, *138*, 149–164.
22. Mohanty, B.P.; Cosh, M.H.; Lakshmi, V.; Montzka, C. Soil Moisture Remote Sensing: State-of-the-Science. *Vadose Zone J.* **2017**, *16*, 1–9.

23. Schmitz, M.; Sourell, H. Variability in Soil Moisture Measurements. *Irrig. Sci.* **2000**, *19*, 147–151.
24. McCutchan, H.; Shackel, K. Stem-Water Potential as a Sensitive Indicator of Water Stress in Prune Trees (Prunus Domestica L. Cv. French). *J. Am. Soc. Hortic. Sci.* **1992**, *117*, 607–611.
25. Jones, H.G. Irrigation Scheduling: Advantages and Pitfalls of Plant-Based Methods. *J. Exp. Bot.* **2004**, *55*, 2427–2436.
26. Scalisi, A.; Bresilla, K.; Simões Grilo, F. Continuous Determination of Fruit Tree Water-Status by Plant-Based Sensors. *Italus Hortus* **2017**, *24*, 39–50.
27. Shackel, K.A.; Ahmadi, H.; Biasi, W.; Buchner, R.; Goldhamer, D.; Gurusinghe, S.; Hasey, J.; Kester, D.; Krueger, B.; Lampinen, B. Plant Water Status as an Index of Irrigation Need in Deciduous Fruit Trees. *HortTechnology* **1997**, *7*, 23–29.
28. Poblete-Echeverría, C.; Ortega-Farías, S.; Lobos, G.; Romero, S.; Ahumada, L.; Escobar, A.; Fuentes, S. Non-Invasive Method to Monitor Plant Water Potential of an Olive Orchard Using Visible and near Infrared Spectroscopy Analysis. *Acta Hortic* **2014**, *1057*, 363–368.
29. Zimmermann, D.; Reuss, R.; Westhoff, M.; Gessner, P.; Bauer, W.; Bamberg, E.; Bentrup, F.-W.; Zimmermann, U. A Novel, Non-Invasive, Online-Monitoring, Versatile and Easy Plant-Based Probe for Measuring Leaf Water Status. *J. Exp. Bot.* **2008**, *59*, 3157–3167.
30. Bennett, J.; Boote, K.; Hammond, L. Alterations in the Components of Peanut Leaf Water Potential during Desiccation. *J. Exp. Bot.* **1981**, 1035–1043.
31. Lo Bianco, R.; Scalisi, A. Water Relations and Carbohydrate Partitioning of Four Greenhouse-Grown Olive Genotypes under Long-Term Drought. *Trees* **2017**, *31*, 717–727.
32. Barrs, H.; Weatherley, P. A Re-Examination of the Relative Turgidity Technique for Estimating Water Deficits in Leaves. *Aust. J. Biol. Sci.* **1962**, *15*, 413–428.
33. Dichio, B.; Xiloyannis, C.; Sofo, A.; Montanaro, G. Osmotic Regulation in Leaves and Roots of Olive Trees during a Water Deficit and Rewatering. *Tree Physiol.* **2006**, *26*, 179–185.
34. Mullan, D.; Pietragalla, J. Leaf Relative Water Content. *Physiol. Breed. II Field Guide Wheat Phenotyping* **2012**, 25–27.
35. Tardieu, F.; Davies, W. Integration of Hydraulic and Chemical Signalling in the Control of Stomatal Conductance and Water Status of Droughted Plants. *Plant Cell Environ.* **1993**, *16*, 341–349.
36. Whitehead, D. Assessment of Water Status in Trees from Measurements of Stomatal Conductance and Water Potential. *NZJ Sci* **1980**, *10*, 159–165.
37. McBurney, T. The Relationship between Leaf Thickness and Plant Water Potential. *J. Exp. Bot.* **1992**, *43*, 327–335.
38. Sakuratani, T. A Heat Balance Method for Measuring Water Flux in the Stem of Intact Plants. *J. Agric. Meteorol.* **1981**, *37*, 9–17.
39. Escalona, J.; Flexas, J.; Medrano, H. Drought Effects on Water Flow, Photosynthesis and Growth of Potted Grapevines. *VITIS-GEILWEILERHOF-* **2002**, *41*, 57–62.
40. Huck, M.G.; Klepper, B. Water Relations of Cotton. II. Continuous Estimates of Plant Water Potential from Stem Diameter Measurements 1. *Agron. J.* **1977**, *69*, 593–597.
41. Intrigliolo, D.; Castel, J. Evaluation of Grapevine Water Status from Trunk Diameter Variations. *Irrig. Sci.* **2007**, *26*, 49–59.
42. Doltra, J.; Oncins, J.A.; Bonany, J.; Cohen, M. Evaluation of Plant-Based Water Status Indicators in Mature Apple Trees under Field Conditions. *Irrig. Sci.* **2007**, *25*, 351–359.
43. Ji, W.; Li, L.; Zhou, W. Design and Implementation of a RFID Reader/Router in RFID-WSN Hybrid System. *Future Internet* **2018**, *10*, 106.
44. Mekonnen, Y.; Namuduri, S.; Burton, L.; Sarwat, A.; Bhansali, S. Machine Learning Techniques in Wireless Sensor Network Based Precision Agriculture. *J. Electrochem. Soc.* **2019**, *167*, 037522.
45. Alexopoulos, A.; Koutras, K.; Ali, S.B.; Puccio, S.; Carella, A.; Ottaviano, R.; Kalogeras, A. Complementary Use of Ground-Based Proximal Sensing and Airborne/Spaceborne Remote Sensing Techniques in Precision Agriculture: A Systematic Review. *Agronomy* **2023**, *13*, 1942.
46. Roma, E.; Catania, P. Precision Oliviculture: Research Topics, Challenges, and Opportunities—A Review. *Remote Sens.* **2022**, *14*, 1668.
47. Asgari, N.; Ayoubi, S.; Jafari, A.; Demattê, J.A. Incorporating Environmental Variables, Remote and Proximal Sensing Data for Digital Soil Mapping of USDA Soil Great Groups. *Int. J. Remote Sens.* **2020**, *41*, 7624–7648.
48. Damásio, M.; Barbosa, M.; Deus, J.; Fernandes, E.; Leitão, A.; Albino, L.; Fonseca, F.; Silvestre, J. Can Grapevine Leaf Water Potential Be Modelled from Physiological and Meteorological Variables? A Machine Learning Approach. *Plants* **2023**, *12*, 4142, doi:10.3390/plants12244142.
49. Thoday, D. On the Water Relations of Plant Cells. *Ann. Bot.* **1950**, *14*, 1–6.

50. Wenkert, W.; Lemon, E.; Sinclair, T. Leaf Elongation and Turgor Pressure in Field-grown Soybean 1. *Agron. J.* **1978**, *70*, 761–764.
51. Rodriguez-Dominguez, C.M.; Buckley, T.N.; Egea, G.; de Cires, A.; Hernandez-Santana, V.; Martorell, S.; Diaz-Espejo, A. Most Stomatal Closure in Woody Species under Moderate Drought Can Be Explained by Stomatal Responses to Leaf Turgor. *Plant Cell Environ.* **2016**, *39*, 2014–2026.
52. Zimmermann, U.; Rüger, S.; Shapira, O.; Westhoff, M.; Wegner, L.; Reuss, R.; Gessner, P.; Zimmermann, G.; Israeli, Y.; Zhou, A. Effects of Environmental Parameters and Irrigation on the Turgor Pressure of Banana Plants Measured Using the Non-invasive, Online Monitoring Leaf Patch Clamp Pressure Probe. *Plant Biol.* **2010**, *12*, 424–436.
53. Green, P.B.; Stanton, F.W. Turgor Pressure: Direct Manometric Measurement in Single Cells of Nitella. *Science* **1967**, *155*, 1675–1676.
54. Zimmermann, U.; Räde, H.; Steudle, E. Kontinuierliche Druckmessung in Pflanzenzellen. *Naturwissenschaften* **1969**, *56*, 634–634.
55. Steudle, E.; Zimmermann, U.; Lüttge, U. Effect of Turgor Pressure and Cell Size on the Wall Elasticity of Plant Cells 1. *Plant Physiol.* **1977**, *59*, 285–289, doi:10.1104/pp.59.2.285.
56. Hüsken, D.; Steudle, E.; Zimmermann, U. Pressure Probe Technique for Measuring Water Relations of Cells in Higher Plants. *Plant Physiol.* **1978**, *61*, 158–163.
57. Howard, R.J.; Ferrari, M.A.; Roach, D.H.; Money, N.P. Penetration of Hard Substrates by a Fungus Employing Enormous Turgor Pressures. *Proc. Natl. Acad. Sci.* **1991**, *88*, 11281–11284.
58. Marino, G.; Scalisi, A.; Guzmán-Delgado, P.; Caruso, T.; Marra, F.P.; Lo Bianco, R. Detecting Mild Water Stress in Olive with Multiple Plant-Based Continuous Sensors. *Plants* **2021**, *10*, 131, doi:10.3390/plants10010131.
59. Marino, G.; Pernice, F.; Marra, F.P.; Caruso, T. Validation of an Online System for the Continuous Monitoring of Tree Water Status for Sustainable Irrigation Managements in Olive (Olea Europaea L.). *Agric. Water Manag.* **2016**, *177*, 298–307.
60. Padilla-Díaz, C.; Rodriguez-Dominguez, C.; Hernandez-Santana, V.; Perez-Martin, A.; Fernández, J. Scheduling Regulated Deficit Irrigation in a Hedgerow Olive Orchard from Leaf Turgor Pressure Related Measurements. *Agric. Water Manag.* **2016**, *164*, 28–37.
61. Ehrenberger, W.; Rüger, S.; Rodríguez-Domínguez, C.M.; Díaz-Espejo, A.; Fernández, J. e.; Moreno, J.; Zimmermann, D.; Sukhorukov, V.L.; Zimmermann, U. Leaf Patch Clamp Pressure Probe Measurements on Olive Leaves in a Nearly Turgorless State. *Plant Biol.* **2012**, *14*, 666–674, doi:10.1111/j.1438-8677.2011.00545.x.
62. Rüger, S.; Netzer, Y.; Westhoff, M.; Zimmermann, D.; Reuss, R.; Ovadiya, S.; Gessner, P.; Zimmermann, G.; Schwartz, A.; Zimmermann, U. Remote Monitoring of Leaf Turgor Pressure of Grapevines Subjected to Different Irrigation Treatments Using the Leaf Patch Clamp Pressure Probe. *Aust. J. Grape Wine Res.* **2010**, *16*, 405–412.
63. Westhoff, M.; Zimmermann, D.; Zimmermann, G.; Gessner, P.; Wegner, L.; Bentrup, F.-W.; Zimmermann, U. Distribution and Function of Epistomatal Mucilage Plugs. *Protoplasma* **2009**, *235*, 101–105.
64. Scalisi, A.; O'Connell, M.G.; Stefanelli, D.; Lo Bianco, R. Fruit and Leaf Sensing for Continuous Detection of Nectarine Water Status. *Front. Plant Sci.* **2019**, *10*, 805.
65. Scalisi, A.; O' Connell, M.; Lo Bianco, R.; Stefanelli, D. Continuous Detection of New Plant Water Status Indicators in Stage I of Nectarine Fruit Growth. *Acta hortic.* **2018,** pp. 9–16.
66. Ballester, C.; Castiella, M.; Zimmermann, U.; Rüger, S.; Martínez Gimeno, M.A.; Intrigliolo, D.S. Usefulness of the ZIM-Probe Technology for Detecting Water Stress in Clementine and Persimmon Trees. **2015**; pp. 105–112.
67. Martínez-Gimeno, M.A.; Castiella, M.; Rüger, S.; Intrigliolo, D.S.; Ballester, C. Evaluating the Usefulness of Continuous Leaf Turgor Pressure Measurements for the Assessment of Persimmon Tree Water Status. *Irrig. Sci.* **2017**, *35*, 159–167.
68. Scalisi, A.; Marino, G.; Marra, F.P.; Caruso, T.; Lo Bianco, R. A Cultivar-Sensitive Approach for the Continuous Monitoring of Olive (Olea Europaea L.) Tree Water Status by Fruit and Leaf Sensing. *Front. Plant Sci.* **2020**, *11*, 340.
69. Massenti, R.; Scalisi, A.; Marra, F.P.; Caruso, T.; Marino, G.; Lo Bianco, R. Physiological and Structural Responses to Prolonged Water Deficit in Young Trees of Two Olive Cultivars. *Plants* **2022**, *11*, 1695.
70. Fernández, J.; Rodriguez-Dominguez, C.; Perez-Martin, A.; Zimmermann, U.; Rüger, S.; Martín-Palomo, M.; Torres-Ruiz, J.; Cuevas, M.; Sann, C.; Ehrenberger, W. Online-Monitoring of Tree Water Stress in a Hedgerow Olive Orchard Using the Leaf Patch Clamp Pressure Probe. *Agric. Water Manag.* **2011**, *100*, 25–35.
71. Sghaier, A.; Chehab, H.; Aissaoui, F.; Naggaz, K.; Ouessar, M.; Boujnah, D. Effect of Three Irrigation Frequencies on Physiological-Biological Aspects of Young Olive Trees (Olea Europaea L. Cvs' Koroneiki'and'Picholine'): Vegetative Growth, Leaf Turgor Pressure, and Fluorescence. *Pol. J. Environ. Stud.* **2019**, *28*.

72. Barriga, J.A.; Blanco-Cipollone, F.; Trigo-Córdoba, E.; García-Tejero, I.; Clemente, P.J. Crop-water assessment in Citrus (*Citrus sinensis* L.) based on continuous measurements of leaf-turgor pressure using machine learning and IoT. *Expert Systems with Applications* **2022**, *209*, 118255.
73. Palomo, J.; Romero, R.; Cuevas, M.V.; Alamo, T.; Muñoz de la Peña, D. Water Stress Estimation from Leaf Turgor Pressure in *Arbequina* Olive Orchards Based on Linear Discriminant Analysis. *Exp. Syst. Appl.* 2024, preprint submitted. Available at SSRN: https://ssrn.com/abstract=4719404.
74. Cecilia, B.; Francesca, A.; Dalila, P.; Carlo, S.; Antonella, G.; Francesco, F.; Marco, R.; Mauro, C. On-Line Monitoring of Plant Water Status: Validation of a Novel Sensor Based on Photon Attenuation of Radiation through the Leaf. *Sci. Total Environ.* **2022**, *817*, 152881.
75. Kaiser, H. A New Device for Continuous Non-Invasive Measurements of Leaf Water Content Using NIR-Transmission Allowing Dynamic Tracking of Water Budgets. *bioRxiv* **2022**, 2022–05.
76. Haworth, M.; Marino, G.; Atzori, G.; Fabbri, A.; Daccache, A.; Killi, D.; Carli, A.; Montesano, V.; Conte, A.; Balestrini, R. Plant Physiological Analysis to Overcome Limitations to Plant Phenotyping. *Plants* **2023**, *12*, 4015.
77. Meidner, H. An Instrument for the Continuous Determination of Leaf Thickness Changes in the Field. *J. Exp. Bot.* **1952**, *3*, 319–325.
78. Scoffoni, C.; Vuong, C.; Diep, S.; Cochard, H.; Sack, L. Leaf Shrinkage with Dehydration: Coordination with Hydraulic Vulnerability and Drought Tolerance. *Plant Physiol.* **2014**, *164*, 1772–1788.
79. Seelig, H.-D.; Stoner, R.J.; Linden, J.C. Irrigation Control of Cowpea Plants Using the Measurement of Leaf Thickness under Greenhouse Conditions. *Irrig. Sci.* **2012**, *30*, 247–257.
80. Rozema, J.; Arp, W. van; Diggelen, J. van; Kok, E.; Letschert, J. An Ecophysiological Comparison of Measurements of the Diurnal Rhythm of the Leaf Elongation and Changes of the Leaf Thickness of Salt-Resistant Dicotyledonae and Monocotyledonae. *J. Exp. Bot.* **1987**, *38*, 442–453.
81. Burquez, A. Leaf Thickness and Water Deficit in Plants: A Tool for Field Studies. *J. Exp. Bot.* **1987**, *38*, 109–114.
82. Giuliani, R.; Koteyeva, N.; Voznesenskaya, E.; Evans, M.A.; Cousins, A.B.; Edwards, G.E. Coordination of Leaf Photosynthesis, Transpiration, and Structural Traits in Rice and Wild Relatives (Genus Oryza). *Plant Physiol.* **2013**, *162*, 1632–1651.
83. Afzal, A.; Duiker, S.W.; Watson, J.E. Leaf Thickness to Predict Plant Water Status. *Biosyst. Eng.* **2017**, *156*, 148–156.
84. Bachmann, F. Studien Über Dickenänderungen von Laubblättern. *Jb F Wiss Bot* **1922**, *61*, 372.
85. Malone, M. Kinetics of Wound-Induced Hydraulic Signals and Variation Potentials in Wheat Seedlings. *Planta* **1992**, *187*, 505–510.
86. Jinwen, L.; Jingping, Y.; Pinpin, F.; Junlan, S.; Dongsheng, L.; Changshui, G.; Wenyue, C. Responses of Rice Leaf Thickness, SPAD Readings and Chlorophyll a/b Ratios to Different Nitrogen Supply Rates in Paddy Field. *Field Crops Res.* **2009**, *114*, 426–432.
87. Sharon, Y.; Bravdo, B.-A. Irrigation Control for Citrus According to the Diurnal Cycling of Leaf Thickness., **1996**; pp. 273–283.
88. Thalheimer, M. A Leaf-Mounted Capacitance Sensor for Continuous Monitoring of Foliar Transpiration and Solar Irradiance as an Indicator of Plant Water Status. *J. Agric. Eng.* **2023**, *54*.
89. Moreshet, S.; Yocum, C. A Condensation Type Porometer for Field Use. *Plant Physiol.* **1972**, *49*, 944–949.
90. Miner, G.L.; Ham, J.M.; Kluitenberg, G.J. A Heat-Pulse Method for Measuring Sap Flow in Corn and Sunflower Using 3D-Printed Sensor Bodies and Low-Cost Electronics. *Agric. For. Meteorol.* **2017**, *246*, 86–97.
91. Afzal, A.; Duiker, S.W.; Watson, J.E.; Luthe, D. Leaf Thickness and Electrical Capacitance as Measures of Plant Water Status. *Trans. ASABE* **2017**, *60*, 1063–1074.
92. Arve, L.E.; Kruse, O.M.O.; Tanino, K.K.; Olsen, J.E.; Futsæther, C.; Torre, S. Daily Changes in VPD during Leaf Development in High Air Humidity Increase the Stomatal Responsiveness to Darkness and Dry Air. *J. Plant Physiol.* **2017**, *211*, 63–69.
93. Maroco, J.P.; Pereira, J.S.; Chaves, M.M. Stomatal Responses to Leaf-to-Air Vapour Pressure Deficit in Sahelian Species. *Funct. Plant Biol.* **1997**, *24*, 381–387.
94. McAdam, S.A.; Brodribb, T.J. The Evolution of Mechanisms Driving the Stomatal Response to Vapor Pressure Deficit. *Plant Physiol.* **2015**, *167*, 833–843.
95. Clauser, L. Precision water management in apple orchards: comparison of technologies. Master degree Thesis, University of Padua, Padua, Italy, 26 February 2024.
96. Jackson, R.D.; Idso, S.; Reginato, R.; Pinter Jr, P. Canopy Temperature as a Crop Water Stress Indicator. *Water Resour. Res.* **1981**, *17*, 1133–1138.
97. Leinonen, I.; Jones, H.G. Combining Thermal and Visible Imagery for Estimating Canopy Temperature and Identifying Plant Stress. *J. Exp. Bot.* **2004**, *55*, 1423–1431.

98. Idso, S.; Jackson, R.; Pinter Jr, P.; Reginato, R.; Hatfield, J. Normalizing the Stress-Degree-Day Parameter for Environmental Variability. *Agric. Meteorol.* **1981**, *24*, 45–55.
99. Yu, L.; Wang, W.; Zhang, X.; Zheng, W. A Review on Leaf Temperature Sensor: Measurement Methods and Application.; *Springer*. **2016**, pp. 216–230.
100. Kim, B. Assessing Accuracy over Warm-up Time of Lepton 3.5 Thermal Imaging for Measuring Leaf Temperature of Crops. *J. Appl. Hortic.* **2023**, *25*.
101. Kim, B. Feasibility of Lepton 3.5 Using Warm-up Time for Measuring Leaf Temperature of Crops. **2023**.
102. Atherton, J.J.; Rosamond, M.C.; Zeze, D.A. A Leaf-Mounted Thermal Sensor for the Measurement of Water Content. *Sens. Actuators Phys.* **2012**, *187*, 67–72.
103. Adachi, H.; Uchida, K.; Saitoh, E.; Maekawa, S. Theory of the Spin Seebeck Effect. *Rep. Prog. Phys.* **2013**, *76*, 036501.
104. Uchida, K.-I.; Takahashi, S.; Harii, K.; Ieda, J.; Koshibae, W.; Ando, K.; Maekawa, S.; Saitoh, E. Observation of the Spin Seebeck Effect. *nature* **2008**, *455*, 778–781.
105. Pou, A.; Diago, M.P.; Medrano, H.; Baluja, J.; Tardaguila, J. Validation of Thermal Indices for Water Status Identification in Grapevine. *Agric. Water Manag.* **2014**, *134*, 60–72.
106. Costa, J.; Egipto, R.; Sánchez-Virosta, A.; Lopes, C.; Chaves, M. Canopy and Soil Thermal Patterns to Support Water and Heat Stress Management in Vineyards. *Agric. Water Manag.* **2019**, *216*, 484–496.
107. Dhillon, R.S.; Upadhaya, S.K.; Rojo, F.; Roach, J.; Coates, R.W.; Delwiche, M.J. Development of a Continuous Leaf Monitoring System to Predict Plant Water Status. *Trans. ASABE* **2017**, *60*, 1445–1455.
108. Dhillon, R.; Rojo, F.; Upadhyaya, S.K.; Roach, J.; Coates, R.; Delwiche, M. Prediction of Plant Water Status in Almond and Walnut Trees Using a Continuous Leaf Monitoring System. *Precis. Agric.* **2019**, *20*, 723–745, doi:10.1007/s11119-018-9607-0.
109. Li, X.H.; Li, M.Z.; Li, J.Y.; Gao, Y.Y.; Liu, C.R.; Hao, G.F. Wearable sensor supports in-situ and continuous monitoring of plant health in precision agriculture era. *Plant Biotechnol. J.* **2024**, 1-20.
110. Muthumalai, K.; Gokila, N.; Haldorai, Y.; Rajendra Kumar, R.T. Advanced Wearable Sensing Technologies for Sustainable Precision Agriculture–a Review on Chemical Sensors. *Adv. Sensor Res.* **2024**, *3*(3), 2300107.
111. Peng, B.; Liu, X.; Yao, Y.; Ping, J.; Ying, Y. A Wearable and Capacitive Sensor for Leaf Moisture Status Monitoring. *Biosens. Bioelectron.* **2024**, *245*, 115804.
112. Wang, Y.; Anderegg, W.R.; Venturas, M.D.; Trugman, A.T.; Yu, K.; Frankenberg, C. Optimization Theory Explains Nighttime Stomatal Responses. *New Phytol.* **2021**, *230*, 1550–1561.
113. Im, H.; Lee, S.; Naqi, M.; Lee, C.; Kim, S. Flexible PI-Based Plant Drought Stress Sensor for Real-Time Monitoring System in Smart Farm. *Electronics* **2018**, *7*, 114.
114. Fernández, J.; Cuevas, M. Irrigation Scheduling from Stem Diameter Variations: A Review. *Agric. For. Meteorol.* **2010**, *150*, 135–151.
115. Hinckley, T.M.; Bruckerhoff, D.N. The Effects of Drought on Water Relations and Stem Shrinkage of Quercus Alba. *Can. J. Bot.* **1975**, *53*, 62–72.
116. Čermák, J.; Kučera, J.; Bauerle, W.L.; Phillips, N.; Hinckley, T.M. Tree Water Storage and Its Diurnal Dynamics Related to Sap Flow and Changes in Stem Volume in Old-Growth Douglas-Fir Trees. *Tree Physiol.* **2007**, *27*, 181–198.
117. Genard, M.; Fishman, S.; Vercambre, G.; Huguet, J.-G.; Bussi, C.; Besset, J.; Habib, R. A Biophysical Analysis of Stem and Root Diameter Variations in Woody Plants. *Plant Physiol.* **2001**, *126*, 188–202.
118. Herzog, K.M.; Häsler, R.; Thum, R. Diurnal Changes in the Radius of a Subalpine Norway Spruce Stem: Their Relation to the Sap Flow and Their Use to Estimate Transpiration. *Trees* **1995**, *10*, 94–101.
119. Molz, F.J.; Klepper, B. On the Mechanism of Water-Stress-Induced Stem Deformation 1. *Agron. J.* **1973**, *65*, 304–306.
120. Molz, F.J.; Klepper, B.; Browning, V.D. Radial Diffusion of Free Energy in Stem Phloem: An Experimental Study 1. *Agron. J.* **1973**, *65*, 219–222.
121. Cochard, H.; Forestier, S.; Améglio, T. A New Validation of the Scholander Pressure Chamber Technique Based on Stem Diameter Variations. *J. Exp. Bot.* **2001**, *52*, 1361–1365.
122. Parlange, J.-Y.; Turner, N.C.; Waggoner, P.E. Water Uptake, Diameter Change, and Nonlinear Diffusion in Tree Stems. *Plant Physiol.* **1975**, *55*, 247–250.
123. Gallardo, M.; Thompson, R.; Valdez, L.; Fernández, M. Response of Stem Diameter Variations to Water Stress in Greenhouse-Grown Vegetable Crops. *J. Hortic. Sci. Biotechnol.* **2006**, *81*, 483–495.
124. Böhmerle, K. Die Pfister'sche Zuwachsuhr. *Zentralblatt Für Gesamte Forstwes.* **1883**, *9*, 83–93.
125. Kozlowski, T.; Winget, C. Diurnal and Seasonal Variation in Radii of Tree Stems. *Ecology* **1964**, *45*, 149–155.
126. Holmes, J.; Shim, S. Diurnal Changes in Stem Diameter of Canary Island Pine Trees (Pinus Canariensis, C. Smith) Caused by Soil Water Stress and Varying Microclimate. *J. Exp. Bot.* **1968**, *19*, 219–232.

127. Valentini, R.; Belelli Marchesini, L.; Gianelle, D.; Sala, G.; Yarovslavtsev, A.; Vasenev, V.; Castaldi, S. New Tree Monitoring Systems: From Industry 4.0 to Nature 4.0. *Ann. Silvic. Res.* **2019**, *43*, 84–88.

128. Hao, G.-Y.; Wheeler, J.; Holbrook, N.; Goldstein, G.; Carrasco, L.; Bucci, S.; Scholz, F.; Campanello, P.; Madanes, N.; Cristiano, P. Water Storage Discharge and Refilling in the Main Stems of Canopy Tree Species Investigated Using Frequency Domain Reflectometry and Electronic Point Dendrometers. *Acta hortic.* **2013**, 17–24.

129. Drew, D.M.; Downes, G.M. The Use of Precision Dendrometers in Research on Daily Stem Size and Wood Property Variation: A Review. *Dendrochronologia* **2009**, *27*, 159–172.

130. Naor, A.; Cohen, S. Sensitivity and Variability of Maximum Trunk Shrinkage, Midday Stem Water Potential, and Transpiration Rate in Response to Withholding Irrigation from Field-Grown Apple Trees. *HortScience* **2003**, *38*, 547–551.

131. Goldhamer, D.A.; Fereres, E.; Mata, M.; Girona, J.; Cohen, M. Sensitivity of Continuous and Discrete Plant and Soil Water Status Monitoring in Peach Trees Subjected to Deficit Irrigation. *J. Am. Soc. Hortic. Sci.* **1999**, *124*, 437–444.

132. Wheeler, W.D.; Black, B.; Bugbee, B. Assessing water stress in a high-density apple orchard using trunk circumference variation, sap flow index and stem water potential. *Front. Plant Sci.* **2023**, *14*, 1214429.

133. Conejero, W.; Alarcón, J.; García-Orellana, Y.; Nicolás, E.; Torrecillas, A. Evaluation of Sap Flow and Trunk Diameter Sensors for Irrigation Scheduling in Early Maturing Peach Trees. *Tree Physiol.* **2007**, *27*, 1753–1759.

134. Mirás-Avalos, J.M.; Pérez-Sarmiento, F.; Alcobendas, R.; Alarcón, J.J.; Mounzer, O.; Nicolás, E. Maximum Daily Trunk Shrinkage for Estimating Water Needs and Scheduling Regulated Deficit Irrigation in Peach Trees. *Irrig. Sci.* **2017**, *35*, 69–82.

135. De la Rosa, J.M.; Dodd, I.C.; Domingo, R.; Pérez-Pastor, A. Early Morning Fluctuations in Trunk Diameter Are Highly Sensitive to Water Stress in Nectarine Trees. *Irrig. Sci.* **2016**, *34*, 117–128, doi:10.1007/s00271-016-0491-y.

136. Martín-Palomo, M.; Andreu, L.; Pérez-López, D.; Centeno, A.; Galindo, A.; Moriana, A.; Corell, M. Trunk Growth Rate Frequencies as Water Stress Indicator in Almond Trees. *Agric. Water Manag.* **2022**, *271*, 107765, doi:10.1016/j.agwat.2022.107765.

137. Vélez-Sánchez, J.E.; Balaguera-López, H.E.; Rodríguez Hernández, P. The Water Status of Pear (Pyrus Communis L.) under Application of Regulated Deficit Irrigation in High Tropical Latitudinal Conditions. *J. Saudi Soc. Agric. Sci.* **2022**, *21*, 460–468, doi:10.1016/j.jssas.2021.12.003.

138. Blanco, V.; Kalcsits, L. Long-Term Validation of Continuous Measurements of Trunk Water Potential and Trunk Diameter Indicate Different Diurnal Patterns for Pear under Water Limitations. *Agric. Water Manag.* **2023**, *281*, 108257, doi:10.1016/j.agwat.2023.108257.

139. Corell, M.; Martín-Palomo, M.J.; Pérez-López, D.; Centeno, A.; Girón, I.; Moreno, F.; Torrecillas, A.; Moriana, A. Approach for Using Trunk Growth Rate (TGR) in the Irrigation Scheduling of Table Olive Orchards. *Agric. Water Manag.* **2017**, *192*, 12–20, doi:10.1016/j.agwat.2017.06.020.

140. Blanco, V.; Domingo, R.; Pérez-Pastor, A.; Blaya-Ros, P.J.; Torres-Sánchez, R. Soil and Plant Water Indicators for Deficit Irrigation Management of Field-Grown Sweet Cherry Trees. *Agric. Water Manag.* **2018**, *208*, 83–94, doi:10.1016/j.agwat.2018.05.021.

141. Conesa, M.R.; Dodd, I.C.; Temnani, A.; De la Rosa, J.M.; Pérez-Pastor, A. Physiological Response of Post-Veraison Deficit Irrigation Strategies and Growth Patterns of Table Grapes (Cv. Crimson Seedless). *Agric. Water Manag.* **2018**, *208*, 363–372, doi:10.1016/j.agwat.2018.06.019.

142. Pagay, V.; Santiago, M.; Sessoms, D.A.; Huber, E.J.; Vincent, O.; Pharkya, A.; Corso, T.N.; Lakso, A.N.; Stroock, A.D. A Microtensiometer Capable of Measuring Water Potentials Below− 10 MPa. *Lab. Chip* **2014**, *14*, 2806–2817.

143. Black, W.L.; Santiago, M.; Zhu, S.; Stroock, A.D. Ex Situ and in Situ Measurement of Water Activity with a MEMS Tensiometer. *Anal. Chem.* **2019**, *92*, 716–723.

144. Pagay, V. Evaluating a Novel Microtensiometer for Continuous Trunk Water Potential Measurements in Field-Grown Irrigated Grapevines. *Irrig. Sci.* **2022**, *40*, 45–54, doi:10.1007/s00271-021-00758-8.

145. Richards, L. Soil Moisture Tensiometer Materials and Construction. *Soil Sci.* **1942**, *53*, 241–248.

146. Lakso, A.N.; Santiago, M.; Stroock, A.D. Monitoring Stem Water Potential with an Embedded Microtensiometer to Inform Irrigation Scheduling in Fruit Crops. *Horticulturae* **2022**, *8*, 1207.

147. Zucchini, M.; Guzmán-Delgado, P.; Santos, E.; Synstelien, T.; Marino, G. Preliminary Observations on the Use of Microtensiometers to Continuously Measure Water Potential in a Mature Olive Orchard. *IEEE*, **2023**, 268–272.

148. Conesa, M.R.; Conejero, W.; Vera, J.; Ruiz-Sánchez, M.C. Assessment of Trunk Microtensiometer as a Novel Biosensor to Continuously Monitor Plant Water Status in Nectarine Trees. *Front. Plant Sci.* **2023**, *14*, 1123045.

149. Blanco, V.; Kalcsits, L. Microtensiometers Accurately Measure Stem Water Potential in Woody Perennials. *Plants* **2021**, *10*, 2780.

150. Kisekka, I.; Peddinti, S.R.; Savchik, P.; Yang, L.; Culumber, M.; Bali, K.; Millioron, L.; Edwards, E.; Nocco, M.; Reyes, C.; Mahoney, R.; Shackel, K.; Fulton, A. Multisite Evaluation of Microtensiometer and Osmotic Cell Stem Water Potential Sensors in Almond Orchards. *SSSN* 2024, preprint submitted. Available at SSSN: https://ssrn.com/abstract=4713202.

151. Gonzalez Nieto, L.; Huber, A.; Gao, R.; Biasuz, E.C.; Cheng, L.; Stroock, A.D.; Lakso, A.N.; Robinson, T.L. Trunk Water Potential Measured with Microtensiometers for Managing Water Stress in "Gala" Apple Trees. *Plants* **2023**, *12*, 1912.

152. Lakso, A.; Zhu, S.; Santiago, M.; Shackel, K.; Volkov, V.; Stroock, A. A Microtensiometer Sensor to Continuously Monitor Stem Water Potentials in Woody Plants Design and Field Testing. *Acta hortic.* **2019**, 317–324.

153. Marra, F.; Marino, G.; Marchese, A.; Caruso, T. Effects of Different Irrigation Regimes on a Super-High-Density Olive Grove Cv."Arbequina": Vegetative Growth, Productivity and Polyphenol Content of the Oil. *Irrig. Sci.* **2016**, *34*, 313–325.

154. Granier, A.; Bréda, N. Modelling Canopy Conductance and Stand Transpiration of an Oak Forest from Sap Flow Measurements. *EDP Sciences*. **1996**, *53*, 537–546.

155. Smith, D.; Allen, S. Measurement of Sap Flow in Plant Stems. *J. Exp. Bot.* **1996**, *47*, 1833–1844.

156. Poyatos, R.; Granda, V.; Molowny-Horas, R.; Mencuccini, M.; Steppe, K.; Martínez-Vilalta, J. SAPFLUXNET: Towards a Global Database of Sap Flow Measurements. *Tree Physiol.* **2016**, *36*, 1449–1455.

157. Flo, V.; Martinez-Vilalta, J.; Steppe, K.; Schuldt, B.; Poyatos, R. A Synthesis of Bias and Uncertainty in Sap Flow Methods. *Agric. For. Meteorol.* **2019**, *271*, 362–374.

158. Granier, A. Une Nouvelle Méthode Pour La Mesure Du Flux de Sève Brute Dans Le Tronc Des Arbres. *EDP Sciences*. **1985**, 42, 193–200.

159. Do, F.; Rocheteau, A. Influence of Natural Temperature Gradients on Measurements of Xylem Sap Flow with Thermal Dissipation Probes. 1. Field Observations and Possible Remedies. *Tree Physiol.* **2002**, *22*, 641–648.

160. Swanson, R.H.; Whitfield, D. A Numerical Analysis of Heat Pulse Velocity Theory and Practice. *J. Exp. Bot.* **1981**, *32*, 221–239.

161. Burgess, S.S.; Adams, M.A.; Turner, N.C.; Beverly, C.R.; Ong, C.K.; Khan, A.A.; Bleby, T.M. An Improved Heat Pulse Method to Measure Low and Reverse Rates of Sap Flow in Woody Plants. *Tree Physiol.* **2001**, *21*, 589–598.

162. Cohen, Y.; Fuchs, M.; Green, G. Improvement of the Heat Pulse Method for Determining Sap Flow in Trees. *Plant Cell Environ.* **1981**, *4*, 391–397.

163. Testi, L.; Villalobos, F.J. New Approach for Measuring Low Sap Velocities in Trees. *Agric. For. Meteorol.* **2009**, *149*, 730–734.

164. Vandegehuchte, M.W.; Steppe, K. Sapflow+: A Four-needle Heat-pulse Sap Flow Sensor Enabling Nonempirical Sap Flux Density and Water Content Measurements. *New Phytol.* **2012**, *196*, 306–317.

165. López-Bernal, Á.; Testi, L.; Villalobos, F.J. A Single-probe Heat Pulse Method for Estimating Sap Velocity in Trees. *New Phytol.* **2017**, *216*, 321–329.

166. Pearsall, K.R.; Williams, L.E.; Castorani, S.; Bleby, T.M.; McElrone, A.J. Evaluating the Potential of a Novel Dual Heat-Pulse Sensor to Measure Volumetric Water Use in Grapevines under a Range of Flow Conditions. *Funct. Plant Biol.* **2014**, *41*, 874–883.

167. Nadezhdina, N. Revisiting the Heat Field Deformation (HFD) Method for Measuring Sap Flow. *IForest-Biogeosciences For.* **2018**, *11*, 118.

168. Čermák, J.; Kučera, J.; Nadezhdina, N. Sap Flow Measurements with Some Thermodynamic Methods, Flow Integration within Trees and Scaling up from Sample Trees to Entire Forest Stands. *Trees* **2004**, *18*, 529–546.

169. Nhean, S.; Isarangkool Na Ayutthaya, S.; Rocheteau, A.; Do, F.C. Multi-Species Test and Calibration of an Improved Transient Thermal Dissipation System of Sap Flow Measurement with a Single Probe. *Tree Physiol.* **2019**, *39*, 1061–1070.

170. Granier, A. Evaluation of Transpiration in a Douglas-Fir Stand by Means of Sap Flow Measurements. *Tree Physiol.* **1987**, *3*, 309–320.

171. Rana, G.; De Lorenzi, F.; Palatella, L.; Martinelli, N.; Ferrara, R.M. Field Scale Recalibration of the Sap Flow Thermal Dissipation Method in a Mediterranean Vineyard. *Agric. For. Meteorol.* **2019**, *269*, 169–179.

172. Fuchs, S.; Leuschner, C.; Link, R.; Coners, H.; Schuldt, B. Calibration and Comparison of Thermal Dissipation, Heat Ratio and Heat Field Deformation Sap Flow Probes for Diffuse-Porous Trees. *Agric. For. Meteorol.* **2017**, *244*, 151–161.

173. Hernandez-Santana, V.; Fernandes, R.D.; Perez-Arcoiza, A.; Fernández, J.; Garcia, J.; Diaz-Espejo, A. Relationships between Fruit Growth and Oil Accumulation with Simulated Seasonal Dynamics of Leaf Gas Exchange in the Olive Tree. *Agric. For. Meteorol.* **2018**, *256*, 458–469.

174. Ferrara, R.M.; Bruno, M.R.; Campi, P.; Camposeo, S.; De Carolis, G.; Gaeta, L.; Martinelli, N.; Mastrorilli, M.; Modugno, A.F.; Mongelli, T.; Piarulli, M.; Ruggieri, S.; Rana, G. Water use of a super high-density olive orchard submitted to regulated deficit irrigation in Mediterranean environment over three contrasted years. *Irrig. Sci.* **2024**, *42*(1), 57-73.

175. Saitta, D.; Consoli, S.; Ferlito, F.; Torrisi, B.; Allegra, M.; Longo-Minnolo, G.; Ramírez-Cuesta, J.M.; Vanella, D. Adaptation of Citrus Orchards to Deficit Irrigation Strategies. *Agric. Water Manag.* **2021**, *247*, 106734.

176. Abdelfatah, A.; Aranda, X.; Savé, R.; de Herralde, F.; Biel, C. Evaluation of the Response of Maximum Daily Shrinkage in Young Cherry Trees Submitted to Water Stress Cycles in a Greenhouse. *Agric. Water Manag.* **2013**, *118*, 150–158.

177. Rawlins, S. Theory for Thermocouple Psychrometers Used to Measure Water Potential in Soil and Plant Samples. *Agric. Meteorol.* **1966**, *3*, 293–310.

178. Andraski, B.J.; Scanlon, B.R. 3.2. 3 Thermocouple Psychrometry. *Methods Soil Anal. Part 4 Phys. Methods* **2002**, *5*, 609–642.

179. Pérez, E.M.M.; Barrio, J.J.C.; García, T.S.C.; Seijo, X.X.N. Use of Psychrometers in Field Measurements of Plant Material: Accuracy and Handling Difficulties. *Span. J. Agric. Res.* **2011**, 313–328.

180. Dixon, M.; Tyree, M. A New Stem Hygrometer, Corrected for Temperature Gradients and Calibrated against the Pressure Bomb. *Plant Cell Environ.* **1984**, *7*, 693–697.

181. Dainese, R.; Lopes, B. de C.F.L.; Fourcaud, T.; Tarantino, A. Evaluation of Instruments for Monitoring the Soil–Plant Continuum. *Geomech. Energy Environ.* **2022**, *30*, 100256.

182. Dainese, R.; de Carvalho Faria Lima Lopes, B.; Tedeschi, G.; Lamarque, L.J.; Delzon, S.; Fourcaud, T.; Tarantino, A. Cross-Validation on Saplings of High-Capacity Tensiometer and Thermocouple Psychrometer for Continuous Monitoring of Xylem Water Potential. **2021**.

183. Kokkotos, E.; Zotos, A.; Patakas, A. The Ecophysiological Response of Olive Trees under Different Fruit Loads. *Life* **2024**, *14*(1), 128.

184. Rodriguez-Dominguez, C.M.; Brodribb, T.J. Declining Root Water Transport Drives Stomatal Closure in Olive under Moderate Water Stress. *New Phytol.* **2020**, *225*, 126–134.

185. Prats, K.A.; Fanton, A.C.; Brodersen, C.R.; Furze, M.E. Starch Depletion in the Xylem and Phloem Ray Parenchyma of Grapevine Stems under Drought. *AoB Plants* **2023**, *15*, plad062.

186. Quick, D.; Espino, S.; Morua, M.; Schenk, H. Effects of Thermal Gradients in Sapwood on Stem Psychrometry. *Acta hortic*. **2016**; pp. 23–30.

187. Kanakaraja, P.; Sundar, P.S.; Vaishnavi, N.; Reddy, S.G.K.; Manikanta, G.S. IoT Enabled Advanced Forest Fire Detecting and Monitoring on Ubidots Platform. *Mater. Today Proc.* **2021**, *46*, 3907–3914.

188. Niccoli, F.; Pacheco-Solana, A.; Delzon, S.; Kabala, J.P.; Asgharinia, S.; Castaldi, S.; Valentini, R.; Battipaglia, G. Effects of Wildfire on Growth, Transpiration and Hydraulic Properties of Pinus Pinaster Aiton Forest. *Dendrochronologia* **2023**, *79*, 126086.

189. Laurin, G.V.; Cotrina-Sanchez, A.; Belelli-Marchesini, L.; Tomelleri, E.; Battipaglia, G.; Cocozza, C.; Niccoli, F.; Kabala, J.P.; Gianelle, D.; Vescovo, L. Comparing Ground Below-Canopy and Satellite Spectral Data for an Improved and Integrated Forest Phenology Monitoring System. *Ecol. Indic.* **2024**, *158*, 111328.

190. Vasenev, V.I.; Slukovskaya, M.V.; Cheng, Z.; Paltseva, A.A.; Nehls, T.; Korneykova, M.V.; Vasenev, I.I.; Romzaykina, O.N.; Ivashchenko, K.V.; Sarzhanov, D.A. Anthropogenic Soils and Landscapes of European Russia: Summer School from Sea to Sea—A Didactic Prototype. *J. Environ. Qual.* **2021**, *50*, 63–77.

191. Fernandes, R.D.M.; Cuevas, M.V.; Diaz-Espejo, A.; Hernandez-Santana, V. Effects of Water Stress on Fruit Growth and Water Relations between Fruits and Leaves in a Hedgerow Olive Orchard. *Agric. Water Manag.* **2018**, *210*, 32–40.

192. Greenspan, M.D.; Schultz, H.R.; Matthews, M.A. Field Evaluation of Water Transport in Grape Berries during Water Deficits. *Physiol. Plant.* **1996**, *97*, 55–62.

193. Carella, A.; Gianguzzi, G.; Scalisi, A.; Farina, V.; Inglese, P.; Bianco, R.L. Fruit Growth Stage Transitions in Two Mango Cultivars Grown in a Mediterranean Environment. *Plants* **2021**, *10*, 1332.

194. Morandi, B.; Rieger, M.; Grappadelli, L.C. Vascular Flows and Transpiration Affect Peach (Prunus Persica Batsch.) Fruit Daily Growth. *J. Exp. Bot.* **2007**, *58*, 3941–3947.

195. Léchaudel, M.; Lopez-Lauri, F.; Vidal, V.; Sallanon, H.; Joas, J. Response of the Physiological Parameters of Mango Fruit (Transpiration, Water Relations and Antioxidant System) to Its Light and Temperature Environment. *J. Plant Physiol.* **2013**, *170*, 567–576.

196. Tukey, L. A Linear Electric Device for Continuous Measurement and Recording of Fruit Enlargement and Contraction. *J Am Soc Hort Sci* **1964**, *84*, 653–660.

197. Higgs, K.; Jones, H. A Microcomputer-Based System for Continuous Measurement and Recording Fruit Diameter in Relation to Environmental Factors. *J. Exp. Bot.* **1984**, *35*, 1646–1655.

198. Thalheimer, M. A New Optoelectronic Sensor for Monitoring Fruit or Stem Radial Growth. *Comput. Electron. Agric.* **2016**, *123*, 149–153.

199. Morandi, B.; Manfrini, L.; Zibordi, M.; Noferini, M.; Fiori, G.; Grappadelli, L.C. A Low-Cost Device for Accurate and Continuous Measurements of Fruit Diameter. *HortScience* **2007**, *42*, 1380–1382.

200. Link, S.; Thiede, M.; Bavel, M. van An Improved Strain-Gauge Device for Continuous Field Measurement of Stem and Fruit Diameter. *J. Exp. Bot.* **1998**, *49*, 1583–1587.

201. Grilo, F.; Scalisi, A.; Pernice, F.; Morandi, B.; Lo Bianco, R. Recurrent Deficit Irrigation and Fruit Harvest Affect Tree Water Relations and Fruitlet Growth in 'Valencia'Orange. *Eur J Hortic Sci* **2019**, *84*, 177–187.

202. Scalisi, A.; Morandi, B.; Inglese, P.; Bianco, R.L. Cladode Growth Dynamics in Opuntia Ficus-Indica under Drought. *Environ. Exp. Bot.* **2016**, *122*, 158–167.

203. Scalisi, A.; O'Connell, M.; Turpin, S.; Lo Bianco, R. Diurnal Irrigation Timing Affects Fruit Growth in Late-Ripening Nectarines. *Acta hortic.* **2019**, 61–68.

204. Peppi, L.M.; Zauli, M.; Manfrini, L.; Grappadelli, L.C.; De Marchi, L.; Traverso, P.A. Low-Cost, High-Resolution and No-Manning Distributed Sensing System for the Continuous Monitoring of Fruit Growth in Precision Farming. *Acta IMEKO,* **2023**, *12*, 1–11.

205. Giovannini, A.; Venturi, M.; Gutiérrez-Gordillo, S.; Manfrini, L.; Corelli-Grappadelli, L.; Morandi, B. Vascular and Transpiration Flows Affecting Apricot (Prunus Armeniaca L.) Fruit Growth. *Agronomy* **2022**, *12*, 989.

206. Morandi, B.; Manfrini, L.; Losciale, P.; Zibordi, M.; Corelli Grappadelli, L. Changes in Vascular and Transpiration Flows Affect the Seasonal and Daily Growth of Kiwifruit (Actinidia Deliciosa) Berry. *Ann. Bot.* **2010**, *105*, 913–923.

207. Brüggenwirth, M.; Winkler, A.; Knoche, M. Xylem, Phloem, and Transpiration Flows in Developing Sweet Cherry Fruit. *Trees* **2016**, *30*, 1821–1830.

208. Morandi, B.; Losciale, P.; Manfrini, L.; Zibordi, M.; Anconelli, S.; Pierpaoli, E.; Grappadelli, L.C. Leaf Gas Exchanges and Water Relations Affect the Daily Patterns of Fruit Growth and Vascular Flows in Abbé Fétel Pear (*Pyrus Communis* L.) Trees. *Sci. Hortic.* **2014**, *178*, 106–113.

209. Carella, A.; Massenti, R.; Lo Bianco, R. Testing Effects of Vapor Pressure Deficit on Fruit Growth: A Comparative Approach Using Peach, Mango, Olive, Orange, and Loquat. *Front. Plant Sci.* **2023**, *14*, 1294195.

210. Boini, A.; Manfrini, L.; Bortolotti, G.; Corelli-Grappadelli, L.; Morandi, B. Monitoring Fruit Daily Growth Indicates the Onset of Mild Drought Stress in Apple. *Sci. Hortic.* **2019**, *256*, 108520.

211. Khosravi, A.; Mohammadi, Z.; Saber, A.; Pourzangbar, A.; Neri, D. Anomaly Detection in Real-time Continuous Fruit-based Monitoring of Olive via Extensimeter. *SSRN* **2023**, 4652476.

212. Morandi, B.; Manfrini, L.; Losciale, P.; Zibordi, M.; Corelli-Grappadelli, L. The Positive Effect of Skin Transpiration in Peach Fruit Growth. *J. Plant Physiol.* **2010**, *167*, 1033–1037.

213. Alvino, A.; Marino, S. Remote Sensing for Irrigation of Horticultural Crops. *Horticulturae* **2017**, *3*, 40.

214. Semmens, K.A.; Anderson, M.C.; Kustas, W.P.; Gao, F.; Alfieri, J.G.; McKee, L.; Prueger, J.H.; Hain, C.R.; Cammalleri, C.; Yang, Y. Monitoring Daily Evapotranspiration over Two California Vineyards Using Landsat 8 in a Multi-Sensor Data Fusion Approach. *Remote Sens. Environ.* **2016**, *185*, 155–170.

215. Messina, G.; Modica, G. Applications of UAV Thermal Imagery in Precision Agriculture: State of the Art and Future Research Outlook. *Remote Sens.* **2020**, *12*, 1491.

216. Jones, H.G.; Sirault, X.R. Scaling of Thermal Images at Different Spatial Resolution: The Mixed Pixel Problem. *Agronomy* **2014**, *4*, 380–396.

217. Matese, A.; Toscano, P.; Di Gennaro, S.F.; Genesio, L.; Vaccari, F.P.; Primicerio, J.; Belli, C.; Zaldei, A.; Bianconi, R.; Gioli, B. Intercomparison of UAV, Aircraft and Satellite Remote Sensing Platforms for Precision Viticulture. *Remote Sens.* **2015**, *7*, 2971–2990.

218. McCabe, M.F.; Rodell, M.; Alsdorf, D.E.; Miralles, D.G.; Uijlenhoet, R.; Wagner, W.; Lucieer, A.; Houborg, R.; Verhoest, N.E.; Franz, T.E. The Future of Earth Observation in Hydrology. *Hydrol. Earth Syst. Sci.* **2017**, *21*, 3879–3914.

219. Lucieer, A.; Malenovský, Z.; Veness, T.; Wallace, L. HyperUAS—Imaging Spectroscopy from a Multirotor Unmanned Aircraft System. *J. Field Robot.* **2014**, *31*, 571–590.

220. Christiansen, M.P.; Laursen, M.S.; Jørgensen, R.N.; Skovsen, S.; Gislum, R. Designing and Testing a UAV Mapping System for Agricultural Field Surveying. *Sensors* **2017**, *17*, 2703.

221. Huang, S.; Tang, L.; Hupy, J.P.; Wang, Y.; Shao, G. A Commentary Review on the Use of Normalized Difference Vegetation Index (NDVI) in the Era of Popular Remote Sensing. *J. For. Res.* **2021**, *32*, 1–6.

222. Shao, G. Optical Remote Sensing. *Int. Encycl. Geogr. People Earth Environ. Technol.* **2016**, 1–12.

223. Carrasco-Benavides, M.; Antunez-Quilobrán, J.; Baffico-Hernández, A.; Ávila-Sánchez, C.; Ortega-Farías, S.; Espinoza, S.; Gajardo, J.; Mora, M.; Fuentes, S. Performance Assessment of Thermal Infrared Cameras of Different Resolutions to Estimate Tree Water Status from Two Cherry Cultivars: An Alternative to Midday Stem Water Potential and Stomatal Conductance. *Sensors* **2020**, *20*, 3596.

224. Fuentes, S.; De Bei, R.; Pech, J.; Tyerman, S. Computational Water Stress Indices Obtained from Thermal Image Analysis of Grapevine Canopies. *Irrig. Sci.* **2012**, *30*, 523–536.

225. Jones, H.G.; Stoll, M.; Santos, T.; Sousa, C. de; Chaves, M.M.; Grant, O.M. Use of Infrared Thermography for Monitoring Stomatal Closure in the Field: Application to Grapevine. *J. Exp. Bot.* **2002**, *53*, 2249–2260.

226. Gonzalez-Dugo, V.; Zarco-Tejada, P.; Nicolás, E.; Nortes, P.A.; Alarcón, J.; Intrigliolo, D.S.; Fereres, E. Using High Resolution UAV Thermal Imagery to Assess the Variability in the Water Status of Five Fruit Tree Species within a Commercial Orchard. *Precis. Agric.* **2013**, *14*, 660–678.

227. Blanco, V.; Willsea, N.; Campbell, T.; Howe, O.; Kalcsits, L. Combining Thermal Imaging and Soil Water Content Sensors to Assess Tree Water Status in Pear Trees. *Front. Plant Sci.* **2023**, *14*, 1197437.

228. Gonzalez-Dugo, V.; Zarco-Tejada, P.J.; Fereres, E. Applicability and Limitations of Using the Crop Water Stress Index as an Indicator of Water Deficits in Citrus Orchards. *Agric. For. Meteorol.* **2014**, *198*, 94–104.

229. Jones, H.G. Use of Infrared Thermometry for Estimation of Stomatal Conductance as a Possible Aid to Irrigation Scheduling. *Agric. For. Meteorol.* **1999**, *95*, 139–149.

230. Jackson, R.D.; Kustas, W.P.; Choudhury, B.J. A Reexamination of the Crop Water Stress Index. *Irrig. Sci.* **1988**, *9*, 309–317.

231. Agam, N.; Cohen, Y.; Berni, J.; Alchanatis, V.; Kool, D.; Dag, A.; Yermiyahu, U.; Ben-Gal, A. An Insight to the Performance of Crop Water Stress Index for Olive Trees. *Agric. Water Manag.* **2013**, *118*, 79–86.

232. Meron, M.; Tsipris, J.; Charitt, D. Remote Mapping of Crop Water Status to Assess Spatial Variability of Crop Stress. In *Precision agriculture. Proceedings of the fourth European conference on precision agriculture.* Academic Publishers, Berlin, Germany; **2003**; pp. 405–410.

233. Möller, M.; Alchanatis, V.; Cohen, Y.; Meron, M.; Tsipris, J.; Naor, A.; Ostrovsky, V.; Sprintsin, M.; Cohen, S. Use of Thermal and Visible Imagery for Estimating Crop Water Status of Irrigated Grapevine. *J. Exp. Bot.* **2007**, *58*, 827–838.

234. Irmak, S.; Haman, D.Z.; Bastug, R. Determination of Crop Water Stress Index for Irrigation Timing and Yield Estimation of Corn. *Agron. J.* **2000**, *92*, 1221–1227.

235. Gerhards, M.; Schlerf, M.; Mallick, K.; Udelhoven, T. Challenges and Future Perspectives of Multi-/Hyperspectral Thermal Infrared Remote Sensing for Crop Water-Stress Detection: A Review. *Remote Sens.* **2019**, *11*, 1240.

236. Apolo-Apolo, O.; Martínez-Guanter, J.; Pérez-Ruiz, M.; Egea, G. Design and Assessment of New Artificial Reference Surfaces for Real Time Monitoring of Crop Water Stress Index in Maize. *Agric. Water Manag.* **2020**, *240*, 106304.

237. Park, S.; Ryu, D.; Fuentes, S.; Chung, H.; O'connell, M.; Kim, J. Dependence of CWSI-Based Plant Water Stress Estimation with Diurnal Acquisition Times in a Nectarine Orchard. *Remote Sens.* **2021**, *13*, 2775.

238. Araújo-Paredes, C.; Portela, F.; Mendes, S.; Valín, M.I. Using Aerial Thermal Imagery to Evaluate Water Status in Vitis Vinifera Cv. Loureiro. *Sensors* **2022**, *22*, 8056.

239. Bian, J.; Zhang, Z.; Chen, J.; Chen, H.; Cui, C.; Li, X.; Chen, S.; Fu, Q. Simplified Evaluation of Cotton Water Stress Using High Resolution Unmanned Aerial Vehicle Thermal Imagery. *Remote Sens.* **2019**, *11*, 267.

240. Cohen, Y.; Alchanatis, V.; Saranga, Y.; Rosenberg, O.; Sela, E.; Bosak, A. Mapping Water Status Based on Aerial Thermal Imagery: Comparison of Methodologies for Upscaling from a Single Leaf to Commercial Fields. *Precis. Agric.* **2017**, *18*, 801–822.

241. Caruso, G.; Palai, G.; Tozzini, L.; Gucci, R. Using Visible and Thermal Images by an Unmanned Aerial Vehicle to Monitor the Plant Water Status, Canopy Growth and Yield of Olive Trees (Cvs. Frantoio and Leccino) under Different Irrigation Regimes. *Agronomy* **2022**, *12*, 1904.

242. Zhou, H.; Zhou, G.; He, Q.; Zhou, L.; Ji, Y.; Lv, X. Capability of Leaf Water Content and Its Threshold Values in Reflection of Soil–Plant Water Status in Maize during Prolonged Drought. *Ecol. Indic.* **2021**, *124*, 107395, doi:10.1016/j.ecolind.2021.107395.

243. Käthner, J.; Ben-Gal, A.; Gebbers, R.; Peeters, A.; Herppich, W.B.; Zude-Sasse, M. Evaluating Spatially Resolved Influence of Soil and Tree Water Status on Quality of European Plum Grown in Semi-Humid Climate. *Front. Plant Sci.* **2017**, *8*, 1053.

244. Zhou, Z.; Majeed, Y.; Naranjo, G.D.; Gambacorta, E.M. Assessment for crop water stress with infrared thermal imagery in precision agriculture: A review and future prospects for deep learning applications. *Comput. Electron. Agric.* **2021**, *182*, 106019.

245. Bellvert, J.; Marsal, J.; Girona, J.; Gonzalez-Dugo, V.; Fereres, E.; Ustin, S.L.; Zarco-Tejada, P.J. Airborne Thermal Imagery to Detect the Seasonal Evolution of Crop Water Status in Peach, Nectarine and Saturn Peach Orchards. *Remote Sens.* **2016**, *8*, 39.

246. Bai, G.; Ge, Y.; Hussain, W.; Baenziger, P.S.; Graef, G. A multi-sensor system for high throughput field phenotyping in soybean and wheat breeding. *Comput. Electron. Agric.* **2016**, *128*, 181-192.

247. Katz, L.; Ben-Gal, A.; Litaor, M.I.; Naor, A.; Peeters, A.; Goldshtein, E.; Lidor, G.; Keisar, O.; Marzuk, S.; Alchanatis, V. How Sensitive Is Thermal Image-Based Orchard Water Status Estimation to Canopy Extraction Quality? *Remote Sens.* **2023**, *15*, 1448.

248. Sánchez-Piñero, M.; Martín-Palomo, M.; Andreu, L.; Moriana, A.; Corell, M. Evaluation of a Simplified Methodology to Estimate the CWSI in Olive Orchards. *Agric. Water Manag.* **2022**, *269*, 107729.

249. Berni, J.; Zarco-Tejada, P.; Sepulcre-Cantó, G.; Fereres, E.; Villalobos, F. Mapping Canopy Conductance and CWSI in Olive Orchards Using High Resolution Thermal Remote Sensing Imagery. *Remote Sens. Environ.* **2009**, *113*, 2380–2388.

250. Ben-Gal, A.; Agam, N.; Alchanatis, V.; Cohen, Y.; Yermiyahu, U.; Zipori, I.; Presnov, E.; Sprintsin, M.; Dag, A. Evaluating Water Stress in Irrigated Olives: Correlation of Soil Water Status, Tree Water Status, and Thermal Imagery. *Irrig. Sci.* **2009**, *27*, 367–376.

251. Gutiérrez-Gordillo, S.; de la Gala González-Santiago, J.; Trigo-Córdoba, E.; Rubio-Casal, A.E.; García-Tejero, I.F.; Egea, G. Monitoring of Emerging Water Stress Situations by Thermal and Vegetation Indices in Different Almond Cultivars. *Agronomy* **2021**, *11*, 1419.

252. Ramírez-Cuesta, J.M.; Ortuño, M.; Gonzalez-Dugo, V.; Zarco-Tejada, P.J.; Parra, M.; Rubio-Asensio, J.S.; Intrigliolo, D.S. Assessment of Peach Trees Water Status and Leaf Gas Exchange Using On-the-Ground versus Airborne-Based Thermal Imagery. *Agric. Water Manag.* **2022**, *267*, 107628.

253. Mohamed, A.Z.; Osroosh, Y.; Peters, R.T.; Bates, T.; Campbell, C.S.; Ferrer-Alegre, F. Monitoring Water Status in Apple Trees Using a Sensitive Morning Crop Water Stress Index. *Irrig. Drain.* **2021**, *70*, 27–41.

254. Jamshidi, S.; Zand-Parsa, S.; Niyogi, D. Assessing Crop Water Stress Index of Citrus Using In-Situ Measurements, Landsat, and Sentinel-2 Data. *Int. J. Remote Sens.* **2021**, *42*, 1893–1916.

255. Gonzalez-Dugo, V.; Zarco-Tejada, P.; Nicolás, E.; Nortes, P.A.; Alarcón, J.; Intrigliolo, D.S.; Fereres, E. Using High Resolution UAV Thermal Imagery to Assess the Variability in the Water Status of Five Fruit Tree Species within a Commercial Orchard. *Precis. Agric.* **2013**, *14*, 660–678.

256. Mortazavi, M.; Ehsani, R.; Carpin, S.; Toudeshki, A. Predicting Tree Water Status in Pistachio and Almond Orchards Using Supervised Machine Learning. *SSRN* 2023, preprint submitted, available at SSRN: https://ssrn.com/abstract=4511076.

257. Li, Z.; Wu, H.; Duan, S.; Zhao, W.; Ren, H.; Liu, X.; Leng, P.; Tang, R.; Ye, X.; Zhu, J. Satellite Remote Sensing of Global Land Surface Temperature: Definition, Methods, Products, and Applications. *Rev. Geophys.* **2023**, *61*, e2022RG000777.

258. Nicolai, B.M.; Beullens, K.; Bobelyn, E.; Peirs, A.; Saeys, W.; Theron, K.I.; Lammertyn, J. Nondestructive Measurement of Fruit and Vegetable Quality by Means of NIR Spectroscopy: A Review. *Postharvest Biol. Technol.* **2007**, *46*, 99–118.

259. Polesello, A.; Giangiacomo, R.; Dull, G.G. Application of near Infrared Spectrophotometry to the Nondestructive Analysis of Foods: A Review of Experimental Results. *Crit. Rev. Food Sci. Nutr.* **1983**, *18*, 203–230.

260. Jorge, J.; Vallbé, M.; Soler, J.A. Detection of Irrigation Inhomogeneities in an Olive Grove Using the NDRE Vegetation Index Obtained from UAV Images. *Eur. J. Remote Sens.* **2019**, *52*, 169–177.

261. Zúñiga Espinoza, C.; Khot, L.R.; Sankaran, S.; Jacoby, P.W. High Resolution Multispectral and Thermal Remote Sensing-Based Water Stress Assessment in Subsurface Irrigated Grapevines. *Remote Sens.* **2017**, *9*, 961.

262. Pettorelli, N.; Vik, J.O.; Mysterud, A.; Gaillard, J.-M.; Tucker, C.J.; Stenseth, N.C. Using the Satellite-Derived NDVI to Assess Ecological Responses to Environmental Change. *Trends Ecol. Evol.* **2005**, *20*, 503–510.

263. Jones, H.G.; Vaughan, R.A. *Remote Sensing of Vegetation: Principles, Techniques, and Applications*; Oxford University Press: Oxford, UK, **2010**; 223, pp. 229-242.

264. Ballester, C.; Zarco-Tejada, P.J.; Nicolás, E.; Alarcón, J.J.; Fereres, E.; Intrigliolo, D.S.; Gonzalez-Dugo, V. Evaluating the Performance of Xanthophyll, Chlorophyll and Structure-Sensitive Spectral Indices to Detect Water Stress in Five Fruit Tree Species. *Precis. Agric.* **2018**, *19*, 178–193.

265. Caruso, G.; Palai, G.; Gucci, R.; Priori, S. Remote and Proximal Sensing Techniques for Site-Specific Irrigation Management in the Olive Orchard. *Appl. Sci.* **2022**, *12*, 1309.

266. Poblete, T.; Ortega-Farías, S.; Moreno, M.A.; Bardeen, M. Artificial Neural Network to Predict Vine Water Status Spatial Variability Using Multispectral Information Obtained from an Unmanned Aerial Vehicle (UAV). *Sensors* **2017**, *17*, 2488.

267. Baluja, J.; Diago, M.P.; Balda, P.; Zorer, R.; Meggio, F.; Morales, F.; Tardaguila, J. Assessment of Vineyard Water Status Variability by Thermal and Multispectral Imagery Using an Unmanned Aerial Vehicle (UAV). *Irrig. Sci.* **2012**, *30*, 511–522.

268. Romero, M.; Luo, Y.; Su, B.; Fuentes, S. Vineyard Water Status Estimation Using Multispectral Imagery from an UAV Platform and Machine Learning Algorithms for Irrigation Scheduling Management. *Comput. Electron. Agric.* **2018**, *147*, 109–117.

269. Zarco-Tejada, P.J.; González-Dugo, V.; Williams, L.; Suarez, L.; Berni, J.A.; Goldhamer, D.; Fereres, E. A PRI-Based Water Stress Index Combining Structural and Chlorophyll Effects: Assessment Using Diurnal Narrow-Band Airborne Imagery and the CWSI Thermal Index. *Remote Sens. Environ.* **2013**, *138*, 38–50.

270. Rallo, G.; Minacapilli, M.; Ciraolo, G.; Provenzano, G. Detecting Crop Water Status in Mature Olive Groves Using Vegetation Spectral Measurements. *Biosyst. Eng.* **2014**, *128*, 52–68.

271. Mwinuka, P.R.; Mourice, S.K.; Mbungu, W.B.; Mbilinyi, B.P.; Tumbo, S.D.; Schmitter, P. UAV-based multispectral vegetation indices for assessing the interactive effects of water and nitrogen in irrigated horticultural crops production under tropical sub-humid conditions: A case of African eggplant. *Agric. Water Manage.* **2022**, *266*, 107516.

272. Tang, Z.; Jin, Y.; Alsina, M.M.; McElrone, A.J.; Bambach, N.; Kustas, W.P. Vine water status mapping with multispectral UAV imagery and machine learning. *Irrig. Sci.* **2022**, *40*(4), 715-730.

273. Zhang, L.; Han, W.; Niu, Y.; Chavez, J.L.; Shao, G.; Zhang, H. Evaluating the sensitivity of water stressed maize chlorophyll and structure based on UAV derived vegetation indices. *Comput. Electron. Agric.* **2021**, *185*, 106174.

274. Stagakis, S.; González-Dugo, V.; Cid, P.; Guillén-Climent, M.L.; Zarco-Tejada, P.J. Monitoring Water Stress and Fruit Quality in an Orange Orchard under Regulated Deficit Irrigation Using Narrow-Band Structural and Physiological Remote Sensing Indices. *ISPRS J. Photogramm. Remote Sens.* **2012**, *71*, 47–61.

275. Fasiolo, D.T.; Pichierri, A.; Sivilotti, P.; Scalera, L. An analysis of the effects of water regime on grapevine canopy status using a UAV and a mobile robot. *Smart Agric. Technol.* **2023**, *6*, 100344.

276. Longo-Minnolo, G.; Consoli, S.; Vanella, D.; Guarrera, S.; Manetto, G.; Cerruto, E. Appraising the stem water potential of citrus orchards from UAV-based multispectral imagery. In *2023 IEEE International Workshop on Metrology for Agriculture and Forestry (MetroAgriFor)*; Pisa, Italy, 06-08 November 2023; IEEE: Piscataway, NJ, US 2023; pp. 120-125.

277. Cohen, Y.; Gogumalla, P.; Bahat, I.; Netzer, Y.; Ben-Gal, A.; Lenski, I.; Michael, Y.; Helman, D. Can Time Series of Multispectral Satellite Images Be Used to Estimate Stem Water Potential in Vineyards? *Precision agriculture'19*, Wageningen Academic Publishers: Wageningen, Holland. **2019;** pp. 1–5.

278. Lin, Y.; Zhu, Z.; Guo, W.; Sun, Y.; Yang, X.; Kovalskyy, V. Continuous Monitoring of Cotton Stem Water Potential Using Sentinel-2 Imagery. *Remote Sens.* **2020**, *12*, 1176.

279. Boren, E.J.; Boschetti, L. Landsat-8 and Sentinel-2 Canopy Water Content Estimation in Croplands through Radiative Transfer Model Inversion. *Remote Sens.* **2020**, *12*, 2803.

280. Jiménez-Bello, M.A.; Martínez Alzamora, F.; Carles Campos Alonso, J.; Amparo Martínez Gimeno, M.; Intrigliolo, D.S. Dynamic Citrus Orchards Irrigation Performance Assessment by a Surface Energy Balance Method Using Landsat Imagery. *EGU General Assembly Conference Abstracts.* **2018**, 14557.

281. Van Beek, J.; Tits, L.; Somers, B.; Coppin, P. Stem Water Potential Monitoring in Pear Orchards through WorldView-2 Multispectral Imagery. *Remote Sens.* **2013**, *5*, 6647–6666, doi:10.3390/rs5126647.

282. Zhang, C.; Marzougui, A.; Sankaran, S. High-Resolution Satellite Imagery Applications in Crop Phenotyping: An Overview. *Comput. Electron. Agric.* **2020**, *175*, 105584.

283. Schut, A.; Stephens, D.; Stovold, R.; Adams, M.; Craig, R. Improved Wheat Yield and Production Forecasting with a Moisture Stress Index, AVHRR and MODIS Data. *Crop Pasture Sci.* **2009**, *60*, 60–70.

284. Satellite Imagery Analytics Available online: https://www.planet.com/products/planet-imagery/.

285. Helman, D.; Bahat, I.; Netzer, Y.; Ben-Gal, A.; Alchanatis, V.; Peeters, A.; Cohen, Y. Using Time Series of High-Resolution Planet Satellite Images to Monitor Grapevine Stem Water Potential in Commercial Vineyards. *Remote Sens.* **2018**, *10*, 1615.

286. Garofalo, S.P.; Giannico, V.; Costanza, L.; Alhajj Ali, S.; Camposeo, S.; Lopriore, G.; Pedrero Salcedo, F.; Vivaldi, G.A. Prediction of Stem Water Potential in Olive Orchards Using High-Resolution Planet Satellite Images and Machine Learning Techniques. *Agronomy* **2024**, *14*, 1, doi:10.3390/agronomy14010001.

287. Gao, B.-C. NDWI—A Normalized Difference Water Index for Remote Sensing of Vegetation Liquid Water from Space. *Remote Sens. Environ.* **1996**, *58*, 257–266.

288. Rodríguez-Fernández, M.; Fandiño, M.; González, X.P.; Cancela, J.J. Estimation Water Status of the Vineyard by Calculating Multispectral Index from Satellite Images. *EGU General Assembly Conference Abstracts*. **2021**, 21-2187.

289. Zhao, T.; Nakano, A.; Iwaski, Y.; Umeda, H. Application of Hyperspectral Imaging for Assessment of Tomato Leaf Water Status in Plant Factories. *Appl. Sci.* **2020**, *10*, 4665.

290. Pu, R. *Hyperspectral Remote Sensing: Fundamentals and Practices*. CRC Press: Boca Raton, FL, US., **2017**; 1,4-5.

291. Sahoo, R.N.; Ray, S.; Manjunath, K. Hyperspectral Remote Sensing of Agriculture. *Curr. Sci.* **2015**, 848–859.

292. Lu, B.; Dao, P.D.; Liu, J.; He, Y.; Shang, J. Recent Advances of Hyperspectral Imaging Technology and Applications in Agriculture. *Remote Sens.* **2020**, *12*, 2659.

293. Natesan, S.; Armenakis, C.; Benari, G.; Lee, R. Use of UAV-Borne Spectrometer for Land Cover Classification. *Drones* **2018**, *2*, 16.

294. Gallo, I.; Boschetti, M.; Rehman, A.U.; Candiani, G. Self-Supervised Convolutional Neural Network Learning in a Hybrid Approach Framework to Estimate Chlorophyll and Nitrogen Content of Maize from Hyperspectral Images. *Remote Sensing* **2023**, *15*(19), 4765.

295. Rodríguez-Pérez, J.R.; Riaño, D.; Carlisle, E.; Ustin, S.; Smart, D.R. Evaluation of Hyperspectral Reflectance Indexes to Detect Grapevine Water Status in Vineyards. *Am. J. Enol. Vitic.* **2007**, *58*, 302–317.

296. Jones, C.L.; Weckler, P.R.; Maness, N.O.; Stone, M.L.; Jayasekara, R. Estimating Water Stress in Plants Using Hyperspectral Sensing. *American Society of Agricultural and Biological Engineers*. **2004**, 1.

297. Da Luz, B.R.; Crowley, J.K. Spectral Reflectance and Emissivity Features of Broad Leaf Plants: Prospects for Remote Sensing in the Thermal Infrared (8.0–14.0 Mm). *Remote Sens. Environ.* **2007**, *109*, 393–405.

1804 298. Zarco-Tejada, P.J.; González-Dugo, V.; Berni, J.A. Fluorescence, Temperature and Narrow-Band Indices Acquired from
1805 a UAV Platform for Water Stress Detection Using a Micro-Hyperspectral Imager and a Thermal Camera. *Remote Sens. Environ.* **2012**,
1806 *117*, 322–337.
1807 299. Loggenberg, K.; Strever, A.; Greyling, B.; Poona, N. Modelling Water Stress in a Shiraz Vineyard Using Hyperspectral
1808 Imaging and Machine Learning. *Remote Sens.* **2018**, *10*, 202.
1809 300. Matese, A.; Di Gennaro, S.F.; Orlandi, G.; Gatti, M.; Poni, S. Assessing Grapevine Biophysical Parameters From Un-
1810 manned Aerial Vehicles Hyperspectral Imagery. *Front. Plant Sci.* **2022**, *13*, 898722.
1811 301. Vasquez, K.; Laroche-Pinel, E.; Partida, G.; Brillante, L. Grapevine water status in a variably irrigated vineyard with NIR
1812 hyperspectral imaging from a UAV. In *Precision agriculture'23*, 1ed.; Wageningen Academic Publishers: Wageningen, Holland, 2023;
1813 pp. 345-350.
1814 302. Gomez-Candon, D.; Labbé, S.; Virlet, N.; Jolivot, A.; Regnard, J.-L. High Resolution Thermal and Multispectral UAV
1815 Imagery for Precision Assessment of Apple Tree Response to Water Stress. *PGM*, **2014,** np.
1816 303. Blanco, V.; Blaya-Ros, P.J.; Castillo, C.; Soto-Vallés, F.; Torres-Sánchez, R.; Domingo, R. Potential of UAS-Based Remote
1817 Sensing for Estimating Tree Water Status and Yield in Sweet Cherry Trees. *Remote Sens.* **2020**, *12*, 2359.
1818 304. Zhao, T.; Doll, D.; Wang, D.; Chen, Y. A New Framework for UAV-Based Remote Sensing Data Processing and Its Ap-
1819 plication in Almond Water Stress Quantification. *IEEE*, **2017**, 1794–1799.
1820 305. Saxton, K.; Rawls, W.; Romberger, J.S.; Papendick, R. Estimating Generalized Soil-water Characteristics from Texture.
1821 *Soil Sci. Soc. Am. J.* **1986**, *50*, 1031–1036.
1822 306. Manrique, L.; Jones, C.; Dyke, P. Predicting Soil Water Retention Characteristics from Soil Physical and Chemical Prop-
1823 erties. *Commun. Soil Sci. Plant Anal.* **1991**, *22*, 1847–1860.
1824 307. Scott, R.L.; Huxman, T.E.; Barron-Gafford, G.A.; Darrel Jenerette, G.; Young, J.M.; Hamerlynck, E.P. When Vegetation
1825 Change Alters Ecosystem Water Availability. *Glob. Change Biol.* **2014**, *20*, 2198–2210.
1826 308. Krstić, Đ.; Vujić, S.; Jaćimović, G.; D'Ottavio, P.; Radanović, Z.; Erić, P.; Ćupina, B. The Effect of Cover Crops on Soil
1827 Water Balance in Rain-Fed Conditions. *Atmosphere* **2018**, *9*, 492.
1828 309. Von Arx, G.; Graf Pannatier, E.; Thimonier, A.; Rebetez, M. Microclimate in Forests with Varying Leaf Area Index and
1829 Soil Moisture: Potential Implications for Seedling Establishment in a Changing Climate. *J. Ecol.* **2013**, *101*, 1201–1213.
1830 310. Matese, A.; Baraldi, R.; Berton, A.; Cesaraccio, C.; Di Gennaro, S.F.; Duce, P.; Facini, O.; Mameli, M.G.; Piga, A.; Zaldei,
1831 A. Estimation of Water Stress in Grapevines Using Proximal and Remote Sensing Methods. *Remote Sens.* **2018**, *10*, 114.
1832 311. Gonzalez-Dugo, V.; Testi, L.; Villalobos, F.J.; López-Bernal, A.; Orgaz, F.; Zarco-Tejada, P.J.; Fereres, E. Empirical Vali-
1833 dation of the Relationship between the Crop Water Stress Index and Relative Transpiration in Almond Trees. *Agric. For. Meteorol.*
1834 **2020**, *292*, 108128.
1835 312. Pasqualotto, G.; Carraro, V.; Suarez Huerta, E.; Bono Rosselló, N.; Gilcher, M.; Retzlaff, R.; Garone, E.; Cristofori, V.;
1836 Anfodillo, T. Tree-Based Sap Flow Monitoring to Validate the Crop Water Stress Index in Hazelnut. *Acta hortic*. **2022**, 277–282.
1837
1838
1839

CHAPTER 2.

Use of thermography and leaf relative water content to estimate water status in young olive trees

Based on the paper:
Carella, A., Massenti, R., Imperiale, V., Lo Bianco, R. Use of thermography ald leaf relative water content to estimate water status in young olive trees. **Submitted** in *Acta Horticolturae.*
Presented at the "X International Symposium on Irrigation of Horticultural Crops", Stellenbosch, South Africa.

Use of thermography and leaf relative water content to estimate water status in young olive trees

A. Carella[1a], R. Massenti[1], V. Imperiale[1], R. Lo Bianco[1]

[1]Department of Agricultural, Food and Forest Sciences, University of Palermo, Palermo, Italy

Abstract

The measurement of plant water potential by pressure chamber is currently the most widely used and reliable method to estimate plant water status. However, this practice is destructive and requires a big amount of time to get a representative measure of orchard water status. For this reason, finding new systems to estimate plant water status is critical for precision irrigation protocols. The aim of this study was to test leaf Relative Water Content (RWC, %) and thermography techniques as potential indicators of plant water status to provide accurate alternative methods to estimate water status in olive. To achieve this purpose, leaf water potential (Ψ_{leaf}), RWC and thermal images were obtained from plants grown in growth chambers under different hydration conditions: from full hydration to very severe stress. Ψ_{leaf}, RWC, and Crop Water Stress Index (CWSI) were correlated to develop a model. Ψ_{leaf} was measured with a pressure chamber; RWC was determined in the laboratory from leaf fresh, turgid and dry weights; single-leaf thermal images were acquired using a hand-held thermal camera. A strong direct relationship was found between Ψ_{leaf} and RWC (R^2 = 0.71). An inverse relationship between Ψ_{leaf} and CWSI was also found (R^2 = 0.61), for Ψ_{leaf} values below -1 MPa. On the other hand, a weaker relationship between RWC and CWSI was detected (R^2 = 0.33). Olive plant water status could be estimated more reliably with a multiple linear regression model combining RWC and CWSI data (R^2 = 0.76). Further on-field studies will be needed to confirm these results and chiefly the importance of using RWC in the model to assess olive tree water status.

Keywords: plant water status, *Olea europaea* L., relative water content, crop water stress index, stem water potential.

INTRODUCTION

Water availability is one of the limiting factors in modern agriculture, mainly due to drought as a result of climate change. Climate change-induced temperature increases will affect water availability due to increased evapotranspiration and consequent changes in rainfall and river flows (Hristov et al., 2021). For this reason, understanding plant responses to water availability is more and more urgent given losses in crop productivity and tree mortality in several ecosystems around the world (Allen et al., 2010; Browne et al., 2020).

The techniques for estimating plant water status are numerous. Available measures of soil or plant water status can be broadly divided into those based on water content or energy status, in terms of water potential (Ψ_w) (H. G. Jones, 2007). The most common water potential indicators are the pre-dawn water potential (Ψ_{pd}), that is the water potential measured in the plant just before dawn, and the leaf (Ψ_{leaf}) and stem (Ψ_{stem}) water potential measured at solar noon (J. Fernández et al., 1997) .The pressure chamber is the most common method of

[a] E-mail: alessandro.carella@unipa.it

measuring plant water potential, used as an accurate indicator of olive water status (Martín-Vertedor et al., 2011; Poblete-Echeverría et al., 2014). However, measuring water potential with the pressure chamber is an invasive and labor-intensive process in which an experienced operator must continuously pressurize and de-pressurize the chamber in which the leaf sample is placed and must carefully determine the pressure at which water exudes from the leaf petiole (Poblete-Echeverría et al., 2014; Zimmermann et al., 2008). To carry out the measurement, usually the single leaf is used, while for plants that have small leaves (e.g. olive) the final portion of the shoots is commonly used. In many cases, physiological mechanisms, such as the ability to adjust osmotically and the vulnerability to embolism of the plant, also affect the sensitivity of Ψ_w as an indicator of water status (Dichio et al., 2006; Ingram and Bartels, 1996; Fernández, 2017; Massenti et al., 2022; Xiloyannis et al., 1997).

One type of measurement that may prove reliable, based on water content, is the Relative Water Content (RWC) method (Barrs and Weatherley, 1962). In contrast to water potential, RWC assesses leaf water deficit and accounts for possible solute accumulation and osmotic adjustment in response to drought (H. G. Jones, 2007; Lo Bianco and Scalisi, 2017; Scalisi et al., 2017). RWC is generally measured with a precision balance using a gravimetric weighing process, where RWC is given as the ratio of the water content of the newly collected leaf over the leaf water content at full turgor (Li et al., 2020; Smart and Bingham, 1974). In other words, RWC is a useful indicator of the state of water balance of a plant essentially because it expresses the percentage missing to saturation., which the plant requires to reach artificial full saturation (González and González-Vilar, 2001). Thus, this kind of measure needs the fresh sample, the full hydration and the drying of the leaf sample. Although RWC may prove to be a reliable technique for determining plant water status, similarly to the determination of water potential using the pressure chamber, it is destructive and time-consuming to obtain and weigh fully saturated and dry samples. An alternative way to estimate leaf water status using leaf weight is the determination of leaf Gravimetric Water Content, that can be assessed in function of dry weight or fresh weight (Datt, 1999). GWC is given as the ratio of the leaf fresh weight minus dry weight of the same leaf, over leaf dry (GWC_d) or fresh weight (GWC_f). In some cases, this may be a more reliable water stress indicator than RWC, because several errors in RWC determination are possible, mainly during sample hydration, i.e. infiltration of water into intercellular spaces during hydration, or inadequate time of hydration (Hd. Barrs, 1968; Diaz-Pérez et al., 1995).

Plant temperature has long been recognized as an indicator of water availability (Jackson et al., 1981). Over the past three decades, thermal infrared (TIR) cameras have been used as effective tools to estimate leaf and canopy temperature (T_c), which has been recognized as a reliable, rapid, and non-destructive indicator of transpiration and plant water status (Carrasco-Benavides et al., 2020; Fuentes et al., 2012; H. G. Jones and Leinonen, 2003). Moreover, thermal cameras can be drone-mounted or hand-held. Temperature is closely related to plant water status, as the physical principle behind canopy temperature variation depends on transpiration (water loss as vapor). In fact, stomatal closure that occurs due to water deficit causes a decrease in leaf transpiration, which consequently causes an increase in leaf temperature. Unfortunately, considering only Tc may lead to many limitations due to the high influence of environmental parameters, such as windspeed, radiation, air humidity, and air temperature (Leinonen and Jones, 2004). For this reason, it is necessary to determine vegetation indices to obtain thermal data that can be easily correlated with plant physiological data. The most widely used vegetation index is Crop Water Stress Index (CWSI), first developed in the early 1980s by Idso and Jackson. It is defined as follows (Jones, 1999):

$$CWSI = \frac{Tc - Twet}{Tdry - Twet} \quad (1)$$

where T_c is the actual canopy temperature obtained by thermal photo, and T_{dry} and T_{wet} are the references representing the non-transpiring leaf (or canopy) temperature and a fully transpiring leaf (or canopy) temperature, respectively. CWSI values can range from 0 (totally transpiring plant) to 1 (non-transpiring plant). Up to now, several natural and artificial wet and dry reference surfaces have been used to estimate T_{wet} and T_{dry}. Apolo-Apolo et al. (2020) developed a paper-based hemispheric surfaces placed in a 3D-printed plastic structure that continuously allows water storage. Jones et al. (2002), proposed the use of leaves sprayed with water and detergent as wet references and leaves where transpiration was inhibited by covering with petroleum jelly as dry references.

Olive (*Olea europaea* L.) is a typical species of the Mediterranean climate, with high levels of drought tolerance. For example, Yields of 'Arbequina' trees with $\Psi_w \leq$ -3.5 MPa are not significantly affected, while -2.5 ≤ $\Psi_w \leq$ -3.5 MPa cause a mild water stress (Marra et al., 2016). Below this water status threshold (-3.5 MPa), the plant begins to suffer drought symptoms. However, in young olive trees, avoiding water stress is crucial (Fernández et al., 2018), so it is important to monitor the water status in a precise, simple and non-destructive way.

On these bases, the aim of this study was to test leaf RWC and thermography techniques (CWSI) as potential indicators of plant water status to provide fast and/or non-destructive alternative methods to Ψ_{leaf} in young potted olive plants. These methods could prove to be useful alternatives at the tree training stage and/or in the nursery, as checking water status of the young plants by a destructive method would compromise their development.

MATERIAL AND METHODS

Experimental design

The experiment was conducted from 13 January to 27 February 2021 at the Department of Agricultural, Food and Forest Sciences of the University of Palermo. Eight 5-year-old olive trees (cv. Nocellara del Belice) potted in 15-liters pots, with uniform growth and morphology were used. The young plants were placed into a growth chamber from the beginning to the end of the trial. In the first 15 days of forcing, the temperature of the chamber was set up at 26 ± 5 °C during the day and at 18 ± 5 °C during the night, and the humidity at 65 ± 5 % to allow a gradual adaptation to the rise in temperature. For the remaining 25 days, the chamber was set up at 30 ± 5 °C during the day and at 21 ± 5 °C during the night, with the humidity at 50 ± 5 % to accelerate the increase of transpiration. The photoperiod was set to simulate the summer season, i.e. with 14 hours of light and 10 hours of darkness (Figure 1).

At time zero (13 January), a full irrigation was applied using approximately 4.2 liters of water per pot (sufficient to reach field capacity).. Afterwards, the plants were not irrigated anymore until the end of the experiment, in order to induce a range of water status as wide as possible. Surveys to assess the water status of plants were carried out twice a week.

Water status measurements

Leaf water potential (LWP), Crop Water Stress Index (CWSI), Relative Water Content (RWC) and Gravimetric Water content relative to fresh and dry weight (GWC_f and GWC_d) were determined to estimate plant water status.

Measurements to assess plants water status were conducted twice a week starting from the initial date. Specifically, on 13, 17, and 20 January, as well as on 3, 7, 10, 14, 16 and 21 February.

LWP was measured in 2 single leaves per plant on each date of measurements, by a pressure chamber (PMS 600, Instrument Company, Albany, OR, USA) according to Ben-Gal et al.(2009) and Liu and Stützel (2002).

CWSI was obtained through thermography techniques. Specifically, thermal photos were taken of the branches containing the leaves used for the other measurements. In the same image, a non-transpiring leaf (as water-stressed baseline), covered with petroleum jelly at least 5 min before the measurement, and a totally transpiring leaf (as non-water-stressed baseline), sprayed with water and detergent, were also included (Jones, 2002). Thermal images were obtained using a FLIR i7 hand-held thermal camera (FLIR Systems, Inc., Wilsonville, OR, USA). The emissivity was set to $\varepsilon = 0.98$, according to Rubio et al. (1997) and Agamet al. (2013). Photos were transferred to a computer and transformed into CSV format to extract a numerical file with temperatures of the image pixels using FLIR tools software. The CSV file was later opened with Image J software (LOCI, University of Wisconsin) to manually select the targeted leaves and extract their temperatures. CWSI was calculated with the equation (2).

Measurements of leaf relative water content (RWC) were carried out following the method of Barrs and Weatherley (1962) and Mullan and Pietragalla (2012). One leaf per plant was wrapped in parafilm and aluminum foil, collected, and transported to a nearby laboratory for determination of fresh weight (FW). Leaf samples were placed in glass tubes with deionized water and, after 24 h at 4 °C, their weight at full turgor (TW) was recorded. Finally, the leaf samples were oven-dried at 70 °C until constant weight (DW). RWC was calculated as (FW − DW)/(TW − DW) × 100. GWC_f was calculated as (FW-DW)/FW, and GWC_d as (FW-DW)/DW.

Statistical data analysis

RWC, CWSI, GWC_d and GWC_f were plotted against LWP as the dependent variable. Data were analyzed by linear and non-linear regression analysis to establish relationships between parameters. Multiple linear regression analysis was performed to evaluate the combined use of RWC and CWSI for estimating leaf water potential. Linear regression and multiple linear regression analyses were performed using the Python module statsmodels (version 0.13.2) (Seabold and Perktold, 2010) Matplotlib library (version 3.6.2) (Hunter, 2007) was used to plot the data.

RESULTS AND DISCUSSION

Continuous trends of Leaf Water Potential, Leaf Water Content and Crop Water Stress Index

LWP showed a decrease throughout the measurement period. From an average value of -0.46 ± 0.14 MPa in January Ψ_{leaf} dropped to -5 ± 1.70 MPa at the end of the trial (21/02/2022; Figure 2A). In particular, a marked decrease was observed right after the VPD levels increased, between 3 and 14 February. The beginning of this period of marked decrease coincided more or less with the time when the growth chamber settings were changed, thus increasing atmospheric deficit levels.

A similar trend was also shown in RWC (%) data. RWC values ranged from 92.22 ± 1.36 % in the first month, to 64.90 ± 8.85 % by the end of the trial, with a sharp decrease occurring

again between 10and 14 February (Figure 2B). Both leaf GWC_f (Figure 2C) and GWC_d (Figure 2D) showed trends similar to the previous parameters.

It is interesting to notice that in the last dates of measurements, the error bars become bigger. This may be because different plants may have different abilities to cope with drought due to differences in growth and morphology of the foliage and root system accumulated over the two months of trial.

As expected, CWSI showed an increasing trend because CWSI is directly related to leaf water stress (Figure 2E).

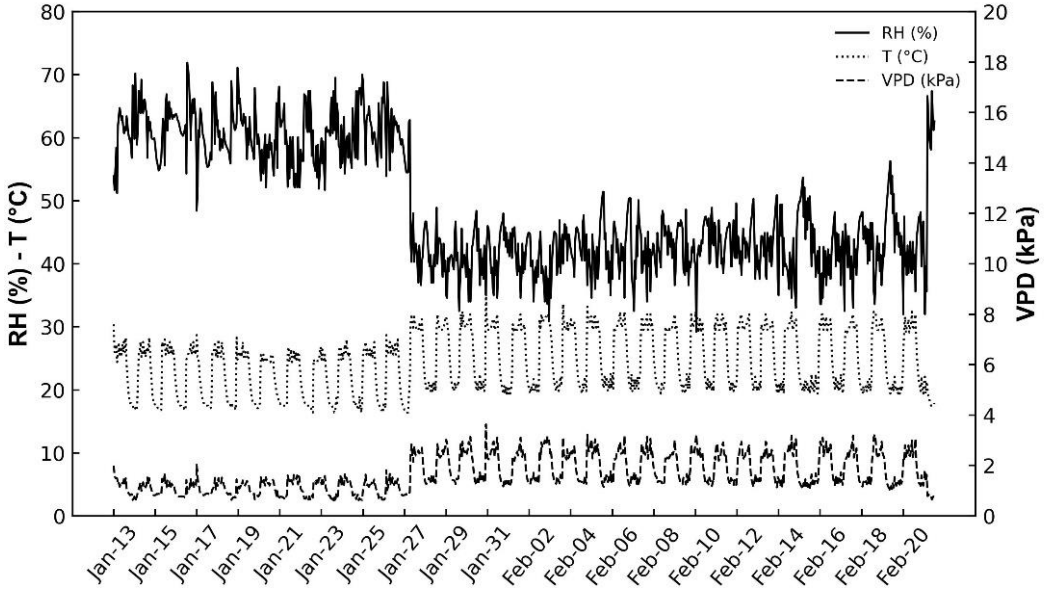

Figure 1. Trends of hourly temperature, Relative Humidity and VPD in the growth chamber during the trial period.

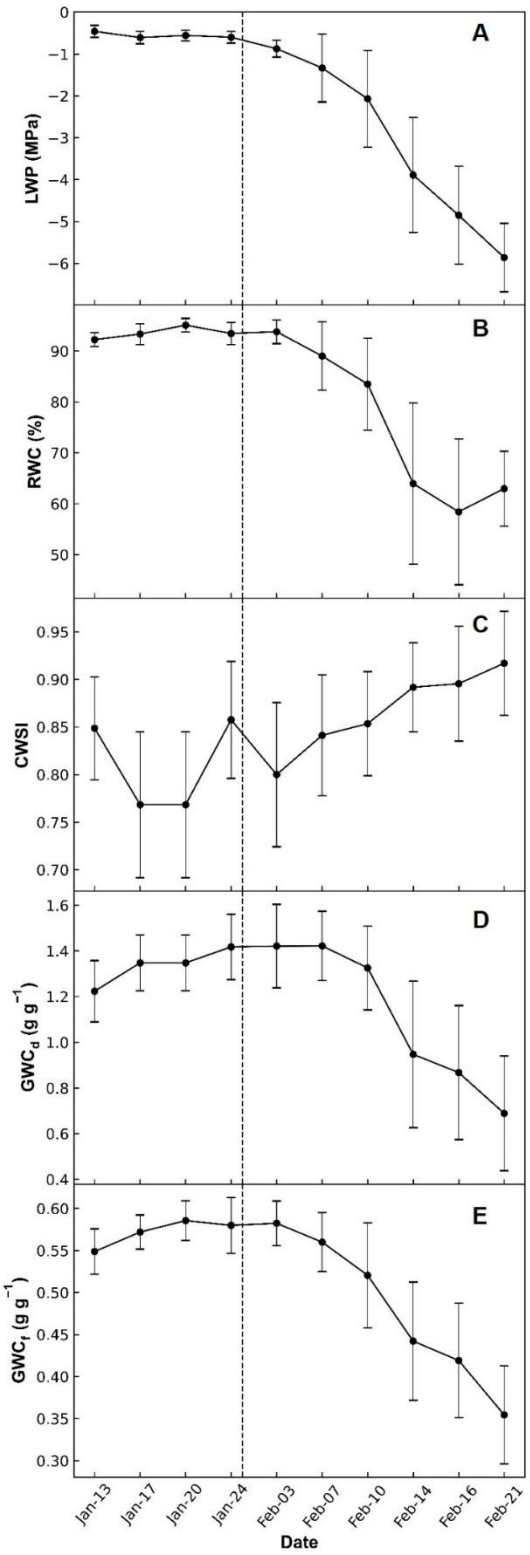

Figure 1. Trends of the measured parameters during the trial period: Leaf Water Potential (LWP) (A), leaf Relative Water Content (RWC) (B), Crop Water Stress Index (CWSI) (C), leaf Gravimetric Water Content in function of dry weight (GWC_d) (D), leaf Gravimetric Water Content in function of fresh weight (GWC_f) (E). The dashed line represents the time when the growth chamber parameters were reset.

Relationships between parameters

LWP values ranged from -0.6 MPa to -7 MPa, while RWC values between 40% and 97% (Figure 3). A direct linear relationship was found between RWC and LWP in leaves, suggesting that RWC may be a useful indicator for assessing plant water status.

On the left side of the graph, at potentials below about -2.5 MPa, there is a slight increase in point scattering. This may be explained by the fact that RWC measures leaf water deficit and since it is based on dry weights, it also considers possible solute accumulation and osmotic adjustment in response to drought conditions (Barrs, 1968). A similar linear relationship was found in young potted olive plant by Dichio et al. (2006). In 2017, Lo Bianco and Scalisi, found a very similar relationship in young potted olive plants of the cv. Minuta, with a similar value of coefficient of determination (0.703) and slope (0.12). Similar relationships were also found in other species, such as orange (Lo Bianco and Massenti, 2012; Mossad et al., 2018) and apple (Jones and Higgs, 1979).

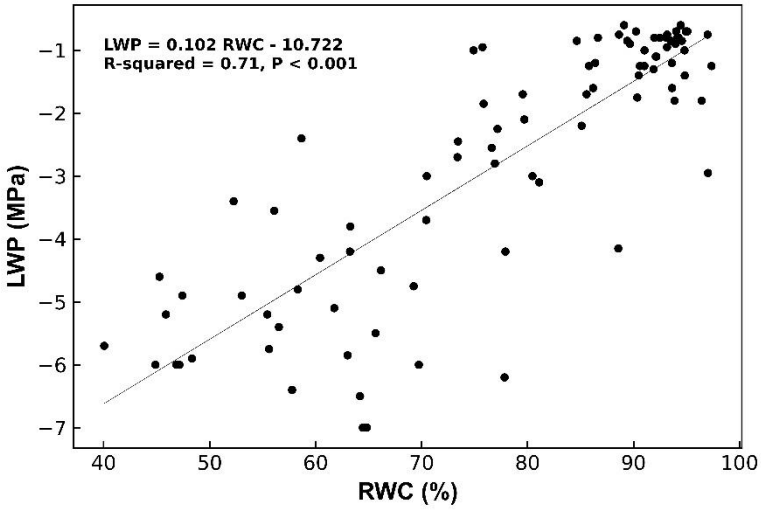

Figure 3. Linear regression analysis between leaf Relative Water Content (RWC, %) and Leaf Water Potential (LWP, MPa). LWP = 0.102 RWC - 10.722; R^2 = 0.71; P < 0.001.

For the relationship between LWP and CWSI only values of LWP below -1 were considered because there was a CWSI point cloud above this level and also because in olive trees, there are no significant metabolic changes for values above -1. As expected, a negative linear relationship was observed between LWP and CWSI (Figure 4). Ben-Gal et al. (2009) and García-Tejero et al. (2017) also found a negative linear relationship between the two parameters. However, the range of CWSI found in their study is different from that found in this work. This may be due to the different monitoring conditions: they worked in the field, with the influence of varying climatic conditions, while we used a growth chamber (e.g., influence of solar radiation (Agam, Cohen, Alchanatis, et al., 2013)), and with adult olive trees. On the other hand, similar results were obtained by Wiriya-Alongkorn et al. (2013) in young longan trees, grown in similar conditions to the plants in this trial.

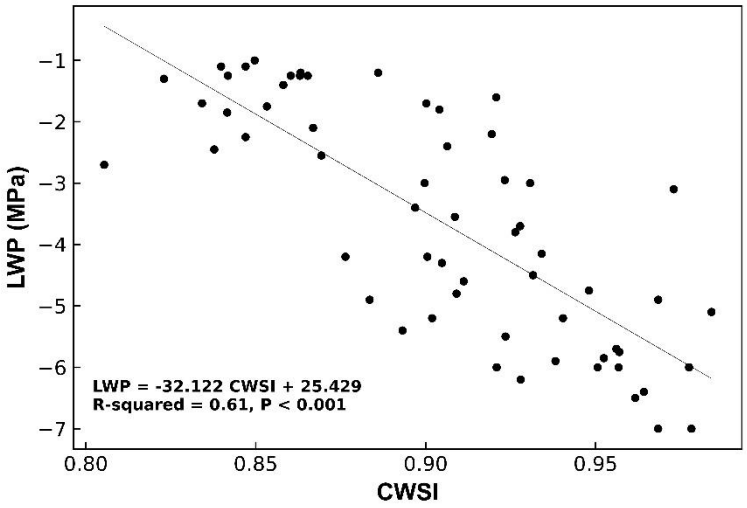

Figure 4. Linear regression analysis between Crop Water Stress Index (CWSI) and Leaf Water Potential (LWP, MPa). LWP = -32.122 CWSI + 25.429; R^2 = 0.61; P < 0.001.

Interesting relationships were found between GWC (GWC_f and GWC_d) and LWP. GWC_d values ranged from 0.40 to 1.61 g g^{-1}, while GWC_f values ranged from 0.27 to 0.66 g g^{-1}. Similarly, to the relationships between RWC and LWP, a positive linear relationship was found between LWP and the two gravimetric parameters (Figures 5A and 5B). However, as the graphs show, the linear relationship is lost at LWP > -1. This could be due to the practical difficulty of measuring water potentials by pressure chamber when the olive plant has high hydration levels. In the case of olive, this result assumes little importance because the leaf is in the range where it is at maximum hydration, not under stress conditions. Moreover, the highest coefficients of determination were obtained for the relationship between GWC_d and LWP (R^2 = 0.77), and between GWC_f and LWP (R^2 = 0.85). Measuring such parameters could be useful as reliable alternative methods for estimating plant water status. However, despite their reliability, these methods are destructive and time-consuming, as opposed to thermography for obtaining CWSI. Unfortunately, in the literature there is not much information on gravimetric leaf water content to assess the olive tree water status. Ahmed et al. (2007) observed a linear relationship between GWC_f (LWC in their study) and stomatal conductance in olive trees (cv. Chemlali). Elsayed et al. (2011) found a significant linear relationship between GWC_f and LWP in maize and wheat. A significant linear relationship between GWC_f and stomatal conductance was also observed by Socias et al. (1997) in clover leaves. Zhou et al. (2021) found a non-linear relationship between GWC_f and net photosynthesis rate (Pn), a parameter strongly related to transpiration rate. Given its reliability, GWC has recently been used as a reference parameter to be determined by optical sensors, especially to assess plant water status from transmission terahertz time-domain spectroscopy (Borovkova et al., 2018; Carter, 1991; Gente et al., 2013).

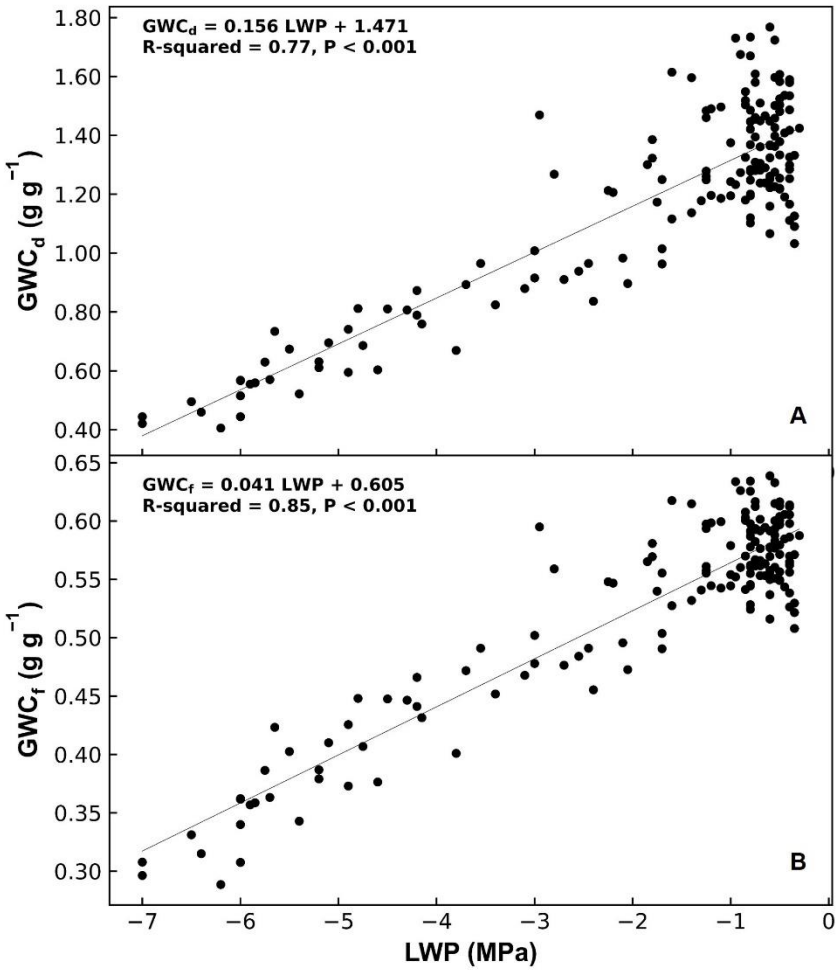

Figure 5. Linear regression analysis between Leaf Water Potential (LWP, MPa) and leaf Gravimetric Water Content in function of dry weight (GWC_d) (A) and leaf Gravimetric Water Content in function of fresh weight (GWC_f) (B). $GWC_d = 0.156$ LWP + 1.471; $R^2 = 0.77$; $P < 0.001$. $GWC_f = 0.041$ LWP + 605; $R^2 = 0.85$; $P < 0.001$.

Finally, an important relationship emerged from a multiple linear regression analysis between LWP and RWC and CWSI ($R^2 = 0.76$, $P < 0.001$). This suggests that the joint use of RWC and CWSI may provide a better estimate of olive water status than using individual parameters. However, using such an approach would be more time-consuming.

CONCLUSION

Considering the tight association with LWP, gravimetric methods, i.e. RWC and especially GWC, proved to be the most reliable for estimating olive water status. However, thermography can also be a useful technique as CWSI values showed a valid, albeit less close relationship than gravimetric parameters, with LWP. Improving this technique could have many advantages, since it is a nondestructive technique and a less time-consuming method than gravimetric measurements (which require at least 3 days in the laboratory).

Based on this experimentation, it is possible to state that the methods presented in this trial could all be useful alternatives for assessing the water status of young olive trees. However, special attention should be paid to the thermographic method for calculating CWSI since this is not performed destructively, thus avoiding the risk of compromising their initial development and future productivity. Further studies, especially in adult plants in the field, are needed to validate the techniques and create appropriate and reliable models.

ACKNOWLEDGEMENTS

The authors want to thank Antonino Ioppolo and all the other colleagues that helped with all the activities.

Literature cited

Agam, N., Cohen, Y., Alchanatis, V., and Ben-Gal, A. (2013). How sensitive is the CWSI to changes in solar radiation? Int. J. Remote. Sens., *34*(17), 6109–6120.

Agam, N., Cohen, Y., Berni, J., Alchanatis, V., Kool, D., Dag, A., Yermiyahu, U., and Ben-Gal, A. (2013). An insight to the performance of crop water stress index for olive trees. Agr. Water. Manage., *118*, 79–86.

Ahmed, C. B., Rouina, B. B., and Boukhris, M. (2007). Effects of water deficit on olive trees cv. Chemlali under field conditions in arid region in Tunisia. Sci. Hortic., *113*(3), 267–277.

Allen, C. D., Macalady, A. K., Chenchouni, H., Bachelet, D., McDowell, N., Vennetier, M., Kitzberger, T., Rigling, A., Breshears, D. D., and Hogg, E. T. (2010). A global overview of drought and heat-induced tree mortality reveals emerging climate change risks for forests. Forest. Ecol. Manag., *259*(4), 660–684.

Apolo-Apolo, O., Martínez-Guanter, J., Pérez-Ruiz, M., and Egea, G. (2020). Design and assessment of new artificial reference surfaces for real time monitoring of crop water stress index in maize. Agr. Water. Manage., *240*, 106304.

Barrs, H., and Weatherley, P. (1962). A re-examination of the relative turgidity technique for estimating water deficits in leaves. Aust. J. Biol. Sci., *15*(3), 413–428.

Barrs, Hd. (1968). Determination of water deficits in plant tissues. Water deficits and plant growth, *Vol. 1*, 235–368.

Ben-Gal, A., Agam, N., Alchanatis, V., Cohen, Y., Yermiyahu, U., Zipori, I., Presnov, E., Sprintsin, M., and Dag, A. (2009). Evaluating water stress in irrigated olives: Correlation of soil water status, tree water status, and thermal imagery. Irrigation Sci., *27*(5), 367–376.

Borovkova, M., Khodzitsky, M., Demchenko, P., Cherkasova, O., Popov, A., and Meglinski, I. (2018). Terahertz time-domain spectroscopy for non-invasive assessment of water content in biological samples. Biomed. Opt. Express, *9*(5), 2266–2276.

Browne, M., Yardimci, N. T., Scoffoni, C., Jarrahi, M., and Sack, L. (2020). Prediction of leaf water potential and relative water content using terahertz radiation spectroscopy. Plant direct, *4*(4), e00197.

Carrasco-Benavides, M., Antunez-Quilobrán, J., Baffico-Hernández, A., Ávila-Sánchez, C., Ortega-Farías, S., Espinoza, S., Gajardo, J., Mora, M., and Fuentes, S. (2020). Performance assessment of thermal infrared cameras of different resolutions to estimate tree water status from two cherry cultivars: An alternative to midday stem water potential and stomatal conductance. Sensors, *20*(12), 3596.

Carter, G. A. (1991). Primary and secondary effects of water content on the spectral reflectance of leaves. Am. J. Bot., *78*(7), 916–924.

Datt, B. (1999). Remote sensing of water content in Eucalyptus leaves. Aust. J. Bot., *47*(6), 909–923.

Diaz-Pérez, J., Shackel, K., and Sutter, E. (1995). Relative water content and water potential of tissue 1. J. Exp. Bot., *46*(1), 111–118.

Dichio, B., Xiloyannis, C., Sofo, A., and Montanaro, G. (2006). Osmotic regulation in leaves and roots of olive trees during a water deficit and rewatering. Tree Physiol., *26*(2), 179–185.

Elsayed, S., Mistele, B., and Schmidhalter, U. (2011). Can changes in leaf water potential be assessed spectrally? Funct. Plant. Biol. , *38*(6), 523–533.

Fernández, J. E. (2017). Plant-based methods for irrigation scheduling of woody crops. *Horticulturae*, *3*(2), 35.

Fernández, J. E., Diaz-Espejo, A., Romero, R., Hernandez-Santana, V., García, J. M., Padilla-Díaz, C. M., and Cuevas, M. V. (2018). Precision irrigation in olive (Olea europaea L.) tree orchards. Water scarcity and sustainable agriculture in semiarid environment (pp. 179–217).

Fernández, J., Moreno, F., Girón, I., and Blázquez, O. (1997). Stomatal control of water use in olive tree leaves. Plant. Soil, *190*(2), 179–192.

Fuentes, S., De Bei, R., Pech, J., and Tyerman, S. (2012). Computational water stress indices obtained from thermal image analysis of grapevine canopies. Irrigation. Sci., *30*(6), 523–536.

García-Tejero, I., Hernández, A., Padilla-Díaz, C., Diaz-Espejo, A., and Fernández, J. (2017). Assessing plant water status in a hedgerow olive orchard from thermography at plant level. Agr. Water Manage., *188*, 50–60.

Gente, R., Born, N., Voß, N., Sannemann, W., Léon, J., Koch, M., and Castro-Camus, E. (2013). Determination of leaf water content from terahertz time-domain spectroscopic data. J. Infrared Millim. Te., *34*(3), 316–323.

González, L., and González-Vilar, M. (2001). Determination of relative water content. Handbook of plant ecophysiology techniques, (pp. 207–212).

Hristov, J., Barreiro-Hurle, J., Salputra, G., Blanco, M., and Witzke, P. (2021). Reuse of treated water in European agriculture: Potential to address water scarcity under climate change. Agr. Water Manage., *251*, 106872.

Hunter, J. D. (2007). Matplotlib: A 2D graphics environment. Comput. Sci. Eng. , *9*(03), 90–95.

Idso, S., Jackson, R., Pinter Jr, P., Reginato, R., and Hatfield, J. (1981). Normalizing the stress-degree-day parameter for environmental variability. Agr. Meteorol., *24*, 45–55.

Ingram, J., and Bartels, D. (1996). The molecular basis of dehydration tolerance in plants. Annu. Rev. Plant Biol., *47*(1), 377–403.

Jackson, R. D., Idso, S., Reginato, R., and Pinter Jr, P. (1981). Canopy temperature as a crop water stress indicator. Water Resour. Res., *17*(4), 1133–1138.

Jones, H. G. (2007). Monitoring plant and soil water status: Established and novel methods revisited and their relevance to studies of drought tolerance. J. Exp. Bot., *58*(2), 119–130. https://doi.org/10.1093/jxb/erl118

Jones, H. G., and Leinonen, I. (2003). Thermal imaging for the study of plant water relations. J. Agric. Meteorol., *59*(3), 205–217.

Jones, H. G., Stoll, M., Santos, T., Sousa, C. de, Chaves, M. M., and Grant, O. M. (2002). Use of infrared thermography for monitoring stomatal closure in the field: Application to grapevine. J. Exp. Bot *., 53*(378), 2249–2260.

Jones, H., and Higgs, K. (1979). Water potential-water content relationships in apple leaves. J. Exp. Bot., *30*(5), 965–970.

Leinonen, I., and Jones, H. G. (2004). Combining thermal and visible imagery for estimating canopy temperature and identifying plant stress. J. Exp. Bot ., *55*(401), 1423–1431.

Li, R., Lu, Y., Peters, J. M., Choat, B., and Lee, A. J. (2020). Non-invasive measurement of leaf water content and pressure–volume curves using terahertz radiation. Sci. Rep., *10*(1), 1–14.

Liu, F., and Stützel, H. (2002). Leaf water relations of vegetable amaranth (Amaranthus spp.) in response to soil drying.Eur. J. Agron., *16*(2), 137–150. https://doi.org/10.1016/S1161-0301(01)00122-8

Lo Bianco, R., and Massenti, R. (2012). *Relazione tra potenziale idrico e contenuto idrico relativo in alberi adulti di arancio'Valencia'*. Acta Italus Hortus, 109–112.

Lo Bianco, R., and Scalisi, A. (2017). Water relations and carbohydrate partitioning of four greenhouse-grown olive genotypes under long-term drought. Trees, *31*(2), 717–727.

Marra, F., Marino, G., Marchese, A., and Caruso, T. (2016). Effects of different irrigation regimes on a super-high-density olive grove cv."Arbequina": Vegetative growth, productivity and polyphenol content of the oil. Irrigation Sci., *34*(4), 313–325.

Martín-Vertedor, A. I., Rodríguez, J. M. P., Losada, H. P., and Castiel, E. F. (2011). Interactive responses to water deficits and crop load in olive (olea europaea L., cv. Morisca) I.–Growth and water relations. Agr. Water Manage., *98*(6), 941–949.

Massenti, R., Scalisi, A., Marra, F. P., Caruso, T., Marino, G., and Lo Bianco, R. (2022). Physiological and Structural Responses to Prolonged Water Deficit in Young Trees of Two Olive Cultivars. Plants, *11*(13), 1695.

Mossad, A., Scalisi, A., and Lo Bianco, R. (2018). Growth and water relations of field-grown 'Valencia'orange trees under long-term partial rootzone drying. Irrigation Sc*i.*, *36*(1), 9–24.

Mullan, D., and Pietragalla, J. (2012). Leaf relative water content. Physiological breeding II: A field guide to wheat phenotyping, pp. 25–27.

Poblete-Echeverría, C., Ortega-Farías, S., Lobos, G., Romero, S., Ahumada, L., Escobar, A., and Fuentes, S. (2014). Non-invasive method to monitor plant water potential of an olive orchard using visible and near infrared spectroscopy analysis. Acta Hortic., *1057*, 363–368.

Rubio, E., Caselles, V., and Badenas, C. (1997). Emissivity measurements of several soils and vegetation types in the 8–14, μm Wave band: Analysis of two field methods. Remote Sens. Environ., *59*(3), 490–521.

Scalisi, A., Bresilla, K., and Simões Grilo, F. (2017). Continuous determination of fruit tree water-status by plant-based sensors. Acta Italus Hortus, *24*(2), 39–50.

Seabold, S., and Perktold, J. (2010). Statsmodels: Econometric and statistical modeling with python. *57*(61), 10–25080.

Smart, R. E., and Bingham, G. E. (1974). Rapid estimates of relative water content. Plant Physiol., *53*(2), 258–260.

Socias, F., Pol, A., Aguilo, F., Vadell, J., and Medrano, H. (1997). Effects of rapidly and gradually induced water stress on plant response in subterranean clover leaves. J. Plant. Physiol, *150*(1–2), 212–219.

Wiriya-Alongkorn, W., Spreer, W., Ongprasert, S., Spohrer, K., Pankasemsuk, T., and Müller, J. (2013). Detecting drought stress in longan tree using thermal imaging. Maejo Int. J. Sci. Tech. , *7*(1), 166.

Xiloyannis, C., Dichio, B., Nuzzo, V., and Celano, G. (1997). Defence strategies of olive against water stres*s*. pp. 423–426.

Zhou, H., Zhou, G., He, Q., Zhou, L., Ji, Y., and Lv, X. (2021). Capability of leaf water content and its threshold values in reflection of soil–plant water status in maize during prolonged drought. Ecological Indicators, *124*, 107395. https://doi.org/10.1016/j.ecolind.2021.107395

Zimmermann, D., Reuss, R., Westhoff, M., Gessner, P., Bauer, W., Bamberg, E., Bentrup, F.-W., and Zimmermann, U. (2008). A novel, non-invasive, online-monitoring, versatile and easy plant-based probe for measuring leaf water status. J. Exp. Bot., *59*(11), 3157–3167.

CHAPTER 3.

Testing effects of vapor pressure deficit on fruit growth: a comparative approach using peach, mango, olive, orange, and loquat

Based on the **published** paper:
Carella, A., Massenti, R., Lo Bianco, R. (2023). Testing effects of vapor pressure deficit on fruit growth: a comparative approach using peach, mango, olive, orange, and loquat. *Frontiers in Plant Science*, *14*, 1294195.
https://doi.org/10.3389/fpls.2023.1294195

frontiers | Frontiers in Plant Science

TYPE Original Research
PUBLISHED 20 December 2023
DOI 10.3389/fpls.2023.1294195

OPEN ACCESS

EDITED BY
Fulai Liu,
University of Copenhagen, Denmark

REVIEWED BY
Gemma Reig,
Institute of Agrifood Research and Technology (IRTA), Spain
Olfa Zarrouk,
Institute of Agrifood Research and Technology (IRTA), Spain

*CORRESPONDENCE
Riccardo Lo Bianco
riccardo.lobianco@unipa.it

RECEIVED 14 September 2023
ACCEPTED 05 December 2023
PUBLISHED 20 December 2023

CITATION
Carella A, Massenti R and Lo Bianco R (2023) Testing effects of vapor pressure deficit on fruit growth: a comparative approach using peach, mango, olive, orange, and loquat. *Front. Plant Sci.* 14:1294195. doi: 10.3389/fpls.2023.1294195

Testing effects of vapor pressure deficit on fruit growth: a comparative approach using peach, mango, olive, orange, and loquat

Alessandro Carella, Roberto Massenti and Riccardo Lo Bianco*

Department of Agricultural, Food and Forest Sciences, University of Palermo, Palermo, Italy

Determining the influence of vapor pressure deficit (VPD) on fruit growth is a key issue under a changing climate scenario. Using a comparative approach across different fruit tree species may provide solid indications of common or contrasting plant responses to environmental factors. Knowing fruit growth responses to VPD may also be useful to optimize horticultural management practices under specific atmospheric conditions. Climate data to calculate VPD and fruit relative growth rates (RGR) by fruit gauges were monitored in peach at cell division, pit hardening and cell expansion stages; in two mango cultivars at cell division, cell expansion and maturation stages; in two olive cultivars, either full irrigated or rainfed, at early and late cell expansion stages; in 'Valencia' orange at early and late cell division stage, before and after mature fruit harvest; in loquat at cell expansion and maturation stages. At the fruit cell division stage, sensitivity of fruit growth to VPD seems to vary with species, time, and probably soil and atmospheric water deficit. 'Keitt' mango and 'Valencia' orange fruit growth responded to VPD in opposite ways, and this could be due to very different time of the year and VPD levels in the monitoring periods of the two species. At pit hardening stage of peach fruit growth, a relatively weak relationship was observed between VPD and RGR, and this is not surprising as fruit growth in size at this stage slows down significantly. A consistent and marked negative relationship between VPD and RGR was observed at cell expansion stage, when fruit growth is directly depending on water intake driving cell turgor. Another behavior common to all observed species was the gradual loss of relationship between VPD and RGR at the onset of fruit maturation, when fruit growth in size is generally programmed to stop. Finally, regardless of fruit type, VPD may have a significant effect on fruit growth and could be a useful parameter to be monitored for tree water management mainly when the cell expansion process prevails during fruit growth.

KEYWORDS

cell division, cell expansion, fruit diameter, fruit gauge, fruit maturation, fruit water relations, precision horticulture, proximal sensing

1 Introduction

In Mediterranean environments, high radiation and air temperature associated with high vapor pressure deficit (VPD) during summer affect both plant water status and production in terms of yield and quality (Somboonkaew and Terry, 2010; Bardi et al., 2022; Noh and Lee, 2022). According to some researchers the global increase in VPD leads to a decrease in plant productivity (Yuan et al., 2019). Increased VPD often causes a closure of leaf stomata resulting in decreased rates of photosynthesis (Fletcher et al., 2007). The transpiration rate of fruits, particularly for those that are well-exposed, is mainly determined by the VPD between the air and the evaporating surface, causing continuous diameter fluctuations. These variations, mainly that of daily contraction, are usually interpreted as elastic changes in tissue volume (Léchaudel et al., 2007). Indeed, the daily diameter variations of fleshy fruits involve a balance between water intake, on one side, and withdrawal through vascular tissue and losses by transpiration, on the other side.

In the early stage of fruit development, at green stage, when the chlorophyll content is high, fruit stomata are sensitive as in leaves. High VPD gradually induce stomatal closure, leading to a reduction in the rate of CO_2 assimilation in the fruit (Blanke and Lenz, 1989; Garrido et al., 2023). These mechanisms should vary in the case of fruits without stomata, such as tomato (Rančić et al., 2010), where water losses from the fruit occur mainly by cuticular transpiration. Transpiration flow in this case may depend on the composition of the cutin and waxy layer and on the concentration of microscopic polar pores (Zarrouk et al., 2018; Fich et al., 2020; Garrido et al., 2023). In peach, it was observed that transpiration, in response to daytime environmental conditions, decreases fruit water content along with a reduction in turgor and water potential, causing fruit shrinkage. Carbohydrates reaching the fruit from the phloem may also accumulate in the vacuole reducing osmotic and ultimately water potential. Later in the day, this, along with resumed xylem flow, attracts greater amounts of water into the fruit from the xylem than are lost through transpiration causing fruit expansion (Morandi et al., 2007b). Drought and VPD, due to the rapid stomatal closure also have a negative effect on photosynthesis (Léchaudel et al., 2013), and thus on the accumulation of dry matter in the fruit. In olive fruits, 10 to 30% of fresh weight (FW) may be that of the endocarp, depending on the cultivar (Del Rio and Caballero, 2008), crop load (Lavee and Wodner, 2004) and water availability (D'Andria et al., 2004; Lavee et al., 2007). In olive under well-watered conditions, Fernandes et al. (2018) showed that fruit contraction was mainly driven by high VPD. In 'Keitt' mango, VPD was the main driving force determining fruit diameter fluctuations (Carella et al., 2021). Also peach fruit shrinkage and growth have been related to high VPD and fruit transpiration (Morandi et al., 2007b; Morandi et al., 2010). An inverse relationship between VPD and fruit relative growth rate was found in 'Valencia' orange when data over a 5-year period were pooled together (Mossad et al., 2018).

Fruit development also plays a key role. In mango, the skin, the flesh and the stone have specific compositions that appear to accumulate water and dry matter at different rates, depending on environmental conditions (Léchaudel et al., 2007). Most fruits can have a sigmoid or double sigmoid growth pattern. These patterns are divided into development stages: cell division, pit hardening (in the case of fruits with double sigmoid pattern), cell expansion, and ripening. Cell division is a high energy demanding process (Li et al., 2012), due to the fast cell division rate in fruit tissues. Thus, ensuring an adequate supply of carbohydrates becomes crucial during this stage. Carbohydrates translocated into the fruit are mainly imported from actively photosynthesizing leaves through the phloem (Génard et al., 2008; Carella et al., 2021). Following the initial stage, fruits enter a phase of linear growth, which primarily involves the expansion of pulp cells caused by water uptake driven by osmotic gradients. This stage is significantly influenced by daily fluctuations in temperature, relative humidity, and vapor pressure deficit (VPD), as these factors play a crucial role in regulating fruit transpiration (Lescourret et al., 2001). Specifically, daily VPD fluctuations drive fruit enlargement during the night and shrinkage during the day. During pit-hardening stage, fruit growth rate is minimal or null (Rahmati et al., 2015), therefore the fruit should respond minimally to VPD changes. The final stage of fruit development is the ripening. In this stage, the fruit reaches sufficient physiological and sexual maturity to be detached from the parent plant, as described in Grierson (2002). At this stage, significant changes in the texture, flavor, and color of the fruit occur, both internally and externally (Lakshminarayana, 1973; Giovannoni, 2001), and the fruit tends to isolate itself from environmental parameters (Morandi et al., 2006; Nordey et al., 2015; Carella et al., 2021).

Several works have shown that the fruit ripening process, in terms of sugar accumulation in the pulp and skin coloration, is markedly influenced and regulated by biotic factors, such as genetic differences and crop load, and by abiotic factors, such as orchard management, ambient temperature and relative humidity, and water availability (Corelli-Grappadelli and Lakso, 2004; Gucci et al., 2009; Hammami et al., 2011). Carbon limitations caused by environmental stress during the early stages of grape berry growth may restrict berry size but do not affect the progression of ripening. On the contrary, if such limitations occur after the lag phase of berry growth, they appear to have an impact on fruit ripening (Keller, 2010).

In climacteric fruits like peaches and mangoes, the peaks in respiration rate and ethylene biosynthesis are reached during the ripening stage. In contrast, in non-climacteric fruits like loquats, oranges and olives, respiration rate and ethylene biosynthesis tend to decrease gradually (Gamage and Rahman, 1999; Rooban et al., 2016). Fruit respiration rate is also dependent on changes in temperature and relative humidity. As temperature increases and relative humidity decreases, respiration rate increases accelerating ripening phenomena (Paul et al., 2012). For these reasons, during fruit ripening, climacteric and non-climacteric fruits may exhibit different responses to environmental conditions.

VPD may be an indirect estimator of water loss in plants, and along with other parameters may provide more accurate information on irrigation scheduling. The non-destructive and continuous monitoring of changes in fruit growth is one of the parameters on which precision agriculture is based, and this is possible using fruit gauges (Morandi et al., 2007a). Fruit diameter variation by fruit

gauges may represent an indirect indicator of plant water status (Lo Bianco and Scalisi, 2019; Scalisi et al., 2019a; Carella et al., 2021), and this type of indicators is needed to avoid permanent stress effects (Tomkiewicz and Piskier, 2012; Fernández, 2014; Marino et al., 2021; Massenti et al., 2022). Monitoring of fruit growth by following the diurnal fluctuation of diameter has been studied in several species, like peach and nectarine (*Prunus persica*) (Morandi et al., 2008; Scalisi et al., 2019b), plum (*Prunus domestica*) (Corelli Grappadelli et al., 2019), apple (*Malus domestica*) (Boini et al., 2019), orange (*Citrus sinensis*) (Grilo et al., 2019), olive (*Olea europaea*) (Marino et al., 2021), mango (*Mangifera indica* L.) (Carella et al., 2016) and also cladode growth in *Opuntia ficus-indica* (Scalisi et al., 2016). The aim of this work was to determine the influence of VPD on fruit growth rates, measured continuously with fruit gauges, using a comparative approach across different fruit tree species. Studying responses across different species like peach, mango, olive, orange, and loquat may serve as a powerful indicator of common or contrasting mechanisms regulating fruit growth. Ultimately, knowing species-specific VPD levels or thresholds that cause changes in fruit growth may be useful to optimize horticultural management practices under specific atmospheric conditions.

2 Materials and methods

2.1 Peach

The trial was conducted on late-ripening 'Tardivo 2000' peach (*Prunus persica* L.) grafted onto 'GF 677' rootstock in a commercial orchard of the Ecofarm company located near Riesi, in south Sicily, Italy (37.25724 N, 14.11922 E), at 330 m a.s.l., from June to September 2022. Ten 12-year-old peach trees trained to small vase and spaced at 6 x 4 m were selected for the experiment. The trial area was located on a sloping, medium-textured sandy loam soil (pH 7.3) with low active carbonates. All plants received the same conventional cultural management, including drip irrigation and fertilization. Trees were irrigated with a seasonal volume of 1443 m^3 ha^{-1}. Fruits were thinned to 1 every 15 cm of shoot on 4 June, before pit hardening.

2.2 Mango

The experiment was carried out in a commercial orchard of the Cupitur farm located near Caronia (38°03' N, and 14°30' E) at 5 m a.s.l. in northeastern Sicily (Italy) from July to October 2019. Mango (*Mangifera indica* L.) trees were protected by windbreaks made of cypress plants (*Cupressus sempervirens* L.), and nonwoven fabric windbreaks supported by 5-m-tall wooden posts. The trial was conducted on six 15-year-old mango trees, three of cv Keitt (late-season ripening) and three of cv Tommy Atkins (early- to mid-season ripening), grafted onto Gomera-3 mango rootstock, with crop loads of 1.3 and 0.7 fruits cm^{-2} of TCSA, respectively. Trees were trained to globe-shaped canopies, reaching 2.5–3 m in height, and spaced at 5 x 4 m. The soil was a loose sandy loam. Trees were fertilized and irrigated through a drip system with a seasonal volume of 3300 m^3 ha^{-1}. Two light pruning operations were carried out, one at the end of winter, before the start of vegetative growth, and one after fruit harvest.

2.3 Olive

The trial was carried out in summer 2016 in a high-density (6 × 3 spacing) olive (*Olea europaea* L.) orchard located near Sciacca, in South-western Sicily (37°29' N and 13°12' E, 138 m a.s.l.). Three-year-old own-rooted trees were trained to "free palmette" along North-South-oriented hedgerows. Sicilian cultivars Nocellara del Belice (NB) and Olivo di Mandanici (MN) were selected for their different fruit characteristics and vigor. The soil was a sandy clay loam (60% sand, 18% silt, and 22% clay) with pH of 7.7 and<5% of active carbonates. Trees were regularly fertilized and pruned according to conventional practices. Two irrigation levels were imposed to generate a large variability in tree water status: full irrigation (FI, 100% ETc) and rainfed (0% of FI). FI trees were irrigated through a drip system with a total volume of 640 m^3 ha^{-1}, while rainfed trees received 189 mm of rainwater.

2.4 Orange

The study was conducted on adult orange trees (*Citrus sinensis* L. Osbeck, cv Valencia) grafted onto sour orange (*Citrus aurantium* L.) in an experimental orchard located at the Department of Agricultural, Food and Forest Sciences, University of Palermo, Italy (30'06 N, 13'21 E), at 31 m a.s.l., in spring 2014. Trees were trained to globe-shaped canopies, reaching 2.5–3 m, and spaced at 4 × 4 m. Micro sprinkler irrigation was applied in 26 events at 2- to 4-day intervals, during the period between June and September. The total irrigation volume was 3870 m^3 ha^{-1}.

2.5 Loquat

In April 2023, 12 adult trees of the Sicilian loquat (*Eriobotrya japonica* Lindl.) cultivar Nespolone di Trabia were selected in a terraced loquat orchard located in Ciaculli, near Palermo (Italy, 38° 06' N, 13°41' E) at 204 m a.s.l. Trees were trained to globe-shaped canopies, reaching 3-3.5 m in height and spaced at 4 × 4 m. The soil was a medium texture loam. Trees were drip irrigated with an average volume of 2100 m^3 ha^{-1} from mid-July to the resumption of fall precipitations, typically in September.

2.6 Fruit growth monitoring

Fruit diameter micrometric changes were recorded at 15-min intervals with the fruit gauges described by Morandi et al. (2007a) connected to a CR-1000 datalogger (Campbell Scientific, Inc., Logan, UT, USA).

In peach, measurements were made from 25 May to 5 September on 10 fruits, one per each tree, over the entire periods

of fruit development: cell division, from 25 May to 23 June; pit hardening, from 24 June to 27 July; cell expansion, from 28 July to 5 September. In 'Keitt' mango, diameter changes were monitored on three fruits from three different plants, over three different periods: cell division, from 27 July to 2 August; cell expansion, from 12 to 23 August; late cell expansion-maturation, from 7 to 21 September. In 'Tommy Atkins' mango, diameter changes were also monitored in the three fruit growth stages: from 20 to 27 July (early cell expansion), from 3 to 12 August (cell expansion), and from 24 August to 7 September (late cell expansion-maturation). In olive, measurements were carried out on one fruit per tree and 8 trees per cultivar at cell expansion (18 August to 9 September) and late cell expansion/early maturation (18 September to 18 October), as during cell division (mid-May to beginning of July) rainfall saturated the soil and canceled any possible effect of deficit irrigation. In 'Valencia' orange, 15 fruits (one per tree) were monitored in two periods, at the time when cell division mechanisms prevailed from 24 to 31 May (early cell division) and from 16 to 21 June (late cell division). Finally, in loquat, measurements were conducted on four fruits (one per tree) during the cell expansion and maturation stages, from 5 to 27 April. For all species, exposed fruits at about mid height of the canopy were selected.

The hourly Absolute Growth Rate (AGR; μm min^{-1}) and Relative Growth Rate (RGR; μm mm^{-1} min^{-1}) were calculated as follows: $AGR = (D_1 - D_0)/(t_1 - t_0)$ and $RGR = AGR/D$. In the equation, D_1 and D_0 are the fruit diameters at time t_1 and t_0, respectively.

2.7 Climate data

In peach, climate data were retrieved from the meteorological station of Riesi (Servizio Informativo Agrometeorologico Siciliano). In mango, data of temperature and humidity were acquired with a PCEHT71 data-logger (PCE Instrument, Jupiter, FL, USA) placed in the field. In orange, climate data were acquired with two weather stations (Pessl Instruments, WZ, Austria) positioned in the experimental plot. In olive, climate data were retrieved from the meteorological station of Sciacca (Servizio Informativo Agrometeorologico Siciliano). In loquat, temperature and relative humidity were measured at one-hour intervals using an Elitech RC-51H sensor (Elitech, London, UK) placed in the farm near the experimental plot.

Data of air temperature and relative humidity were used to calculate vapor pressure deficit (VPD, kPa) using the following equation:

$$VPD = VP_s - VP_a,$$

Where:

$$VP_s(\text{saturated vapor pressure}) = 0.6108 \exp[17.27T/(T + 237.3)]$$

$$VP_a(\text{actual vapor pressure}) = RH/100VP_s .$$

2.8 Statistical analysis

SYSTAT procedures (Systat Software Inc., Chicago, IL, USA) were used to carry out the daily linear regressions by group between VPD and RGR in order to obtain the coefficients (slopes) of each regression. Relationships between VPD and RGR over the whole fruit growth stages were obtained using Sigmaplot 14.0 procedures (Systat Software Inc., Chicago, IL, USA). Subsequently, the slopes of each period were compared by analysis of variance using the coefficients and standard errors from the regression output, followed by Tukey's multiple range test ($P< 0.05$) when appropriate.

3 Results and discussion

3.1 Climate data

During peach fruit monitoring, the average temperature was 26.8°C, with a maximum daily average temperature of 32.2°C reached on 5 July, and a minimum daily average temperature of 18.6°C reached on 28 May. The average relative humidity (RH) of the period was 46.3%, with a minimum daily average value of 22.0% recorded on 28 June. The maximum daily average RH was 79.2% recorded on 11 August mainly due to a heavy rainfall event (49.4 mm). The average VPD was 2.1 kPa, with a maximum daily average value of 3.84 kPa reached on 5 July (corresponding to the maximum daily average temperature), and the minimum daily average value of 0.72 kPa on 11 August (corresponding to the maximum daily average RH and the heaviest rainfall event) (Figure 1A).

During mango fruit monitoring, the average temperature was 25.9°C, with a maximum daily average temperature of 35.9°C reached on 22 July, and a minimum daily average temperature of 18.0°C reached on 3 October. The average RH of the period was 68.1%, with a minimum daily average value of 32.0% recorded on 8 August. The maximum daily average RH was 98.9%, recorded on 4 September during rainfall events (6.8 mm). Consequently, the maximum VPD was recorded on 8 August (1.97 kPa) and the minimum VPD on 4 September (0.23 kPa), with an average VPD of 1.11 kPa (Figure 1B).

During olive fruit monitoring, the average temperature was 23.5°C, while the maximum temperature was 27.4°C, reached on 29 August, and the minimum temperature was 18.9°C, reached on 12 October. The average RH was 66.4%, with a minimum value of 46.7% recorded on 29 August and a maximum RH of 82.6% recorded on 2 October, probably because of a rainfall event (15.8 mm). The average VPD was 1.1 kPa, with a maximum value reached on 29 August (2.15 kPa) (corresponding to the maximum temperature day), and the minimum value on 25 September (0.51 kPa) (corresponding to a rainfall event of 12.4 mm) (Figure 1C).

During orange fruit monitoring, the average temperature was 21.7°C, with a maximum temperature of 26.2°C reached on 15 June, and a minimum temperature of 18.2°C reached on 18 May. The average RH of the period was 64.4%, with a minimum value of

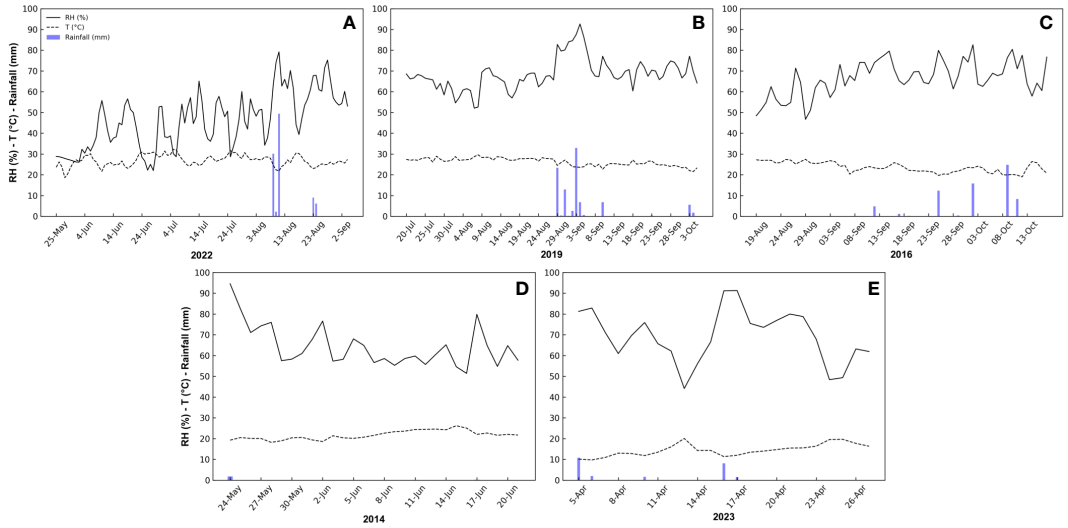

FIGURE 1
Daily trend of relative humidity (RH), temperature (T), rainfall, and vapor pressure deficit (VPD) during the monitoring periods of peach **(A)**, mango **(B)**, olive **(C)**, orange **(D)** and loquat **(E)** fruits at different locations and times in Sicily.

51.4% recorded on 16 June and a maximum RH of 100% recorded on 24 May, probably due to a rainfall event (1.8 mm). The average VPD was 1.1 kPa, with a maximum value reached on 15 June (1.8 kPa) (corresponding to the maximum temperature day), and the minimum value on 24 may (0.1 kPa) (corresponding to the day of maximum RH) (Figure 1D).

During loquat fruit monitoring, the average temperature was 14.4°C, with a maximum of 20.1°C reached on 13 April, and a minimum of 9.8°C reached on 6 April. The average RH of the period was 69.3 %, with a minimum of 44.2 % reached on 13 April and a maximum of 91.3 % reached on 17 April, probably due to a rainfall event (1.5 mm). The average VPD was 0.6 kPa, with a maximum reached on 13 April (1.4 kPa) (corresponding to the day with maximum temperature and minimum RH), and the minimum on 17 April (0.1 kPa) (corresponding to the day of maximum RH) (Figure 1E).

3.2 Peach

During cell division, VPD ranged widely between 0 and 6.3 kPa, but the majority of measurements was between 0.5 and 2.5 kPa (Figure 2A), while RGR ranged between -0.04 and 0.04 µm mm^{-1} min^{-1}, with most values concentrated between 0.02 and -0.02 µm mm^{-1} min^{-1} (Figure 2B).

A significant weak negative linear relationship between VPD and RGR was found at this stage (Figure 3A). Under the environmental conditions of the site and the period of the year, an inverse relationship may be expected since high levels of VPD may induce stomatal closure, resulting in reduced photosynthesis and fruit growth (Guichard et al., 2005).

A negative linear relationship between these two parameters was detected also at pit hardening (Figure 3B). At this stage, RGR ranged between -0.022 and 0.026 µm mm^{-1} min^{-1} but most of the values were in the range between -0.005 and 0.01 µm mm^{-1} min^{-1}, while VPD ranged widely between 0 and 7.2 kPa with most values between 1 and 4 kPa (Figure 2). As expected, in this period fluctuations in fruit RGR were smaller than at cell division (Lo Bianco and Scalisi, 2019; Scalisi et al., 2019a).

At cell expansion, RGR ranged between -0.04 and 0.04 µm mm^{-1} min^{-1} but most of the values were included between 0 and 0.02 µm mm^{-1} min^{-1}. VPD ranged between 0 and 6.7 kPa, with most of the values concentrated between 0 and 3.5 kPa (Figure 2). At this stage, a negative linear relationship between VPD and RGR similar to the previous two stages was detected (Figure 3C). The inverse relationship between VPD (one of the parameters driving transpiration) and fruit RGR at this stage could be attributed to changes in leaf conductance and their consequent ability to absorb water along the day, as well as to the competition for water between leaves and fruit (Grilo et al., 2019). It is worth noting that a significant portion of xylem water is directed towards transpiring leaves in the morning and during the midday, while fruit xylem inflow and RGR remain relatively low, as evidenced in peach (Morandi et al., 2007b), apple (Lang, 1990) and kiwifruit (Morandi et al., 2006). During this daytime, leaves act as strong water sinks (primarily influenced by VPD), and there is even a possibility of water loss by the fruit through backflow (Constantinescu et al., 2020). This causes a reduction in fruit growth. Large fluctuations in fruit RGR are the result of partial dehydration of the plants in part due to high VPD values (Figure 2B), in line with previous observations (Scalisi et al., 2019a).

Surprisingly, the dependence of RGR on VPD at cell expansion, when fruit water content is highest and cell growth strongly depends on water-driven cell turgor, was similar to the one at cell division, when water content is less directly involved in fruit growth. This suggests that similar levels of leaf stomatal limitation at the two

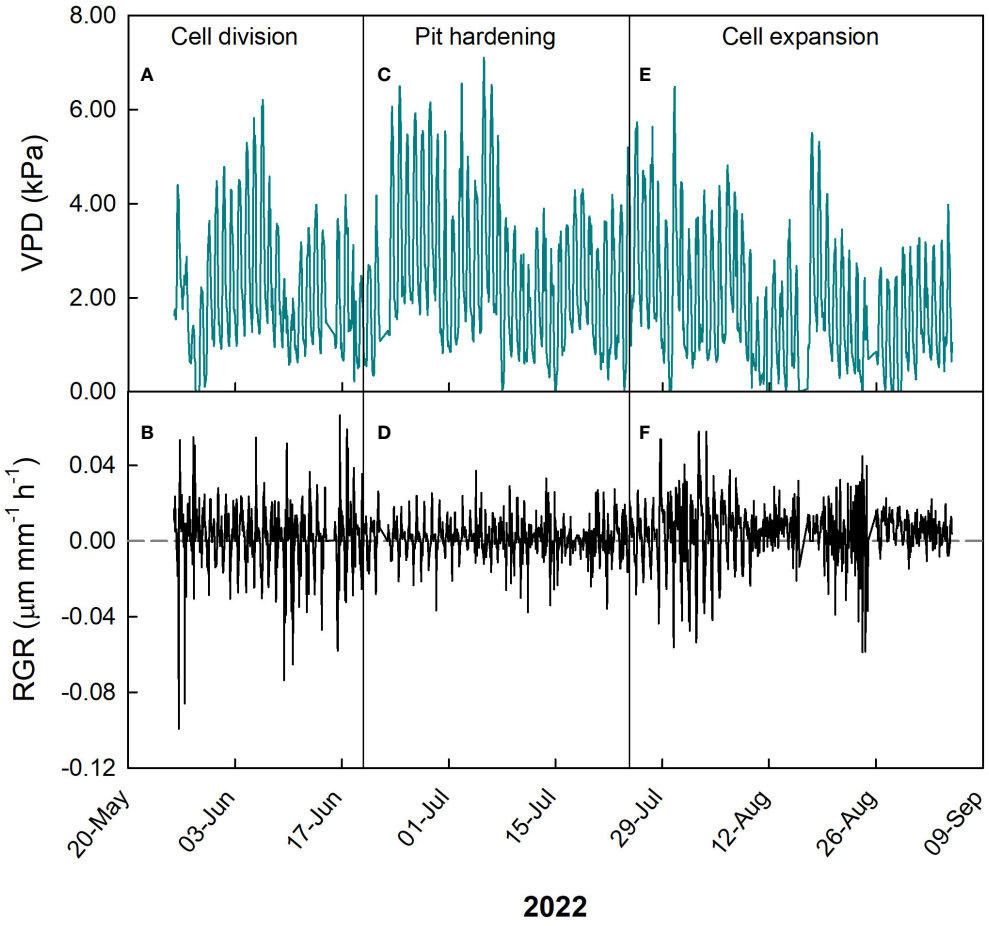

FIGURE 2
Hourly trends of vapor pressure deficit (VPD, **A**, **C**, **E**) and fruit relative growth rate (RGR, **B**, **D**, **F**) during growth stages of 'Tardivo 2000' peach in 2022 near Riesi, south Sicily.

fruit growth stages (cell division and cell expansion) may generate similar fruit growth regulation operated through totally different mechanisms, carbon fixation at cell division and water flows at cell expansion. This ultimately generates similar responses of fruit growth to atmospheric conditions. These results agree with results obtained by Morandi et al. (2007b), who found that patterns of daily fruit growth and phloem, xylem and transpiration flows are similar at cell division and expansion stages. Moreover, strong and similar linear relationships between fruit transpiration rate and VPD were found at both cell division and expansion.

Regarding the slopes of the daily relationships between VPD and RGR, only negative values can be seen during the period from late May to mid-July (Figure 4). Very negative values were found on June 14 and 15 (cell division stage), in which fruit growth was strongly influenced by VPD (Figure 4). In mid/late July, at the end of the pit hardening phase, a peak of positive values was found, indicating a period of optimum plant hydration as a result of frequent and abundant irrigation events. During cell expansion stage, a general linear increase of the slopes of the daily VPD-to-RGR relationships was found, indicating a transition from inverse to no relationship between VPD and RGR, i.e. a loss of fruit sensitivity to the atmospheric conditions.

3.3 Mango

In 'Keitt', during the cell division stage, RGR values ranged from -0.03 to 0.06 µm mm^{-1} min^{-1}, and VPD from 0.71 to 2.81 kPa (Figure 5).

A 2-segment piecewise linear relationship was found during the cell division stage (R^2 = 0.36, P< 0.001), with the following system (Figure 6A):

$$RGR = \begin{cases} \frac{0.033(1.591-VPD)-0.008(VPD-VPD_{min})}{1.591-VPD_{min}}, VPD \leq 1.591kPa \\ \frac{-0.008(VPD_{max}-VPD)+0.014(VPD-1.591)}{VPD_{max}-1.591}, VPD > 1.591kPa \end{cases}$$

The first segment of the piecewise has a negative slope, while the second has a positive slope. The breakpoint corresponds to a VPD value of 1.591 kPa. This means that the fruit, beyond the breakpoint value, increased its growth rate along with increasing VPD. The points after the breakpoint corresponded to times from 17:00 to 19:00, so when the fruits were regaining turgidity. This likely occurred because beyond that value, the plant tended to favor fruit growth instead of leaf carbon and water accumulation in the afternoon hours. A similar behavior was observed by Leonardi et al. (2000) in tomato fruit, where around 17:00 the fruit increased its

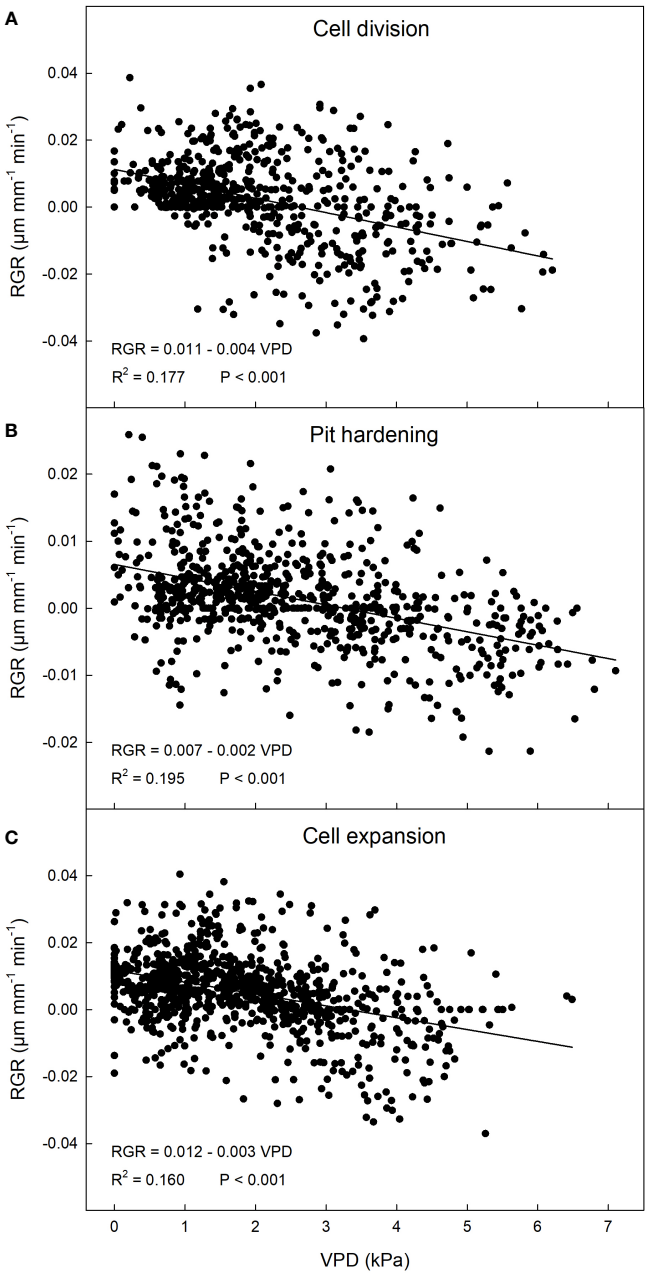

FIGURE 3
Relationship between vapor pressure deficit (VPD) and relative growth rate (RGR) in 'Tardivo 2000' peach at cell division **(A)**, pit hardening **(B)** and cell expansion **(C)** in 2022 near Riesi, south Sicily.

growth rate despite high VPD values, but no explanation was provided by the Authors. At cell expansion stage, RGR values ranged from -0.04 to 0.04 µm mm^{-1} min^{-1}, and VPD from 0.74 to 2.19 kPa (Figure 5A). In this case, a negative linear relationship between VPD and RGR was detected (R^2 = 0.56, P< 0.001) (Figure 6B). When cell expansion mechanisms prevail, water exchanges between the fruit and the atmosphere or the rest of the tree are main drivers of fruit growth, i.e., cell expansion is strongly influenced by the daily fluctuations of VPD. In addition, an increase in VPD, often caused by high temperatures, results in an increase in transpiration, which in turn reduces the xylem water potential and consequently decreases the xylem flow to the fruit, slowing down its enlargement (Tombesi et al., 2014). During the late cell expansion-maturation stage, RGR values ranged from -0.03 to 0.02 µm mm^{-1} min^{-1}, and VPD from 0.23 to 1.71 kPa (Figure 5A). Also at this stage, a negative linear relationship between the two parameters was identified (Figure 6C). However, the slope of the regression line at this stage is significantly less negative than the one at the cell expansion stage (P< 0.05). This indicates that the fruit, as maturation approaches, becomes less dependent on atmospheric environment probably due to both stomatal and xylem isolation mechanisms that prevent fruit water loss, while water inflow still

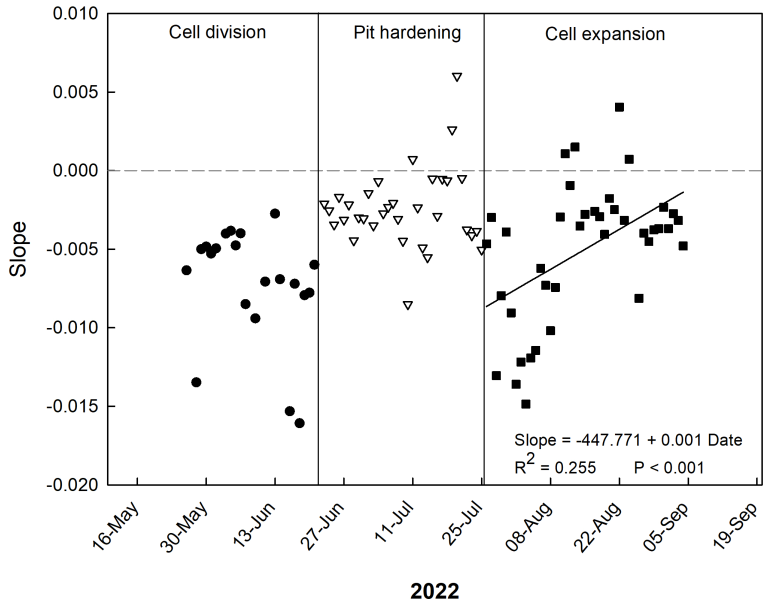

FIGURE 4
Trends of coefficients (slopes) of the daily linear regressions between VPD and RGR at the three stages of 'Tardivo 2000' peach fruit growth in 2022 near Riesi, south Sicily.

occurs via the phloem. Xylem interruption mechanisms near maturation have been documented in kiwifruit (Montanaro et al., 2012), grape (Keller et al., 2006; Choat et al., 2009), sweet cherry (Grimm et al., 2017) and apple (Dražeta et al., 2004).

Such responses are confirmed by the trend of the daily slopes of the relationships between VPD and RGR during the entire monitoring period (Figure 7A). At the cell division and late cell expansion-maturation stages, fruit growth was less influenced by VPD compared to the cell expansion stage, where coefficients were generally more negative, and an inverse trend was detected. This is in line with the principle that, at this stage, fruit growth is directly linked to water relations and xylem functionality, and thereby it responds quickly to VPD changes. Hence, going forward along this stage, the most negative slope values were reached. In the late cell expansion-maturation stage, the trend of daily slopes follows a piecewise pattern. Initially fruit growth responded to changes in

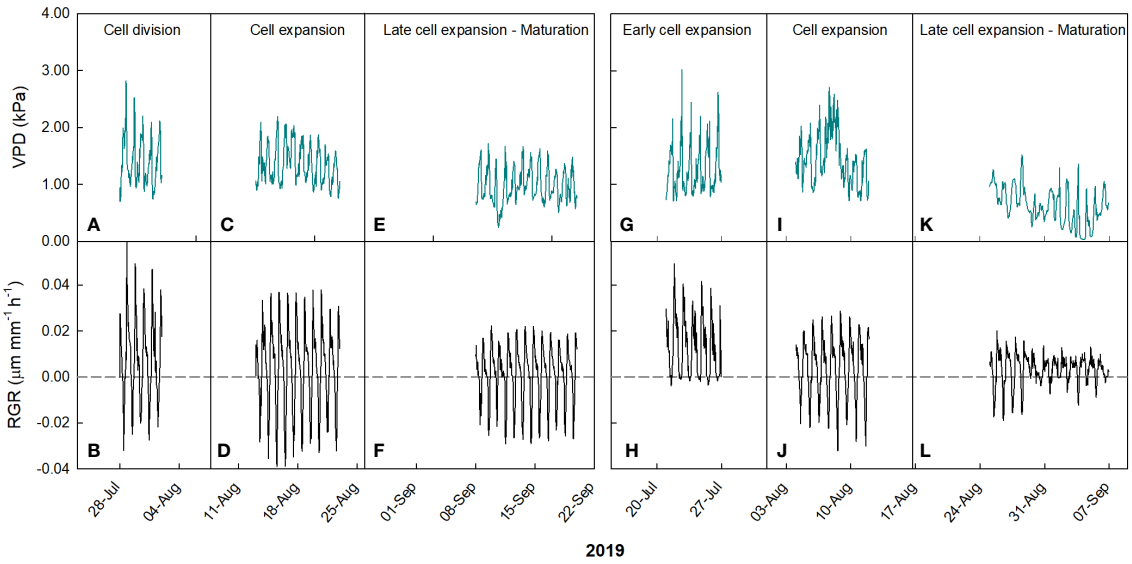

FIGURE 5
Hourly trends of vapor pressure deficit (VPD) in 'Keitt' **(A, C, E)** and 'Tommy Atkins' **(G, I, K)** mango and fruit relative growth rate (RGR) in 'Keitt' **(B, D, F)** and 'Tommy Atkins' **(H, J, L)** during growth stages in 2019 near Caronia, northeast Sicily.

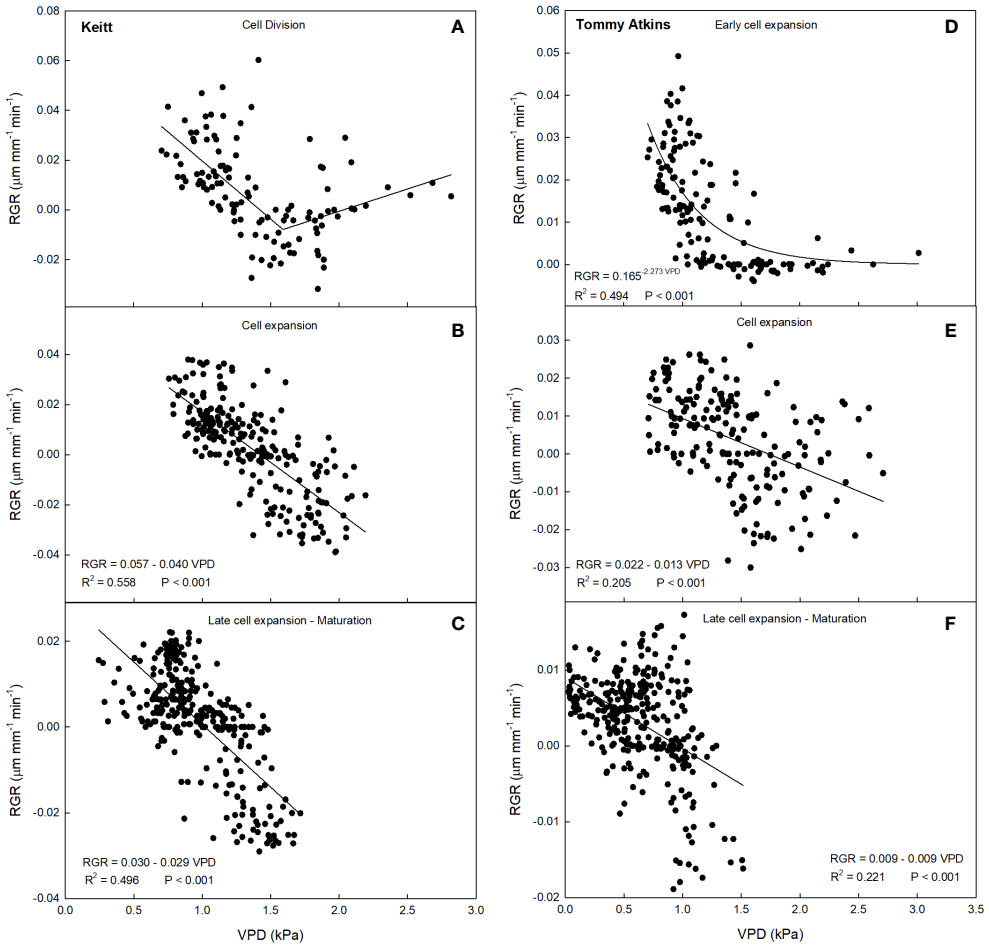

FIGURE 6
Relationship between vapor pressure deficit (VPD) and relative growth rate (RGR) in 'Keitt' **(A–C)** and 'Tommy Atkins' **(D–F)** mango during different fruit growth stages in 2019 near Caronia, northeast Sicily.

VPD similarly to cell expansion. At this specific point, climacteric fruits are characterized by a sharp increase of respiration, which is highly influenced by VPD and has been found to account for up to 39% of water losses in pear fruits (Xanthopoulos et al., 2017). However, a breakpoint is reached on 14 September (43722; days since 1 January 1900) at RGR = -0.044, and after that the fruit tended to respond less and less to VPD (Figure 7A). The piecewise model was the following:

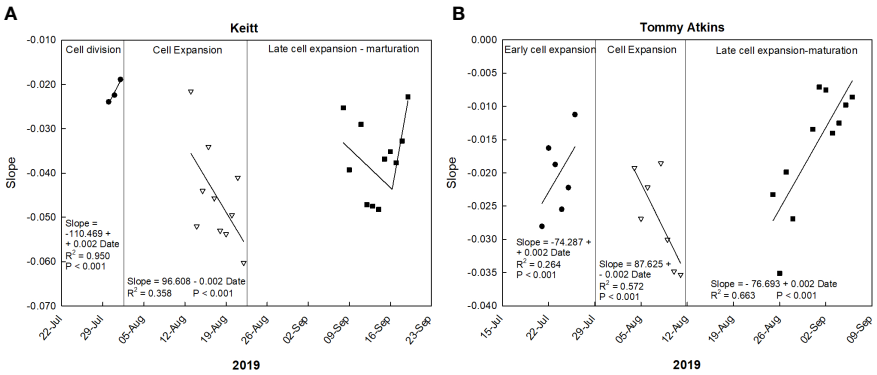

FIGURE 7
Trends of coefficients (slopes) of the daily linear regressions between VPD and RGR at different growth stages of 'Keitt' **(A)** and 'Tommy Atkins' **(B)** mango fruit in 2019 near Caronia, northeast Sicily.

$$Slope = \begin{cases} \frac{-0.033(43722.306-Date)-0.044(Date-Date_{min})}{43722.306-Date_{min}}, Date \leq 43722.306 \\ \frac{-0.044(Date_{max}-Date)-0.024(Date-43722.306)}{Date_{max}-43722.306}, VPD > 43722.306 \end{cases}$$

This may be because during maturation xylem flows and functionality are reduced and the fruit depends more on the phloem functionality and thereby on the vacuole osmotic gradient (Nordey et al., 2015). Moreover, it could be that at maturation, there is a threshold of water entering to the fruit, and the rest of water is recycled by backflow through xylem as observed in grapes (Keller et al., 2015). In 'Tommy Atkins', during the early cell expansion stage, RGR ranged from 0 to 0.05 μm mm^{-1} min^{-1}, and VPD from 0.70 to 3.01 kPa (Figure 5B). At this stage, the relationship between VPD and RGR was best described by an exponential decay model (Figure 6D). The model shows a strong inverse relation at the VPD interval 0.7 to 1.2 kPa, becoming gradually weaker until a VPD of about 1.5 kPa after which the effect on RGR is lost. At full cell expansion stage, RGR values ranged from -0.03 to 0.02 μm mm^{-1} min^{-1} and VPD from 0.71 to 2.70 kPa (Figure 5B). At this stage, a negative linear relationship between VPD and RGR was detected (Figure 6E), like in 'Keitt'. Finally, in the transition period between late cell expansion and maturation, RGR values ranged from -0.02 to 0.02 μm mm^{-1} min^{-1} and VPD from 0.01 to 1.52 kPa. A negative linear relationship was also found at this stage (Figure 6F), but with a significantly lower slope of the regression line compared to the cell expansion stage ($P< 0.05$). This difference confirms the trends observed in 'Keitt' fruit, i.e., the fruit tends to be decreasingly dependent on the atmospheric environment as maturation approaches.

Also in 'Tommy Atkins', these responses are confirmed by the trend of the daily slopes of the relationships between VPD and RGR during the entire monitoring period (Figure 7B). The strongest effect of VPD on fruit growth appears to be just in the middle of the cell expansion phase (end of July-beginning of August), while it tends to disappear after 2 September, when maturation processes begin.

3.4 Olive

In olive, two cultivars (Nocellara del Belice and Olivo di Mandanici) were considered at two different irrigation levels and at two fruit growth stages, cell expansion and late cell expansion-maturation. At the early cell expansion stage, the range of VPD was the same in both cultivars and irrigation treatments, from 0.02 to 4.01 kPa (Figure 8A). In 'Nocellara del Belice', RGR varied from

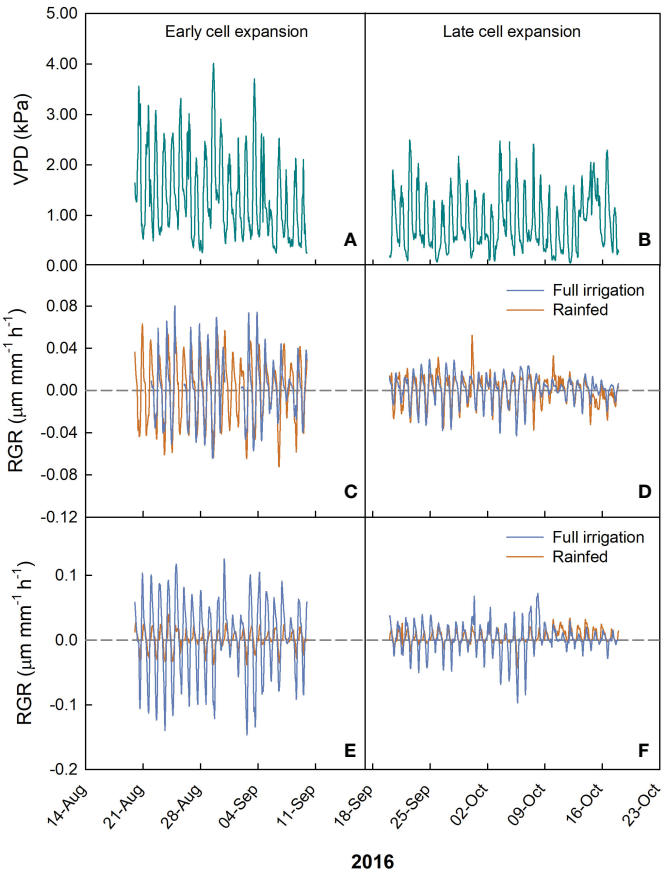

FIGURE 8
Hourly trends of vapor pressure deficit (VPD; **A, D**) and fruit relative growth rate (RGR) during early and late cell expansion stages of fruit growth in 'Nocellara del Belice' **(B, E)** and 'Olivo di Mandanici' **(C, F)** olive under full irrigation (blue lines) and rainfed (orange lines) conditions in 2016 near Sciacca, in southwestern Sicily.

-0.04 to 0.05 μm mm^{-1} min^{-1} in rainfed trees, and -0.06 to 0.08 μm mm^{-1} min^{-1} in full irrigated trees (Figure 8B), showing a relatively small but significant negative effect of water deficit on fruit growth. In 'Olivo di Mandanici', the range of RGR during early cell expansion was -0.04 to 0.04 μm mm^{-1} min^{-1} in fruits of rainfed trees and -0.14 to 0.12 μm mm^{-1} min^{-1} in fruits of full irrigated trees (Figure 8C), showing a relatively bigger effect of water deficit on fruit growth of this cultivar compared to Nocellara del Belice.

At late cell expansion-maturation stage, the range of VPD for both cultivars and irrigation treatments was from 0.04 to 2.46 kPa (Figure 8D). In 'Nocellara del Belice' fruit, the range of RGR was -0.04 to 0.03 μm mm^{-1} min^{-1} in full irrigated trees, and -0.04 to 0.05 μm mm^{-1} min^{-1} in rainfed trees (Figure 8E), showing no effect of water deficit on fruit growth. In 'Olivo di Mandanici' fruit, RGR ranged from -0.09 to 0.07 μm mm^{-1} min^{-1} in full irrigated trees and from -0.04 to 0.04 μm mm^{-1} min^{-1} in rainfed trees (Figure 8F), showing again major reductions of fruit growth in response to water deficit.

At the early cell expansion stage, a negative linear relationship was found between RGR and VPD in both fruits from rainfed and full irrigated trees (Figure 9A). Yet, the slope of the regression line from rainfed trees was more negative than the one from full irrigated trees (P< 0.001) during the early cell division. This indicates that at this stage, the negative effect of VPD on fruit RGR of 'Nocellara del Belice' is greater under non-optimal water conditions than under full irrigation, suggesting that irrigation compensates the fruit growth reduction due to VPD.

Negative linear relationships between RGR and VPD were found in both rainfed and full irrigated 'Olivo di Mandanici' trees (Figure 9B). In this case, the slope of full irrigated trees was significantly more negative than that of rainfed trees (P< 0.001), which was barely different from 0. This suggests that fruits of 'Olivo di Mandanici' trees under water deficit are able to keep adequate hydration by reducing growth and not responding to VPD changes. This may be accomplished by accumulating organic solutes and lowering fruit osmotic potential to maintain good hydration levels under unfavorable tree water status, indicating a greater ability of 'Olivo di Mandanici' to adjust osmotically, and a lower degree of isohydricity, compared to 'Nocellara del Belice' (Lo Bianco et al., 2013; Lo Bianco and Scalisi, 2017). It may be assumed that the relationship between RGR and VPD is strictly related to the ability of the plant to tolerate water deficit: the more tolerant the plant is, the less the fruit will be affected by VPD. This is in line with results found by Scalisi et al. (2020) indicating that 'Olivo di Mandanici' is more tolerant to water deficit than 'Nocellara del Belice', i.e. an evident genetic component.

Also at late cell expansion-maturation stage, negative linear relationships were found between VPD and RGR in rainfed and in full irrigated 'Nocellara del Belice' trees (Figure 9C). Similar to the early cell expansion stage, the slope of the regression line from rainfed trees was more negative than the one from full irrigated trees (P = 0.013). At both stages, 'Nocellara del Belice' showed the tendency of not reducing fruit growth under water deficit, probably at the expenses of tree water status.

At this stage, in 'Olivo di Mandanici', weaker negative linear relationships (in terms of slope and R^2) (Figure 9D) between VPD and RGR were found in both irrigation treatments compared to the early cell expansion stage (Figure 6D). This happened probably

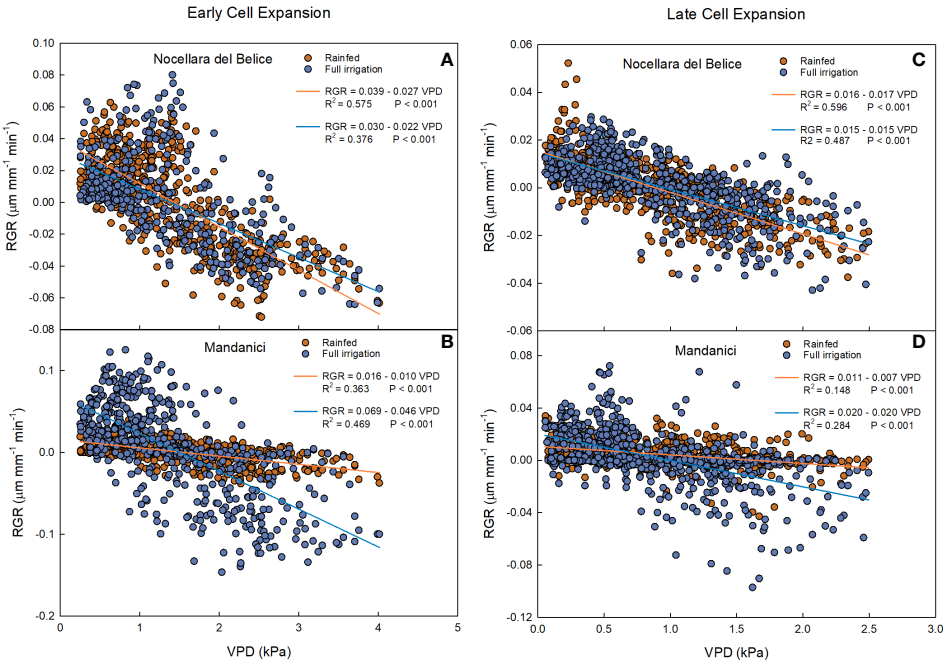

FIGURE 9
Relationship between vapor pressure deficit (VPD) and fruit relative growth rate (RGR) at early cell expansion (left) and late cell expansion (right) stages in 'Nocellara del Belice' **(A, C)** and 'Olivo di Mandanici' **(B, D)** olive trees under full irrigation (blue) and rainfed (orange) conditions in 2016 near Sciacca, in southwestern Sicily.

because the fruit of 'Olivo di Mandanici' was getting close to maturity and tended to isolate itself from environmental factors (VPD), so the fruit response to VPD changes was decreasing. Opposite to what happened in 'Nocellara del Belice', the slope of the regression line of full irrigated 'Olivo di Mandanici' trees was significantly more negative than that of rainfed trees (P< 0.001). This outcome can be related to the previous information: when a plant (such as the 'Olivo di Mandanici') shows greater tolerance to water stress, it suffers less impact on fruit growth from VPD.

The trends of the daily slopes of the relationships between VPD and RGR during the entire monitoring period showed a linear increase in all cases but in 'Olivo di Mandanici' under water deficit (Figure 10). In this last case, slopes remained constantly high, near 0 (Figure 10B), indicating a general lack of effect of VPD on fruit growth. The increasing trends confirm that the effect of VPD on fruit growth at this stage is linked to cell expansion activity. Indeed, cell expansion activity is directly associated to fruit water relations and therefore influenced by daily fluctuations in temperature, relative humidity, and vapor pressure deficit (VPD) (Lescourret et al., 2001).

3.5 Orange

In the case of 'Valencia' orange, two periods were monitored at the time when cell division mechanisms prevailed: before harvest of previous season fruit (24-31 May 2014) and after their harvest (16-21 June 2014). In May, VPD ranged from 0 (corresponding to rainy days) to 2.8 kPa (Figure 11A), while RGR ranged from -0.02 to 0.04 μm mm^{-1} min^{-1} (Figure 11B). On the other hand, in June, VPD ranged from 0.2 to 2.5 kPa (Figure 11C), and the fruit showed a wider range of RGR, from -0.04 to 0.08 μm mm^{-1} min^{-1} (Figure 11D).

Fruit growth dynamics were significantly influenced by VPD in both measurement periods. Specifically, a two-segment piece-wise model was found that accurately describes the relationship between

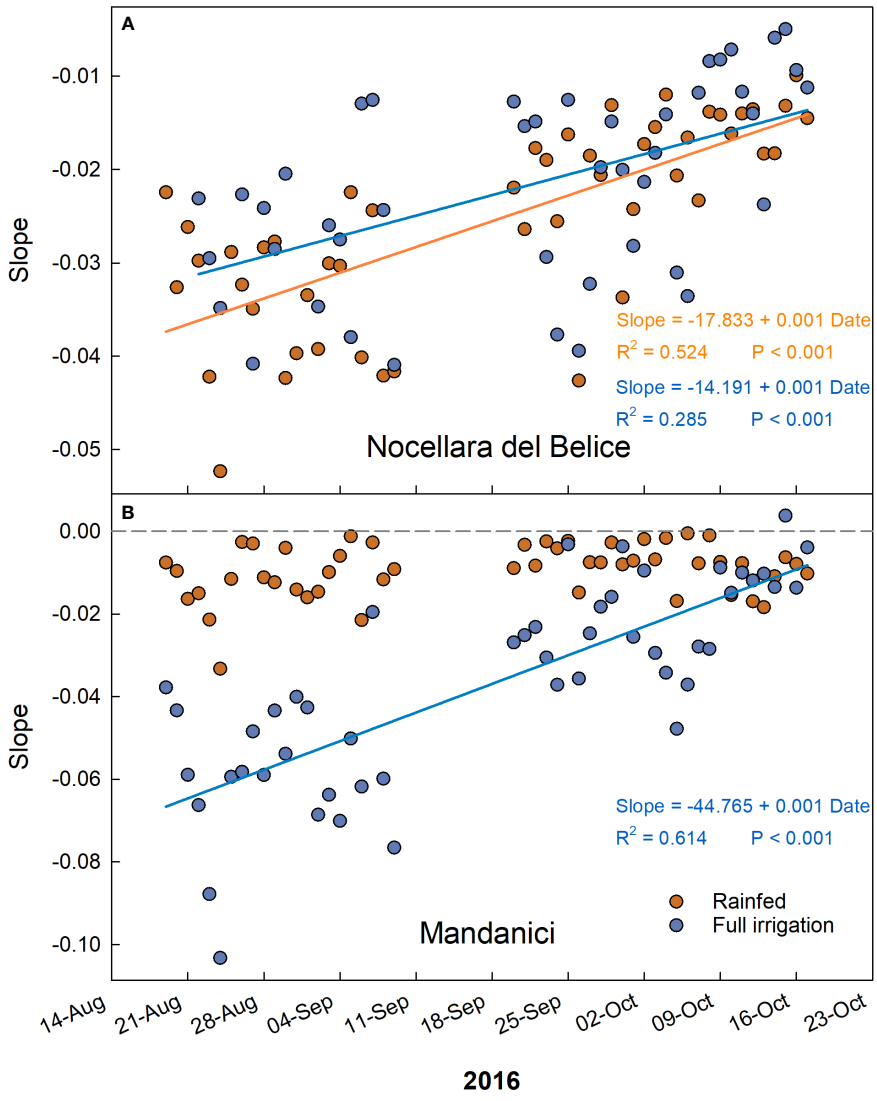

FIGURE 10
Trends of coefficients (slopes) of the daily linear regressions between VPD and RGR across early to late cell expansion stages of 'Nocellara del Belice' **(A)** and 'Olivo di Mandanici' **(B)** olive fruit growth in 2016 near Sciacca, in southwestern Sicily.

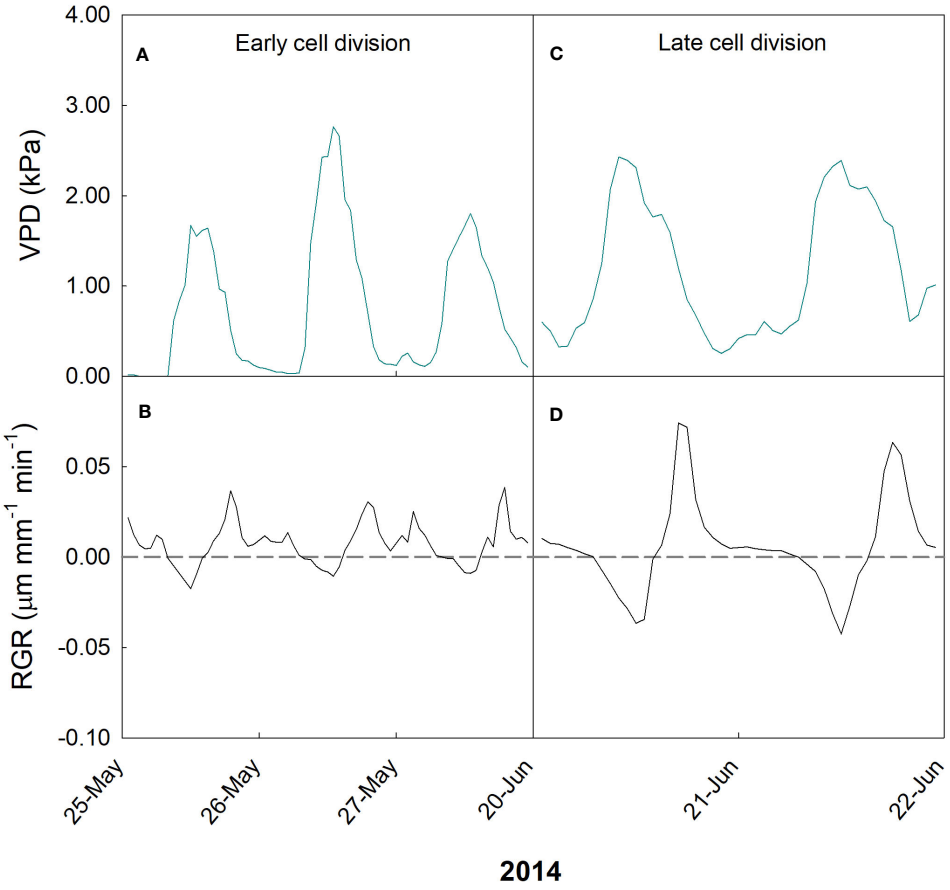

FIGURE 11
Hourly trends of vapor pressure deficit (VPD; **A, C**) and fruit relative growth rate (RGR; **B, D**) during early **(A, B)** and late **(C, D)** cell division stages of fruit growth in 'Valencia' orange in 2014 at the University of Palermo, Sicily.

VPD and fruit RGR (Figure 12). In May, the piecewise system was the following:

$$RGR = \begin{cases} \frac{0.007(0.524-VPD)+0.022(VPD-VPD_{min})}{0.524-VPD_{min}}, VPD \leq 0.524kPa \\ \frac{0.022(VPD_{max}-VPD)-0.019(VPD-0.524)}{VPD_{max}-0.524}, VPD > 0.524kPa \end{cases}$$

In June, the piecewise system was the following:

$$RGR = \begin{cases} \frac{-0.007(1.229-VPD)+0.064(VPD-VPD_{min})}{1.229-VPD_{min}}, VPD \leq 1.229kPa \\ \frac{0.064(VPD_{max}-VPD)-0.041(VPD-1.229)}{VPD_{max}-1.229}, VPD > 1.229kPa \end{cases}$$

At lower VPD values (during the night and early morning), there was a direct linear relationship between VPD and RGR, whereas an inverse relationship was observed at high VPD levels during the day and evening. These trends were consistent for both May and June, with a significant ($P< 0.001$) difference in the breakpoints, where the relationship inverted its trend. The inverse relationship between VPD and RGR shown in the second segment of the piecewise regression is similar to that observed in other fruits (see above) and can be explained by the negative effect of high VPD levels on stomatal conductance, which reduces fruit growth by limiting carbon assimilation. During the evening, there is typically a reduction in leaf transpiration (Matos et al., 1998; Morandi et al., 2014), and consequently stem sap flow also decreases, in accordance with VPD. This period is commonly when fruits initiate rehydration through xylem transportation (Morandi et al., 2010; Morandi et al., 2014), leading to an increase in RGR. In our study, this resulted in an inverse relationship between RGR and VPD. A breakpoint at higher VPD in June than in May can be explained by the removal of older fruits competing for carbon and water with young fruitlets (Grilo et al., 2019).

In the case of 'Valencia' orange, no specific trend of the coefficients (slopes) of the daily linear regressions between VPD and RGR was found, most likely because the two monitored periods were close in time and part of the same fruit development stage, early vs late cell division.

3.6 Loquat

During cell expansion stage of loquat fruit growth, VPD ranged between 0 and 2.6 kPa, but the majority of measurements was between 0.5 and 1.2 kPa (Figure 13A), while RGR ranged between -0.02 and 0.04 µm mm^{-1} min^{-1}, with most values concentrated between -0.005 and 0.02 µm mm^{-1} min^{-1} (Figure 13B). At the fruit maturation stage, VPD ranged between 0.07 and 2.1 kPa (Figure 13C), while RGR ranged

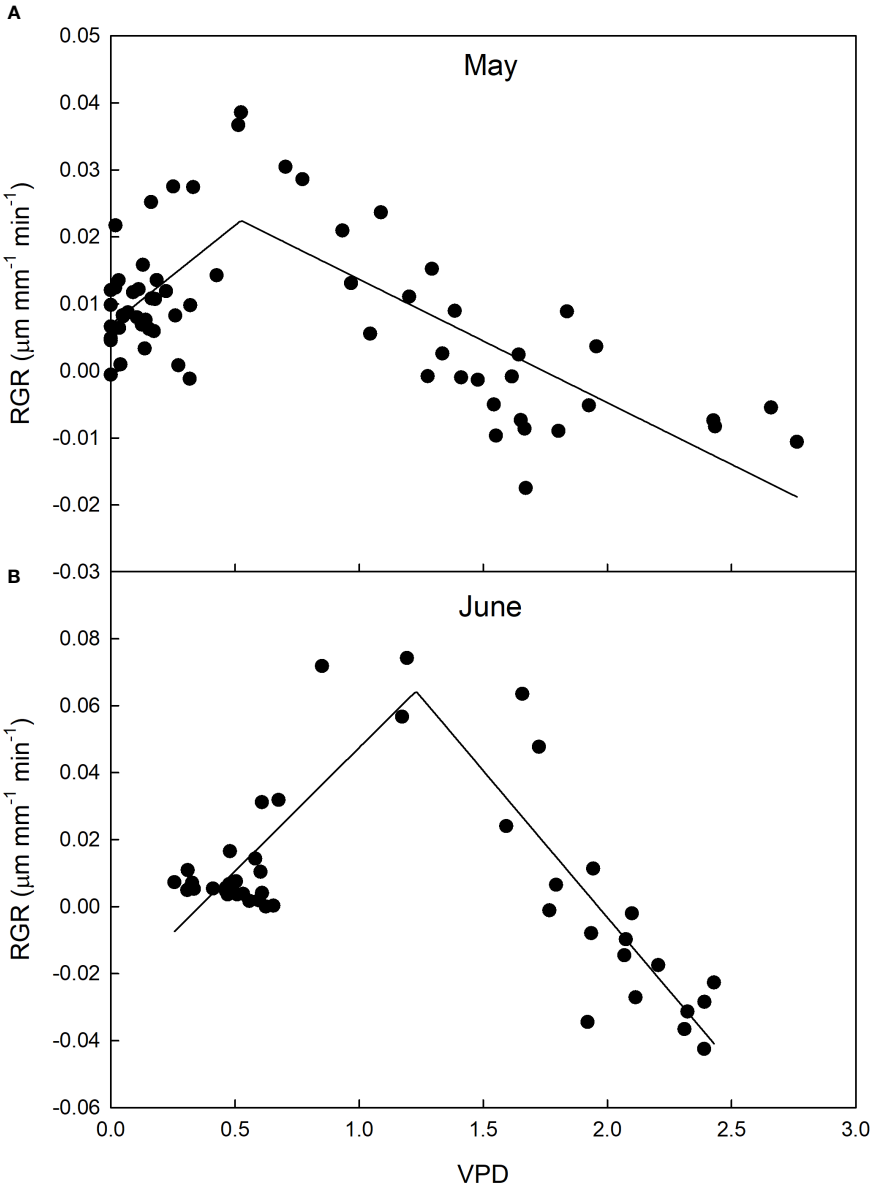

FIGURE 12
Relationship between vapor pressure deficit (VPD) and relative growth rate (RGR) of 'Valencia' orange fruit at cell division stage in May **(A)** and June **(B)**, before and after harvest of mature fruit, respectively in 2014 at the University of Palermo, Sicily.

between -0.002 and 0.03 µm mm^{-1} min^{-1} (Figure 13D), showing a relatively lower fluctuation of RGR compared to cell expansion stage. The latter is consistent with the beginning of fruit maturation.

At cell expansion stage, a weak negative linear relationship between VPD and RGR was found (Figure 14A). Considering the relatively mild VPD conditions due to the period of the year, a weak effect on fruit growth can be expected. At fruit maturation, a negative hyperbolic decay model best described the relationship between VPD and RGR (Figure 14B). Just like in olive and mango, this indicates that, as maturation progresses, the fruit becomes less dependent on atmospheric environment probably due to both the lowering of fruit osmotic potential and xylem isolation mechanisms that prevent fruit water loss.

As for the slopes of the daily relationships between RGR and VPD, a hyperbolic trend tending to 0 (non-significant relationship) was observed (Figure 15). In other words, as the fruit goes from cell expansion stage to maturation, its response to changes in VPD becomes weaker and weaker until it reaches a quasi-steady state of no response during maturation. Our results are in line with previous observations showing that, starting at veraison and all throughout maturation, the growth rate of the fruit is not particularly affected by climatic factors (Gariglio et al., 2002). The maturation period is indeed mainly characterized by decreasing acidity, sugar accumulation, color development, softening of the pulp tissue, and a rapid increase in the fresh weight of the pulp tissue (Lin et al., 1999).

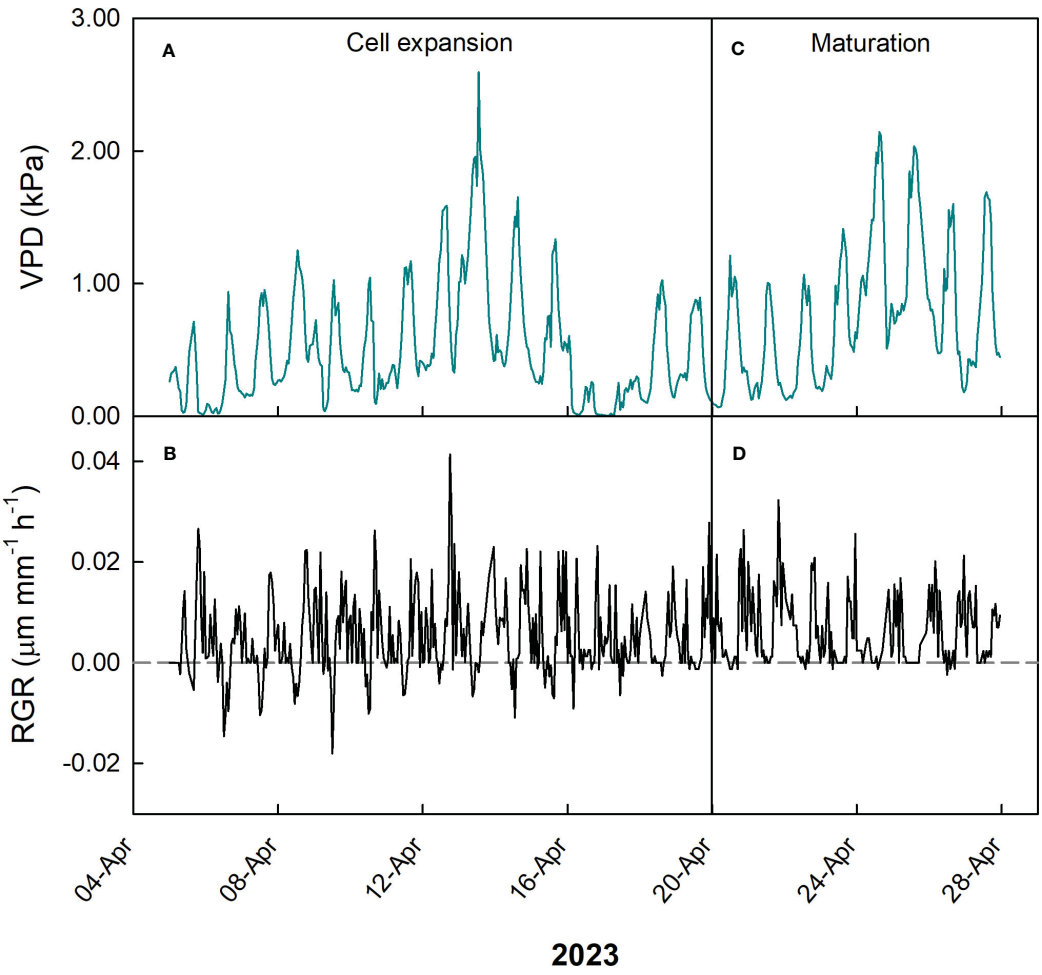

FIGURE 13
Hourly trends of vapor pressure deficit (VPD; **A, C**) and fruit relative growth rate (RGR; **B, D**) during cell expansion **(A, B)** and maturation **(C, D)** stages of fruit growth in 'Nespolone di Trabia' loquat in 2023 in Ciaculli, near Palermo, Sicily.

4 Conclusions

Overall, data collected at different growth stages of peach, mango, olive, orange and loquat fruits indicate a general effect of atmospheric water demand on fruit growth. Specifically, a consistent and more marked negative relationship between VPD and RGR was observed at cell expansion stage, when fruit growth is directly depending on water intake driving cell turgor. This indicates that, regardless of fruit type, VPD could be a powerful indicator of fruit growth and a useful parameter to be monitored for tree water management at this stage. Another behavior common to all observed species (with climacteric and non-climacteric fruits) was the gradual loss of relationship between VPD and RGR at the onset of fruit maturation. At this stage, fruit growth in size is generally programmed to stop and little to no effect of ambient conditions on RGR is observed, either because fruits tend to get hydraulically isolated from the outside and the rest of the plant or because excess of water entering the fruit may be recycled by backflow through the xylem. Sensitivity of fruit growth to ambient conditions at the fruit cell division stage seems to vary with species, time, and probably soil and atmospheric water deficit. We only have data from peach, mango, and orange and they do not seem to express a common behavior or mechanism. Especially 'Keitt' mango and 'Valencia' orange fruit growth responded to VPD in opposite ways; of course, time of the year and VPD levels were very different in the monitoring periods of the two species. At pit hardening stage of peach fruit growth, a relatively weak relationship was observed between VPD and RGR, and this is not surprising as fruit growth in size at this stage slows down significantly masking off any effect of atmospheric water demand on fruit growth. Finally, according to our findings, we can say that VPD may be a useful indicator of fruit growth and tree irrigation needs mainly when the cell expansion process prevails during fruit growth. These results are important especially considering the global change scenario predicting more tropical nights with higher temperatures and relative humidity but also temperature and drought extremes during summer days. Collection of more data at the cell division stage from fruits of different species might serve to clarify the role of atmospheric water demand on fruit growth and the possible usefulness of VPD as an indicator of tree irrigation needs.

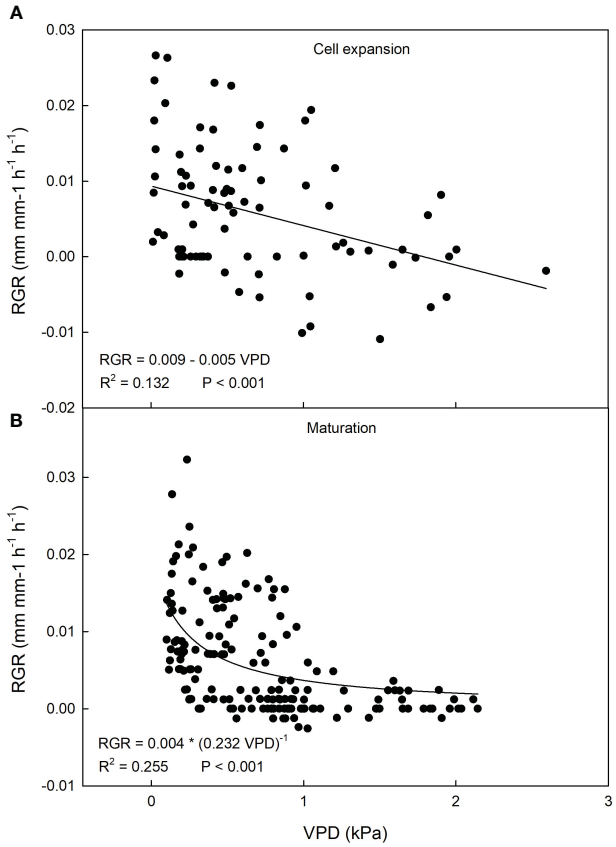

FIGURE 14
Relationship between vapor pressure deficit (VPD) and relative growth rate (RGR) of 'Nespolone di Trabia' loquat fruit at cell expansion **(A)** and maturation stage **(B)** in 2023 in Ciaculli, near Palermo, Sicily.

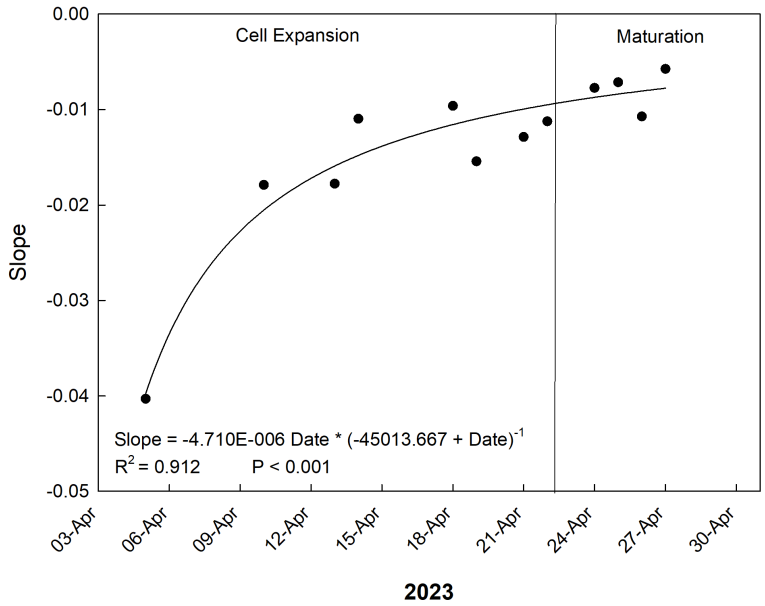

FIGURE 15
Trends of coefficients (slopes) of the daily linear regressions between VPD and RGR across late cell expansion to maturation stages of 'Nespolone di Trabia' loquat in 2023 in Ciaculli, near Palermo, Sicily.

Data availability statement

The raw data supporting the conclusions of this article will be made available by the authors, without undue reservation.

Author contributions

RB: Conceptualization, Data curation, Formal analysis, Funding acquisition, Methodology, Project administration, Supervision, Writing – original draft, Writing – review & editing. AC: Data curation, Formal analysis, Investigation, Validation, Visualization, Writing – original draft. RM: Data curation, Formal analysis, Funding acquisition, Investigation, Project administration, Writing – original draft.

Funding

The author(s) declare financial support was received for the research, authorship, and/or publication of this article. The present study was partly funded by the projects: Ecosistema dell'innovazione Sicilian MicronanoTech Research And Innovation Center -SAMOTHRACE. Fondo Finalizzato alla Ricerca di Ateneo FFR_D13_008811. European Project H2020-MSCA-RISE-2020 - ref. 101007702.

Acknowledgments

We would like to thank the farms Eco Farm s.r.l. (peach), Cupitur s.r.l. (mango), Rosario Bono (olive), Giuseppe Levantino (loquat) for hosting our trials. We would like also to thank the Sicilian agrometeorological service (Servizio Informativo Agrometeorologico Siciliano) for providing climate data of the peach and olive plots.

Conflict of interest

The authors declare that the research was conducted in the absence of any commercial or financial relationships that could be construed as a potential conflict of interest.

The author(s) declared that they were an editorial board member of Frontiers, at the time of submission. This had no impact on the peer review process and the final decision.

Publisher's note

References

Bardi, L., Nari, L., Morone, C., Solomita, M., Mandalà, C., Faga, M. G., et al. (2022). Kiwifruit adaptation to rising vapor pressure deficit increases the risk of kiwifruit decline syndrome occurrence. *Horticulturae* 8 (10), 906. doi: 10.3390/horticulturae8100906

Blanke, M. M., and Lenz, F. (1989). Fruit photosynthesis. *Plant Cell Environ.* 12 (1), 31–46. doi: 10.1111/j.1365-3040.1989.tb01914.x

Boini, A., Manfrini, L., Bortolotti, G., Corelli-Grappadelli, L., and Morandi, B. (2019). Monitoring fruit daily growth indicates the onset of mild drought stress in apple. *Sci. Hortic.* 256, 108520. doi: 10.1016/j.scienta.2019.05.047

Carella, A., Gianguzzi, G., Scalisi, A., Farina, V., Inglese, P., and Lo Bianco, R. (2021). Fruit growth stage transitions in two mango cultivars grown in a Mediterranean environment. *Plants* 10 (7), 1332. doi: 10.3390/plants10071332

Choat, B., Gambetta, G. A., Shackel, K. A., and Matthews, M. A. (2009). Vascular function in grape berries across development and its relevance to apparent hydraulic isolation. *Plant Physiol.* 151 (3), 1677–1687. doi: 10.1104/pp.109.143172

Constantinescu, D., Vercambre, G., and Génard, M. (2020). Model-assisted analysis of the peach pedicel–fruit system suggests regulation of sugar uptake and a water-saving strategy. *J. Exp. Bot.* 71 (12), 3463–3474. doi: 10.1093/jxb/eraa103

Corelli-Grappadelli, L., and Lakso, A. N. (2004). Fruit development in deciduous tree crops as affected by physiological factors and environmental conditions. *Acta Hortic.* 636, 425–441. doi: 10.17660/ActaHortic.2004.636.52

D'Andria, R., Lavini, A., Morelli, G., Patumi, M., Terenziani, S., Calandrelli, D., et al. (2004). Effects of water regimes on five pickling and double aptitude olive cultivars (*Olea europaea* L.). *J. Hortic. Sci. Biotechnol.* 70, 18–25. doi: 10.1080/14620316.2004.11511731

Del Rio, C., and Caballero, J. M. (2008). Variability and classification of olive cultivars by fruit weight, flesh/stone ratio and oil percentage. *Acta Hortic.* 791, 39–44. doi: 10.17660/ActaHortic.2008.791.2

Dražeta, L., Lang, A., Hall, A. J., Volz, R. K., and Jameson, P. E. (2004). Causes and effects of changes in xylem functionality in apple fruit. *Ann. Bot.* 93 (3), 275–282. doi: 10.1093/aob/mch040

Fernandes, R. D. M., Cuevas, M. V., Diaz-Espejo, A., and Hernandez-Santana, V. (2018). Effects of water stress on fruit growth and water relations between fruits and leaves in a hedgerow olive orchard. *Agr. Water Manage.* 210, 32–40. doi: 10.1016/j.agwat.2018.07.028

Fernández, J. E. (2014). Plant-based sensing to monitor water stress: Applicability to commercial orchards. *Agr. Water Manage.* 142, 99–109. doi: 10.1016/j.agwat.2014.04.017

Fich, E. A., Fisher, J., Zamir, D., and Rose, J. K. (2020). Transpiration from tomato fruit occurs primarily *via* trichome-associated transcuticular polar pores. *Plant Physiol.* 184 (4), 1840–1852. doi: 10.1104/pp.20.01105

Fletcher, A. L., Sinclair, T. R., and Allen, L. H.Jr. (2007). Transpiration responses to vapor pressure deficit in well watered 'slow-wilting' and commercial soybean. *Environ. Exp. Bot.* 61, 145–151. doi: 10.1016/j.envexpbot.2007.05.004

Gamage, T. V., and Rahman, M. S. (1999). *Postharvest handling of foods of plant origin* (New York, NY, USA: Marcel Dekker), 11–46.

Gariglio, N., Castillo, Á., Juan, M., Almela, V., and Agustí, M. (2002). *El Nispero japones. Técnicas para mejorar la calidad del fruto* (Valencia: Generalitat Valenciana, Conselleria d'Agricultura, Peixca i Alimentació), 61 pp.

Garrido, A., Conde, A., Serôdio, J., De Vos, R. C. H., and Cunha, A. (2023). Fruit photosynthesis: more to know about where, how and why. *Plants* 12 (13), 2393. doi: 10.3390/plants12132393

Génard, M., Dauzat, J., Franck, N., Lescourret, F., Moitrier, N., Vaast, P., et al. (2008). Carbon allocation in fruit trees: from theory to modelling. *Trees* 22, 269–282. doi: 10.1007/s00468-007-0176-5

Giovannoni, J. (2001). Molecular biology of fruit maturation and ripening. *Annu. Rev. Plant Biol.* 52, 725–749. doi: 10.1146/annurev.arplant.52.1.725

Grappadelli, L. C., Morandi, B., Manfrini, L., and O'Connell, M. (2019). Apoplasmic and simplasmic phloem unloading mechanisms: Do they co-exist in Angeleno plums under demanding environmental conditions? *J. Plant Physiol.* 237, 104–110. doi: 10.1016/j.jplph.2019.04.005

Grierson, W. (2002). "Fruit development, maturation and ripening," in *Handbook of Plant and Crop Physiology* (Boca Raton, FL, USA: CRC Press), 143–160.

Grilo, F. S., Scalisi, A., Pernice, F., Morandi, B., and Lo Bianco, R. (2019). Recurrent deficit irrigation and fruit harvest affect tree water relations and fruitlet growth in 'Valencia' orange. *Eur. J. Hortic. Sci.* 84 (3), 177–187. doi: 10.17660/eJHS.2019/84.3.8

Grimm, E., Pflugfelder, D., van Dusschoten, D., Winkler, A., and Knoche, M. (2017). Physical rupture of the xylem in developing sweet cherry fruit causes progressive decline in xylem sap inflow rate. *Planta* 246, 659–672. doi: 10.1007/s00425-017-2719-3

Gucci, R., Lodolini, E. M., and Rapoport, H. F. (2009). Water deficit-induced changes in mesocarp cellular processes and the relationship between mesocarp and endocarp during olive fruit development. *Tree Physiol.* 29, 1575–1585. doi: 10.1093/treephys/tpp086

Guichard, S., Gary, C., Leonardi, C., and Bertin, N. (2005). Analysis of growth and water relations of tomato fruits in relation to air vapor pressure deficit and plant fruit load. *J. Plant Growth Regul.* 24, 201–213. doi: 10.1007/s00344-005-0040-z

Hammami, S. B., Manrique, T., and Rapoport, H. F. (2011). Cultivar-based fruit size in olive depends on different tissue and cellular processes throughout growth. *Sci. Hortic.* 130, 445–451. doi: 10.1016/j.scienta.2011.07.018

Keller, M. (2010). Managing grapevines to optimise fruit development in a challenging environment: a climate change primer for viticulturists. *Aust. J. Grape Wine Res.* 16, 56–69. doi: 10.1111/j.1755-0238.2009.00077.x

Keller, M., Smith, J. P., and Bondada, B. R. (2006). Ripening grape berries remain hydraulically connected to the shoot. *J. Exp. Bot.* 57 (11), 2577–2587. doi: 10.1093/jxb/erl020

Keller, M., Zhang, Y., Shrestha, P. M., Biondi, M., and Bondada, B. R. (2015). Sugar demand of ripening grape berries leads to recycling of surplus phloem water *via* the xylem. *Plant Cell Envir.* 38, 1048–1059. doi: 10.1111/pce.12465

Lakshminarayana, S. (1973). Respiration and ripening patterns in the life cycle of the mango fruit. *J. Hortic. Sci.* 48, 227–233. doi: 10.1080/00221589.1973.11514525

Lang, A. (1990). Xylem, phloem and transpiration flows in developing apple fruits. *J. Exp. Bot.* 41 (6), 645–651. doi: 10.1093/jxb/41.6.645

Lavee, S., Hanoch, E., Wodner, M., and Abramowitch, H. (2007). The effect of predetermined deficit irrigation in the performance of cv. Muhasan (*Olea europaea* L.) in the eastern coastal plain of Israel. *Sci. Hortic.* 112, 156–163. doi: 10.1016/j.scienta.2006.12.017

Lavee, S., and Wodner, M. (2004). The effect of yield, harvest time and fruit size on the oil content in fruits of irrigated olive trees (*Olea europaea*), cvs. Barnea and Manzanillo. *Sci. Hortic.* 99, 267–277. doi: 10.1016/S0304-4238(03)00100-6

Léchaudel, M., Lopez-Lauri, F., Vidal, V., Sallanon, H., and Joas, J. (2013). Response of the physiological parameters of mango fruit (transpiration, water relations and antioxidant system) to its light and temperature environment. *J. Plant Physiol.* 170 (6), 567–576. doi: 10.1016/j.jplph.2012.11.009

Léchaudel, M., Vercambre, G., Lescourret, F., Normand, F., and Génard, M. (2007). An analysis of elastic and plastic fruit growth of mango in response to various assimilate supplies. *Tree Physiol.* 27 (2), 219–230. doi: 10.1093/treephys/27.2.219

Leonardi, C., Guichard, S., and Bertin, N. (2000). High vapour pressure deficit influences growth, transpiration and quality of tomato fruits. *Sci. Hortic.* 84, 285–296. doi: 10.1016/S0304-4238(99)00127-2

Lescourret, F., Génard, M., Habib, R., and Fishman, S. (2001). Variation in surface conductance to water vapor diffusion in peach fruit and its effects on fruit growth assessed by a simulation model. *Tree Physiol.* 21, 735–741. doi: 10.1093/treephys/21.11.735

Li, M., Feng, F., and Cheng, L. (2012). Expression patterns of genes involved in sugar metabolism and accumulation during apple fruit development. *PloS One* 7, e33055. doi: 10.1371/journal.pone.0033055

Lin, S., Sharpe, R. H., and Janick, J. (1999). Loquat: botany and horticulture. *Hortic. Rev.* 23, 233–276.

Lo Bianco, R., Panno, G., and Avellone, G. (2013). Characterization of Sicilian olive genotypes by multivariate analysis of leaf and fruit chemical and morphological properties. *J. Agr. Sci.* 5, 229–245. doi: 10.5539/jas.v5n11p229

Lo Bianco, R., and Scalisi, A. (2017). Water relations and carbohydrate partitioning of four greenhouse-grown olive genotypes under long-term drought. *Trees* 31, 717–727. doi: 10.1007/s00468-016-1502-6

Lo Bianco, R., and Scalisi, A. (2019). Phloem and xylem flow contributions to nectarine fruit development. *Acta Hortic.* 1314, 463–470. doi: 10.17660/ActaHortic.2021.1314.57

Marino, G., Scalisi, A., Guzmán-Delgado, P., Caruso, T., Marra, F. P., and Lo Bianco, R. (2021). Detecting mild water stress in olive with multiple plant-based continuous sensors. *Plants* 10 (1), 131. doi: 10.3390/plants10010131

Massenti, R., Scalisi, A., Marra, F. P., Caruso, T., Marino, G., and Lo Bianco, R. (2022). Physiological and structural responses to prolonged water deficit in young trees of two olive cultivars. *Plants* 11 (13), 1695. doi: 10.3390/plants11131695

Matos, M. C., Matos, A. A., Mantas, A., Cordeiro, V., and Vieira da Silva, J. B. (1998). Photosynthesis and water relations of almond tree cultivars grafted on two rootstocks. *Photosynthetica* 34, 249–256. doi: 10.1023/A:1006896708742

Montanaro, G., Dichio, B., Xiloyannis, C., and Lang, A. (2012). Fruit transpiration in kiwifruit: environmental drivers and predictive model. *AoB Plants* 2012, pls036. doi: 10.1093/aobpla/pls036

Morandi, B., Corelli Grappadelli, L., Rieger, M., and Lo Bianco, R. (2008). Carbohydrate availability affects growth and metabolism in peach fruit. *Physiol. Plant* 133 (2), 229–241. doi: 10.1111/j.1399-3054.2008.01068.x

Morandi, B., Losciale, P., Manfrini, L., Zibordi, M., Anconelli, S., Pierpaoli, E., et al. (2014). Leaf gas exchanges and water relations affect the daily patterns of fruit growth and vascular flows in Abbé Fétel pear (*Pyrus communis* L.) trees. *Sci. Hortic.* 178, 106–113. doi: 10.1016/j.scienta.2014.08.009

Morandi, B., Losciale, P., Manfrini, L., Zibordi, M., Studhalter, M., and Corelli Grappadelli, L. (2006). The growth of the kiwifruit in its final stages. *Acta Hortic.* 753, 369–374. doi: 10.17660/ActaHortic.2007.753.46

Morandi, B., Manfrini, L., Losciale, P., Zibordi, M., and Corelli-Grappadelli, L. (2010). The positive effect of skin transpiration in peach fruit growth. *J. Plant Physiol.* 167 (13), 1033–1037. doi: 10.1016/j.jplph.2010.02.015

Morandi, B., Manfrini, L., Zibordi, M., Noferini, M., Fiori, G., and Corelli Grappadelli, L. (2007a). A low-cost device for accurate and continuous measurements of fruit diameter. *HortScience* 42 (6), 1380–1382. doi: 10.21273/HORTSCI.42.6.1380

Morandi, B., Rieger, M., and Grappadelli, L. C. (2007b). Vascular flows and transpiration affect peach (Prunus persica Batsch.) fruit daily growth. *J. Exp. Bot.* 58 (14), 3941–3947. doi: 10.1093/jxb/erm248

Mossad, A., Scalisi, A., and Lo Bianco, R. (2018). Growth and water relations of field-grown 'Valencia' orange trees under long-term partial rootzone drying. *Irrig. Sci.* 36, 9–24. doi: 10.1007/s00271-017-0562-8

Noh, H., and Lee, J. (2022). The effect of vapor pressure deficit regulation on the growth of tomato plants grown in different planting environments. *Appl. Sci.* 12 (7), 3667. doi: 10.3390/app12073667

Nordey, T., Léchaudel, M., and Génard, M. (2015). The decline in xylem flow to mango fruit at the end of its development is related to the appearance of embolism in the fruit pedicel. *Funct. Plant Biol.* 42, 668–675. doi: 10.1071/FP14306

Paul, V., Pandey, R., and Srivastava, G. C. (2012). The fading distinctions between classical patterns of ripening in climacteric and non-climacteric fruit and the ubiquity of ethylene—An overview. *J. Food Sci. Tech.* 49, 1–21. doi: 10.1007/s13197-011-0293-4

Rahmati, M., Davarynejad, G. H., Génard, M., Bannayan, M., Azizi, M., and Vercambre, G. (2015). Peach water relations, gas exchange, growth and shoot mortality under water deficit in semi-arid weather conditions. *PloS One* 10 (4), e0120246. doi: 10.1371/journal.pone.0120246

Rančić, D., Quarrie, S. P., and Pećinar, I. (2010). Anatomy of tomato fruit and fruit pedicel during fruit development. *Microscopy: Science technology Appl. Educ.* 2, 851–861.

Rooban, R., Shanmugam, M., Venkatesan, T., and Tamilmani, C. (2016). Physiochemical changes during different stages of fruit ripening of climacteric fruit of mango (*Mangifera indica* L.) and non-climacteric of fruit cashew apple (*Anacardium occidentale* L.). *J. Appl. Adv. Res.* 1 (2), 53–58. doi: 10.21839/jaar.2016.v1i2.27

Scalisi, A., Marino, G., Marra, F. P., Caruso, T., and Lo Bianco, R. (2020). A cultivar-sensitive approach for the continuous monitoring of olive (Olea europaea L.) tree water status by fruit and leaf sensing. *Front. Plant Sci.* 11, 340. doi: 10.3389/fpls.2020.0034.0

Scalisi, A., Morandi, B., Inglese, P., and Lo Bianco, R. (2016). Cladode growth dynamics in Opuntia ficus-indica under drought. *Environ. Exp. Bot.* 122, 158–167. doi: 10.1016/j.envexpbot.2015.10.003

Scalisi, A., O'Connell, M. G., Stefanelli, D., and Lo Bianco, R. (2019a). Fruit and leaf sensing for continuous detection of nectarine water status. *Front. Plant Sci.* 10. doi: 10.3389/fpls.2019.00805

Scalisi, A., O'Connell, M. G., Turpin, S. R., and Lo Bianco, R. (2019b). Diurnal irrigation timing affects fruit growth in late-ripening nectarines. *Acta Hortic.* 1314, 61–68. doi: 10.17660/ActaHortic.2021.1314.9

Somboonkaew, N., and Terry, L. A. (2010). Altered physiology and biochemistry of imported litchi fruit held under different vapor pressure deficits. *J. Agr. Food Chem.* 58, 6209–6218. doi: 10.1021/jf100023x

Tombesi, S., Day, K. R., Johnson, R. S., Phene, R., and DeJong, T. M. (2014). Vigour reduction in girdled peach trees is related to lower midday stem water potentials. *Funct. Plant Biol.* 41, 1336–1341. doi: 10.1071/FP14089

Tomkiewicz, D., and Piskier, T. (2012). A plant-based sensing method for nutrition stress monitoring. *Precis. Agric.* 13, 370–383. doi: 10.1007/s11119-011-9252-3

Xanthopoulos, G. T., Templalexis, C. G., Aleiferis, N. P., and Lentzou, D. I. (2017). The contribution of transpiration and respiration in water loss of perishable agricultural products: The case of pears. *Biosyst. Engin.* 158, 76–85. doi: 10.1016/j.biosystemseng.2017.03.011

Yuan, W., Zheng, Y., Piao, S., Ciais, P., Lombardozzi, D., Wang, Y., et al. (2019). Increased atmospheric vapor pressure deficit reduces global vegetation growth. *Sci. Adv.* 5, eaax1396. doi: 10.1126/sciadv.aax1396

Zarrouk, O., Pinheiro, C., Misra, C. S., Fernández, V., and Chaves, M. M. (2018). Fleshy fruit epidermis is a protective barrier under water stress. *Water Scarcity Sust. Agric. Semiarid Envir.* chap. 20, 507–533. doi: 10.1016/B978-0-12-813164-0.00020-X

CHAPTER 4.

Combining proximal and remote sensing to assess ‘Calatina’ olive water status

Based on the paper:
Carella, A., Massenti, R., Marra, F.P., Catania, P., Roma, E., Lo Bianco, R. (2024). Combining proximal and remote sensing to assess ‘Calatina’ olive water status. **Submitted** in *Frontiers in Plant Science*

Combining proximal and remote sensing to assess 'Calatina' olive water status

Alessandro Carella*, Roberto Massenti, Francesco Paolo Marra, Pietro Catania, Eliseo Roma, & Riccardo Lo Bianco

Department of Agricultural, Food and Forest Sciences (SAAF), University of Palermo, 90128 Palermo, Italy
*Corresponding author.
Email of corresponding author: alessandro.carella@unipa.it

Abstract

Developing an efficient and sustainable precision irrigation strategy is crucial in contemporary agriculture. This study aimed to integrate proximal and remote sensing techniques to show the benefits of using both monitoring methods, simultaneously assessing the water status and response of 'Calatina' olive under two distinct irrigation levels: full irrigation (FI), and drought stress (DS, -3.5 to 4 MPa). Stem water potential (Ψ_{stem}) and stomatal conductance (g_s) were monitored weekly as reference indicators of plant water status. Crop water stress index (CWSI) and stomatal conductance index (Ig) were calculated through ground-based infrared thermography. Fruit gauges were used to monitor continuously fruit growth and data were converted in fruit daily weight fluctuations (ΔW) and relative growth rate (RGR). Normalized difference vegetation index (NDVI), normalized difference RedEdge index (NDRE), green normalized difference vegetation index (GNDVI), chlorophyll vegetation index (CVI), modified soil-adjusted vegetation index (MSAVI), water index (WI), normalized difference greenness index (NDGI) and green index (GI) were calculated from data collected by UAV-mounted multispectral camera. Data obtained from proximal sensing were correlated with both Ψ_{stem} and g_s, while remote sensing data were correlated only with Ψ_{stem}. Regression analysis showed that both CWSI and Ig proved to be reliable indicators of Ψ_{stem} and g_s. Of the two fruit growth parameters, ΔW exhibited a stronger relationship, primarily with Ψ_{stem}. Finally, NDVI, GNDVI, WI and NDRE emerged as the vegetation indices that correlated most strongly with Ψ_{stem}, achieving high R^2 values. Further studies on integrating proximal and remote sensing data will be necessary in order to find strategic combinations of sensors and establish intervention thresholds.

Introduction

In recent years, climate change has created serious problems regarding the availability and use of water in agriculture, especially in areas characterized by scarce rainfall and high temperatures during the summer (Konapala et al. 2020; Pokhrel et al. 2021). These conditions of severe drought are occurring in the Mediterranean basin, creating significant challenges for local agriculture (Carella et al. 2023).

Deficit irrigation has been demonstrated to be the most effective method for achieving optimum yields and efficient water use in regions confronted with water scarcity (Nikolaou et al. 2020). The objective of implementing a deficit irrigation strategy is to achieve satisfactory crop yields by supplying the crop with a reduced irrigation volume compared to its potential water requirements (Tong et al. 2022). Growing crops that are well-adapted to water deficit conditions (deficit irrigation) is one of the strategies to achieve satisfactory productivity without the overuse of water resources (Gómez-Bellot et al. 2024). In this context, the olive tree (*Olea europaea* L.) emerges as a highly resilient species to water stress, with its production being influenced not only by climatic factors but also by management practices (Massenti et al. 2022b).

Another important aspect of current olive cultivation is the trend towards adopting high-density (HD) planting systems and mechanizing cultural operations. Combining the advantages of comprehensive mechanization, precision agriculture techniques, and the use of local cultivars that well adapt to the climate and soil can greatly reduce production costs associated with labor expenses (Lo Bianco et al. 2021). An olive cultivar that fits well modern growing systems (i.e., high planting density and level of mechanization) is 'Calatina', a minor Sicilian cultivar recently rediscovered thanks to its low vigor and high yield efficiency. 'Calatina' also possesses a degree of shoot bending and branching density suitable for HD and super-high-density (SHD) planting systems along with high harvesting efficiency (large fruits), demonstrating similar or better productive performance than 'Arbequina', the most widespread cultivar for HD and SHD systems (Caruso et al. 2021; Carella et al. 2022; Massenti et al. 2022a). Under HD and SHD systems, water needs and irrigation management become crucial to reach optimum yields and high quality final products. However, there are no studies on 'Calatina' water status assessment and irrigation management.

Studying how olive orchards respond to external influences presents significant challenges due to the diverse range of environments across the Mediterranean and the wide variety of planting systems employed. Prolonged periods of drought stress can trigger various physiological responses in olive trees. These include the closure of stomata (Mairech et al. 2021; Carella et al. 2023), limitation of photosynthesis (Melaouhi et al. 2021), decreased gas exchange (Pierantozzi et al. 2020), and osmotic adjustments (Scalisi et al. 2020; Marino et al. 2021; Abboud et al. 2021). When favorable water conditions return after a period of water deficit, olive trees undergo partial recovery in processes such as transpiration, photosynthesis, chlorophyll fluorescence indices, and osmotic potential (Connor 2005; Fernandez 2014). This implies that while tissue water content may rapidly increase, leaf function may take several days to fully restore, depending on the severity of the preceding stress (Fernandez 2014; Wahab et al. 2022).

The timing of irrigation events can be supported by data related to either soil moisture content or plant water status (Bazzi et al. 2019). The established conventional method for assessing plant water status is by measuring Ψ_{stem} using Scholander's pressure chamber. However, this method is labor-intensive and time-consuming, and requires high skills by

operators. In recent years, technological advancements have enabled the testing and introduction of various plant-based sensors for assessing plant water status and improve irrigation water management in orchard systems. While many of these sensors do not directly measure plant water status, they monitor specific physiological processes that demonstrate varying correlations with plant water status. However, due to the multitude of factors influencing tree physiological responses, such as tree phenological stage, environmental conditions, and genotype-specific traits, the development of simplified and standardized water management protocols using these sensors remains complex (Cocozza et al. 2015; Scalisi et al. 2020). In the mean time, remote and proximal sensing technologies for assessing field variability are becoming increasingly common in precision agriculture. This trend is propelled by their relatively lower costs and non-invasive nature compared to conventional methods (Caruso et al. 2022a).
The use of proximal sensing techniques, such as infrared thermography (Ben-Gal et al. 2009) and daily fruit diameter variation by fruit gauges (Morandi et al. 2007; Boini et al. 2019; Giovannini et al. 2022; Khosravi et al. 2022; Carella et al. 2023), are potentially effective and continuous methods to assess plant water status. Scalisi et al. (2020) observed that coupling Ψ_{stem} with fruit gauges and leaf patch clamp pressure probes (LPCP probes) data can be a reliable tool for evaluating fruit tree water status and smarter irrigation management. Moreover, García-Tejero et al., (2018) determined that the infrared thermography approach has a great advantage due to the large amount of information provided. The use of infrared thermography has proved to be a suitable technique for monitoring the water status of fruit trees (Egea et al. 2016; García-Tejero et al. 2018; Blanco et al. 2023). In details, the most utilized method for plant water status assessment involves the normalization of canopy temperature through the calculation of some indices, e.g., crop water stress index (CWSI) and stomatal conductance index (Ig) (Jackson et al. 1981; Idso 1982; Jones et al. 2002).
Remote sensing techniques enable the rapid detection of spatial variability over large areas using thermal or multispectral cameras. Among the most common platforms used in remote sensing for detailed scale irrigation management are Unmanned Aerial Vehicles (UAVs), suitable for non-intensive agriculture (Roma and Catania 2022). Several studies have found that remote sensing over olive orchards can provide an accurate estimation of tree water status. Most studies emphasize that remote sensing with thermal cameras is highly correlated with plant water status (Ben-Gal et al. 2009; Egea et al. 2016; Caruso et al. 2022b). However, these techniques have some limitations, mainly related to the calculation method used to determine the CWSI (Berni et al., 2009). Nonetheless, detection of spectral plant condition also allows for an estimation of plant water status (Marino et al. 2014; Rallo et al. 2014; Marques et al. 2023). Indeed, several studies have obtained correlations between various vegetation indices and plant water conditions. Among the most used indices, we find normalized difference vegetation index (NDVI, Rouse et al., 1974), normalized difference RedEdge (NDRE, Maccioni et al., 2001), and indices that utilize the Short Wave InfraRed (SWIR) band. Although the latter indices are very efficient, they cannot be obtained from normal multispectral cameras, but only from spectroradiometers or hyperspectral cameras (Herrmann et al. 2010). For this reason, water stress conditions are increasingly being investigated and detected with normal multispectral cameras, as they are cheaper and easier to use.
The combined use of proximal and remote sensing techniques can offer a more comprehensive and accurate indication of plant water status and irrigation requirements. Proximal sensors provide accurate and continuous real-time data for individual plants, while data from UAVs or satellites can extend coverage across the field (Matese et al. 2018; Jin et al. 2022). Remote sensing data provide valuable information on spatial variability through effective field mapping, allowing the strategic positioning of proximal sensors only in certain areas of the field (Alexopoulos et al. 2023; Roma et al. 2023). Data collected by soil electrical conductivity sensors and UAVs were used by Caruso et al. (2022) to delineate homogeneous zones within a densely irrigated olive orchard. They observed that tree water use efficiency (WUE) varies according to the placement within the orchard. Furthermore, they found that tree vigor emerges as a predominant factor affecting the final fruit yield under optimal water availability.
On these bases, this study aims to integrate proximal and remote sensing techniques to show the benefits of using both monitoring methods, while simultaneously assessing the water status and response of 'Calatina' olive under two distinct irrigation regimes.

Material and Methods

The experiment was conducted from summer to fall 2023, in a high-density olive orchard (6 x 2 spacing, 833 trees/ha) located near Sciacca (37°29' N and 13°12' E, 138 m a.s.l., Fig. 1A). Eleven-year-old own-rooted trees were trained to "free palmette" along North-South-oriented hedgerows. The Sicilian cultivar Calatina was selected as potentially suitable for new high-density plantings mainly due to its low vigor, high productivity and good olive oil quality (Massenti et al. 2022a). The soil is a sandy-clay-loam (60% sand, 18% silt, 22% clay), with pH 7.7 and low active carbonates (<5 %). Trees were regularly fertilized and pruned according to ordinary practices.

Air temperature (T) and relative humidity (RH) were measured at one-hour interval using an Elitech RC-51H data-logger (Elitech, London, UK), placed in the orchard within the experimental plot. RH and T data were used to calculate vapor pressure deficit (VPD, kPa) with the following equation: $VPD = VP_s - VP_a$, where VP_s (saturated vapor pressure) = $0.6108 \exp[17.27\ T / (T + 237.3)]$ and VP_a (actual vapor pressure) = $RH/100\ VP_s$.
Trees were irrigated weekly using two self-compensating in-line drippers per tree, each delivering 16 L/h. Two irrigation levels were imposed, selected based on two ranges of stem water potential: Full Irrigation (FI), maintaining the tree water

potential at approximately -1.5 to -2.5 MPa (conventional farm management), and Drought Stress (DS), maintaining the tree water potential within the range of -3.5 to -4 MPa, according to the thresholds defined in Marra et al. (2016) and Marino et al. (2018). Nine plants per treatment were selected, as illustrated in the diagram provided in Fig. 1B: Measurements were carried out at stages III (cell expansion) and IV (maturation) of fruit development.

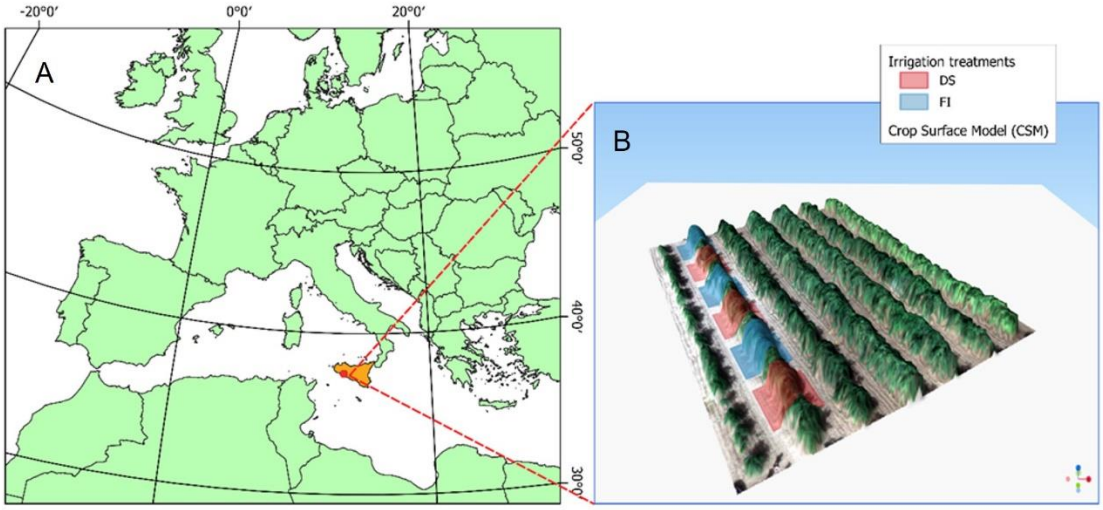

Fig. 1 - Experimental site location (A); Experimental plot with Crop Surface Model (CSM) of the olive orchard, and full irrigation (FI) and drought stress (DS) treatments design (B).

Plant Water Status

Midday stem water potential (Ψ_{stem}; MPa) was the main reference for evaluation of plant water status. Ψ_{stem} was measured with a Scholander's pressure chamber (PMS 600, Instrument Company, Albany, OR, USA). Measurements were taken at around 13:00 on four shoots per plant, each covered with aluminum foil 1 hour before measurement. Leaf stomatal conductance (g_s; mmol H_2O m^{-2} s^{-2}) and net photosynthesis (P_n; µmol CO_2 m^{-2} s^{-2}) were measured weekly using a portable gas exchange system CIRAS-2 (PP Systems®, Hitchin, UK) on two sun-exposed leaves per plant. Both parameters were measured once a week, specifically on 14 July, 1, 8, 16, 22 and 29 August; 6, 11, 19 and 26 September; and 3 and 10 October.

Proximal sensing measurements

Thermal imaging

Infrared thermal images were taken with a FLIR i7 hand-held thermal camera (FLIR systems, Wilsonville, Oregon, USA), with a resolution of 140 x 140 pixels and a spectral range of 7.5-13 µm. The camera has a thermal sensitivity of 0.1 °C and an accuracy of ± 2%. Emissivity was set at 0.98, according to Rubio et al. (1997). Thermal images were taken weekly, at the same time of the other measurements. Each image included the canopy of each individual tree, along with a fully transpiring reference (T_{wet}, as a non-water stressed baseline) and a non-transpiring reference (T_{dry}). The references were obtained following the methodology proposed by Jones et al. in 2002. T_{wet} was determined using leaves sprayed with water and a drop of detergent (0.01 % v/v) (Fuentes et al. 2012) 1 minute before taking the thermal image as wet references. For T_{dry}, leaves were covered with petroleum jelly about 1 h before measurement to artificially close stomata and inhibit transpiration. Crop water stress index (CWSI) was calculated using the following equation:

$$CWSI = \frac{T_c - T_{wet}}{T_{dry} - T_{wet}}$$

T_c represented the actual temperature of the canopy. Thermal data were extracted using the ThermaCAM Researcher Pro 2.10 software (FLIR systems, Wilsonville, Oregon, USA) by manually selecting the regions of interest (ROIs), avoiding the empty spaces, and the wet and dry references. All temperature values corresponded to the average temperature of pixels within the selected area. In addition, according to Jones et al. (2002) a further index related to stomatal conductance (stomatal conductance index - Ig) was calculated by using the same references of CWSI, i.e., with the following equation:

$$Ig = \frac{T_{dry} - T_{canopy}}{T_{canopy} - T_{wet}}$$

Ig may also represent a reliable index for assessing plant water status, as it is theoretically proportional to g_s, as observed in several studies (Jones et al. 2002; Costa et al. 2012; Belfiore et al. 2019). Thermal images were taken on 1, 8, 16, 22 and 29 August; 6, 11, 19 and 26 September; and 3 and 10 October.

Fruit-based sensing

Fruit diameter was continuously monitored during the entire period, at 15-min intervals, with the fruit gauges described by Morandi et al. (2007), wired to a CR-1000 data logger (Campbell Scientific, Inc., Logan, UT, USA). Drupes were continuously measured using 10 fruit gauges, with one sensor per plant for a total of five plants per treatment. Fruit gauges were placed on sun exposed fruits at about 1.5 m from the ground (corresponding to medium canopy height). At the end of the measurement period, the fruit equatorial diameter was converted to fruit weight, as suggested by Morandi et al. (2007b). The following equation was used for the conversion:

$$W(g) = a \times D(mm)^b$$

where W is the fruit weight and D the diameter. For our fruit in the experiment a and b were 0.003 (± 0.0004 S.E.) and 2.59 (± 0.052 S.E.), respectively, with $R^2 = 0.960$. This equation was obtained by regressing diameter and weight data of 200 fruits from the orchard where the experiment was carried out. Subsequently, fruit daily weight fluctuations (ΔW, g) and relative growth rate (RGR, g g^{-1} min^{-1}), were calculated. ΔW was obtained from the subtraction between the maximum and the minimum daily diameter averaged for all monitored fruits. RGR was calculated from the absolute growth rate (AGR, g min^{-1}) of individual fruits. In details, AGR and RGR were calculated as follows: $AGR = (D_1 - D_0)/(t_1 - t_0)$ and $RGR = AGR/D_1$. In the equation, D_1 and D_0 are the fruit diameters at time t_1 and t_0, respectively. RGR provides an indication of dry mass accumulation in the fruit, while ΔW is primarily related to fruit water exchanges through the xylem and transpiration (Carella et al. 2021). Such parameters were correlated with Ψ_{stem} and g_s in order to evaluate how the fruits responded to changes in plant water status, in terms of water exchanges and carbohydrates uptake.

Remote sensing measurements

Flight scheduling and multispectral data acquisition

A rotary-wing Unmanned Aerial Vehicle (UAV) equipped with a multispectral camera was used to obtain the reflectance in different narrow bands of the electromagnetic spectrum of each plant. Specifically, the camera has six 1/2.9″ CMOS sensors, i.e. one RGB sensor and five monochrome sensors with band centers in Blue (B, 450 ± 16nm), Green (G, 560 ± 16nm), Red (R, 650 ± 16nm), RedEdge (RE, 730 ± 16nm) and Near InfraRed (NIR, 840 ± 26nm). Two flights were carried out on 19 September and 10 October with automatic flight configuration using the way-points and RTK mode for correcting the GNSS signal. The flights were performed at about 13:00 at an altitude of 70 m, generating a Ground Surface Distance (GSD) of 3.6 cm. Before each flight, a calibration panel and 10 Ground Control Points (GCP) were positioned and georeferenced with the Stonex S7-G instrument according to Roma et al. (2023). The image acquisition was made in stop-and-go mode with 70% front and side overlap ratio, while the gimbal pitch was set at 90° (downwards).

Image processing

The photogrammetric reconstruction was carried out with Agisoft Photoscan Professional 1.7.3. (Agisoft Metashape, Saint Petersburg, Russia) using structure-from-motion (SfM) algorithms to obtain the multi-band orthomosaic and Digital Elevation Model (DEM). The OBIA (Object-Based Image Analysis) of geo-spatial and multispectral data was performed in the open-source software QGIS 3.2 (QGIS Geographic Information System). Specifically, orthomosaic segmentation and classification to separate the canopy from the background were carried out using the machine learning algorithm implemented in the Orfeo Tool Box (OTB tool). Once the canopies were obtained, the spectral information for each tree was extracted using Statistical Zone tools (Stateras and Kalivas, 2020; Roma et al., 2023). To obtain the information of each tree, a centroid of plants was identified, and a sub-plot of 6 x 2 m was built for each one (Fig. 2). The digital numbers (DN) inside of each sub-plot were used to evaluate the spectral and geometric features per plant.

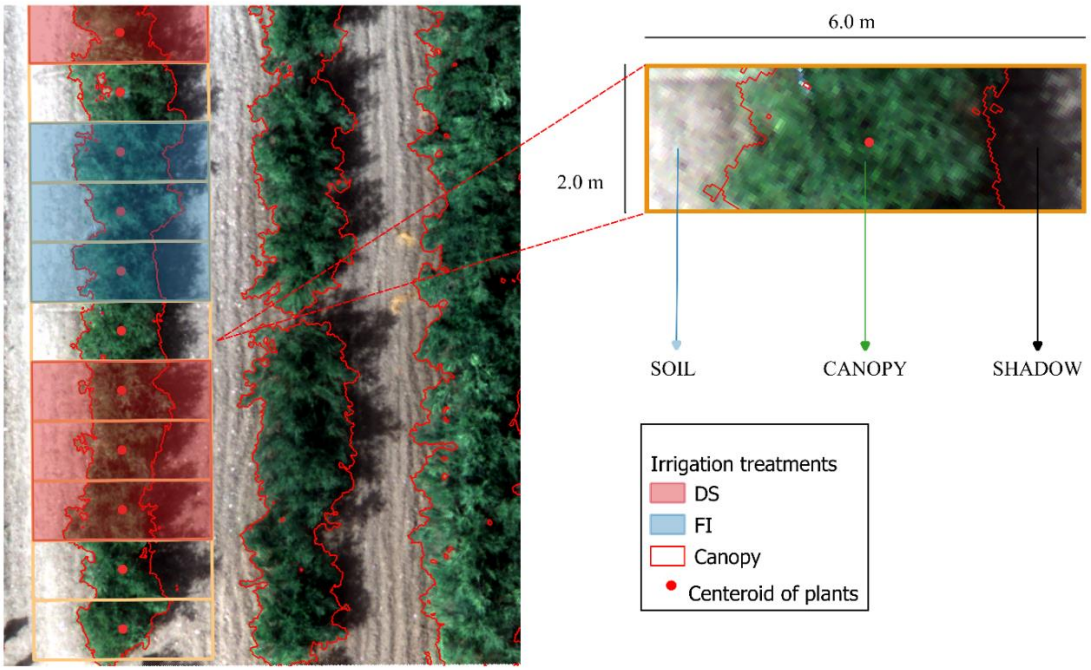

Fig. 2. Representation of sub-plots used to obtain the spectral and geometric information per plant. FI = full irrigated, DS = drought stressed.

The spectral information was related to the determination of several water sensitive vegetation indices used in the literature (Table 1).

Table 1. Vegetation indices considered to determine tree water status, using wavelengths within the VIS-NIR range. G = Green, R = Red, NIR = Near Infrared spectral bands, ρ = reflectance.

Vegetation index	Acronym	Equation	Reference
Chlorophyll Vegetation Index	*CVI*	(ρNIR/ρG) * (ρR+ρG)	Vincini et al. (2007)
Green Index	*GI*	ρG/ρR	Zarco-Tejada et al. (2005)
Green Normalized Difference Vegetation Index	*GNDVI*	(ρNIR−ρG) / (ρNIR+ρG)	Gitelson and Merzlyak (1994)
Modified Soil-Adjusted Vegetation Index	*MSAVI*	0.5 * {2 ρNIR +1 – SQRT[(2 ρNIR+1)^2 – 8 (ρNIR – ρR)]}	Qi et al. (1994)
Normalized Differential Greenness Index	*NDGI*	(ρG−ρR) / (ρG+ρR)	Gitelson et al. (1996)
Normalized Difference RedEdge Index	*NDRE*	(ρNIR−ρRedEdge) / (ρNIR+ρRedEdge)	Maccioni et al. (2001)
Normalized Difference Vegetation Index	*NDVI*	(ρNIR−ρR) / (ρNIR+ρR)	Rouse et al. (1974)
Water Index	*WI*	ρR/ρNIR	Peñuelas et al. (1993)

Statistical analysis

The means of Ψ_{stem} , g_s and P_n of FI and DS plants were compared by using repeated measure ANOVA at the 0.05 significance level using Jamovi 2.4.14 procedures (The Jamovi Project, 2023). Linear and nonlinear regression analysis were performed to relate the parameters obtained from proximal and remote sensing with Ψ_{stem} and g_s using Sigmaplot 14.0 (Systat Software Inc., Chicago, IL, USA) procedures. The remote sensing data were analyzed with two-way analysis of variance using date and irrigation levels as main factors, followed by Tukey's post hoc test.

Results and Discussion

Climate and Irrigation data

As expected, the highest values of VPD were recorded in July. Specifically, the highest VPD was recorded on 18 July. In contrast, the lowest level was reached on 16 October (Fig. 3A). Seven rainfall events occurred during the trial, totaling 51.2 mm of rain. The most intense rainfall events occurred on September 8 and 23 (22 mm and 12 mm, respectively). In FI trees, irrigation was carried out weekly with a total of 40 mm (Fig. 3B), for a total of 571.2 mm (Table 1) (including rainfall). No irrigation was applied between 6 September and 20 September due to a district water shortage. In DS trees, emergency irrigation was carried out when Ψ_{stem} went below -4 MPa, and near fruit ripening, totaling 291.2 mm (including rainfall).

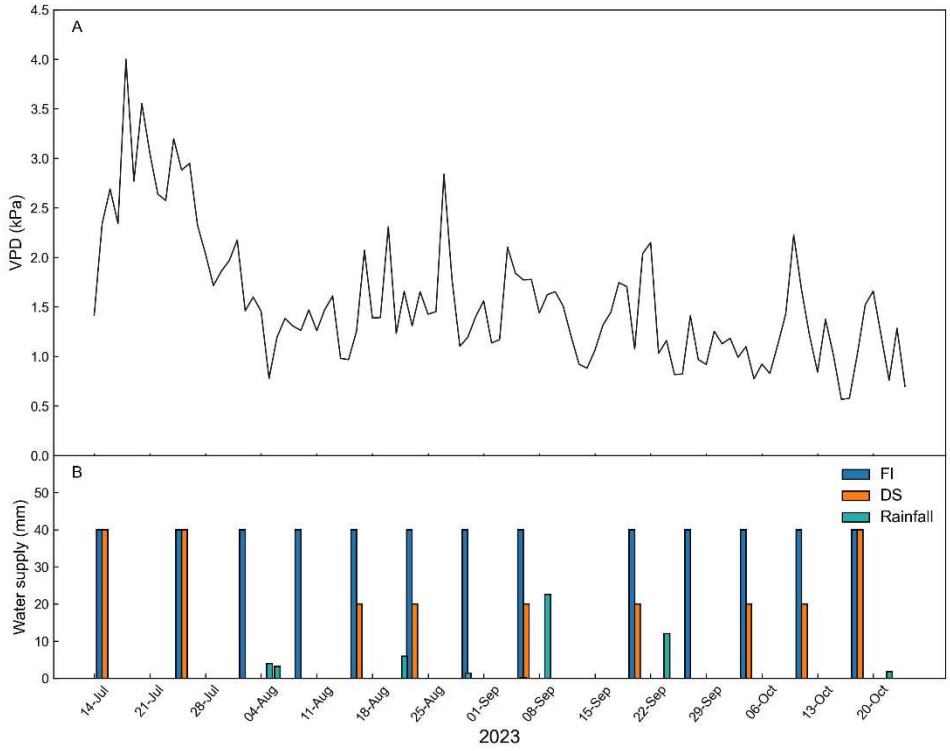

Fig. 3. Daily mean vapor pressure deficit (VPD, A) and water supply (irrigation and rainfall, B) to full irrigated (FI), and drought stressed (DS) 'Calatina' olive trees.

Tree water status and gas exchange

At the beginning of the trial, all trees received the same amount of irrigation water; indeed, no significant differences were found between FI and DS trees in terms of Ψ_{stem}, g_s, and P_n (Fig. 4). Regarding Ψ_{stem}, significant differences were observed between irrigation treatments from 1 August until 19 September (Fig. 4A). No significant differences were observed from 26 September until the end of the experiment (10 October). On 26 September, Ψ_{stem} values were above -2 MPa in both FI and DS trees, due to both rewatering and a rainy event on 23 September. A slight increase in Ψ_{stem} in DS plants was observed on 29 August, following a light rainfall event. The lowest Ψ_{stem} level was recorded on 19 September in DS plants; however, a low value (< 2.5 MPa) was also observed in FI plants on the same date. This was due to a temporary water network failure, so no irrigation was carried out on 18 September.

The trend of g_s over time was consistent with that of Ψ_{stem} for almost the entire experiment (Fig. 4B). On 1 August, despite the differences in Ψ_{stem}, no significant differences of g_s were observed between the two irrigation treatments. Most likely, hydration levels were not sufficiently low for the trees to exhibit different stomatal opening behavior. In subsequent dates, significant differences in g_s between irrigation treatments were observed until 19 September. After this date, despite the rainfall events and rewatering, 'Calatina' trees seemed to keep memory of the watering differences. Indeed, DS significantly reduced g_s on 3 October. This behavior may have been mediated by chemical signals like abscisic acid, possibly accumulated in the roots.

Regarding P_n, no significant differences between the two irrigation treatments were observed until 8 August (Fig. 4C). On this date, despite differences in g_s, P_n of FI and DS trees was not statistically different. In other words, despite the reduction in stomatal closure, similar levels of CO_2 were assimilated, suggesting an increase water use efficiency. This

usually happens when stomatal closure is only partial and it decreases water loss more then CO_2 intake due to the different partial pressures of the two gasses (Lawson and Blatt 2014). On 15 and 22 August, P_n was significantly reduced by DS. As in Ψ_{stem}, no significant differences of P_n were observed from 26 September until the end of the experiment.

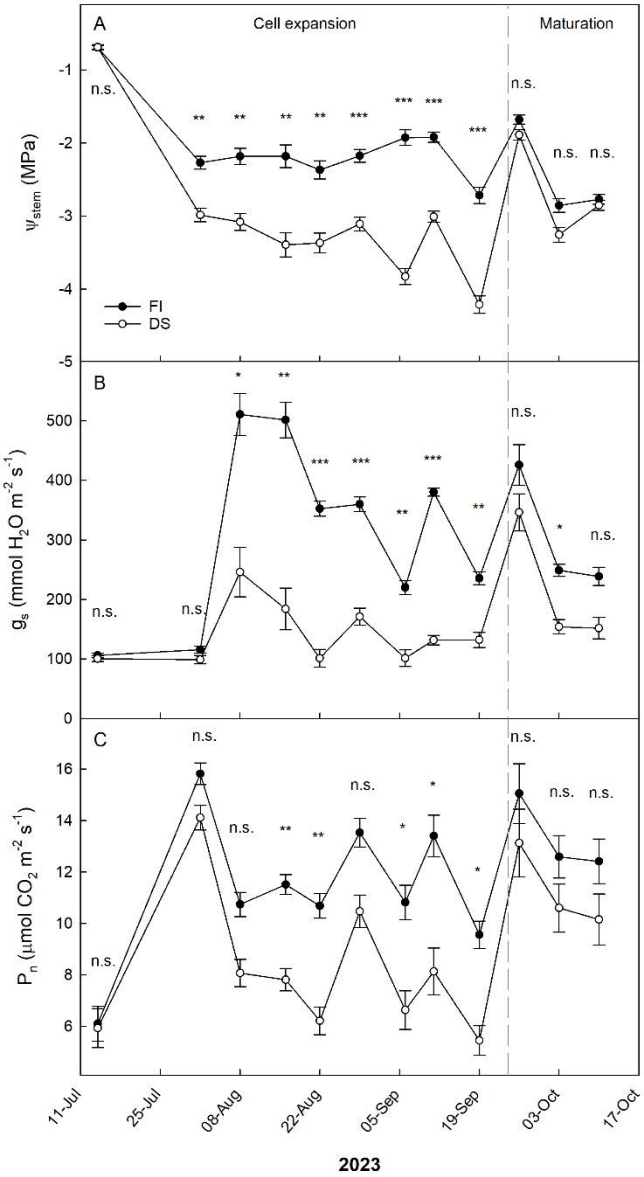

Fig. 4. Trends of midday stem water potential (Ψ_{stem}, A), stomatal conductance (g_s, B) and net photosynthesis (P_n, C) in 'Calatina' olive trees from 14 July to 10 October 2023. Black and white dots represent full irrigated (FI) and drought stressed (DS) trees, respectively. Error bars indicate standard errors of means. n.s., no significantly different; *, significantly different for $P < 0.05$; **, significantly different for $P < 0.01$; ***, significantly different for $P < 0.001$.

Within the observed Ψ_{stem} range (from -4.7 to -1.7), the relationship with g_s was described by a direct exponential model (Fig. 5A). Specifically, the model shows a strong direct relationship from -1.7 to -2.7 MPa, exhibiting a continuous decrease in g_s sensitivity as Ψ_{stem} decreases. In other words, as water stress progresses, stomatal response loses sensitivity and the stomatal closure is gradually lost; as a result, minimal transpiration is maintained. This behavior has been already reported in olive (Moriana et al. 2012; Marino et al. 2018).

P_n ranged from 4.9 to 18.3 µmol CO_2 m^{-2} s^{-1}. In the observed Ψ_{stem} range, the relationship between Ψ_{stem} and P_n was also best represented by a direct exponential model. As Ψ_{stem} decreased, P_n decreased more slowly, gradually reducing sensitivity to Ψ_{stem}. This kind of relationship was also observed in 'Arbequina' olive (Marino et al. 2018; Ahumada-Orellana et al. 2019).

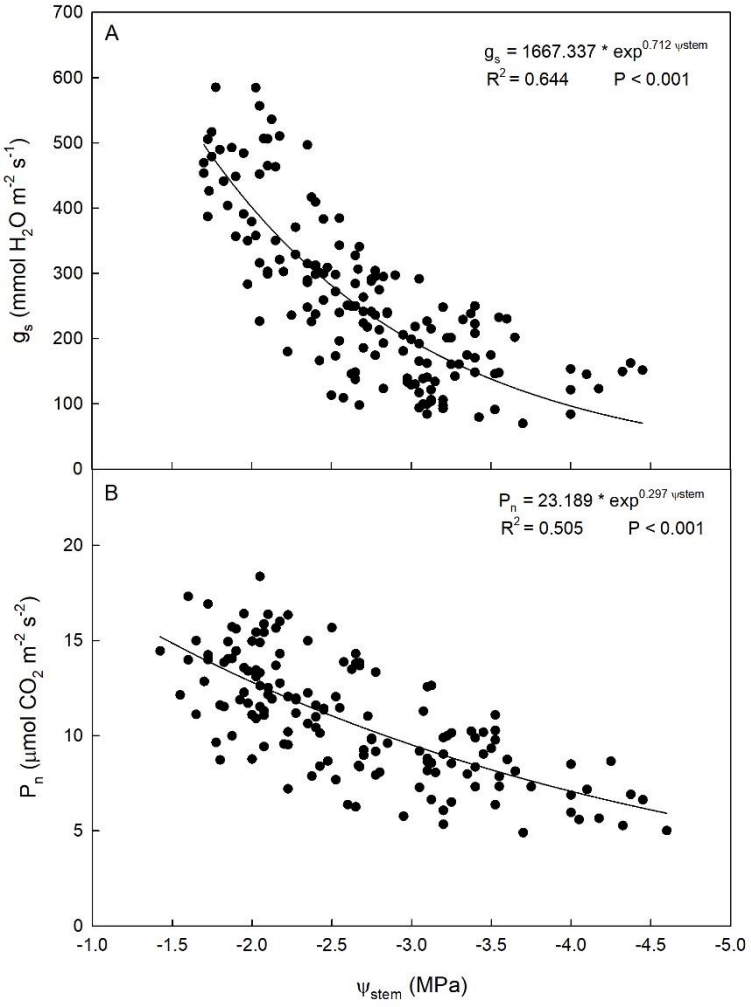

Fig. 5. Relationships between stem water potential (Ψ_{stem}) and stomatal conductance (g_s, A) and net photosynthesis (P_n, B) in 'Calatina' olive trees from 1 August to 10 October 2023.

Proximal sensing

Thermal imaging

A negative linear relationship between CWSI and Ψ_{stem} was observed (Fig. 6A). CWSI ranged from approximately 0.35 to 0.8, while Ψ_{stem} ranged from about -1.5 to -4.8. This indicates that canopy temperature normalized with CWSI is proportional to changes in the water status of 'Calatina' trees. Therefore, CWSI calculated using thermal imagery proved to be a useful parameter for plant water stress assessment, serving as an alternative to the more laborious measurement of Ψ_{stem} by using the pressure chamber. Similar ranges and relationships between Ψ_{stem} and CWSI have been documented in 'Arbequina' (Egea et al. 2016) and in 'Barnea' and 'Cobrançosa' (Ben-Gal et al. 2009; Marques et al. 2023) olive. Caruso et al. (2022b) found a significant relationship between remotely sensed CWSI and Ψ_{stem} in 'Frantoio' and 'Leccino' olive, with values comparable to those observed in this study. Linear relationships between the two parameters have also been documented in other fruit species such as cherry (Blaya-Ros et al. 2020), apple (Mohamed et al. 2021), peach (Ramírez-Cuesta et al. 2022) and grapevine (Pou et al. 2014).

On the other hand, the relationship between CWSI and g_s followed an inverse exponential model (Fig. 6B) similar to the one between Ψ_{stem} and g_s. In this case, CWSI increased almost linearly as g_s decreased up to approximately 200 mmol H_2O m^{-2} s^{-1}. Below this value, CWSI was more sensitive to g_s changes, and increased more rapidly. To date, mainly linear relationships between CWSI and g_s have been documented in olive (García-Tejero et al. 2017; Marques et al. 2023). However, due to the small number of olive cultivars on which this relationship has been studied, it is likely that the latter may vary depending on the cultivar.

The relationship between g_s and Ψ_{stem} also followed a direct exponential function (Fig. 6C). Since Ig was developed as thermal index for estimation of stomatal conductance, the relationship between Ig and Ψ_{stem} was similar to the one between

Ψ_{stem} and g_s. Specifically, from -1.5 toward -4.6 MPa there was a tendency of Ig to lose sensitivity to changes in Ψ_{stem} as the latter decreased.
A positive linear relationship between Ig and g_s was observed (Fig. 6D), confirming that Ig is a more direct estimator of stomatal conductance. Similar relationships were found in several studies with other species (Jones et al. 2002; Reinert et al. 2012; Yu et al. 2015).

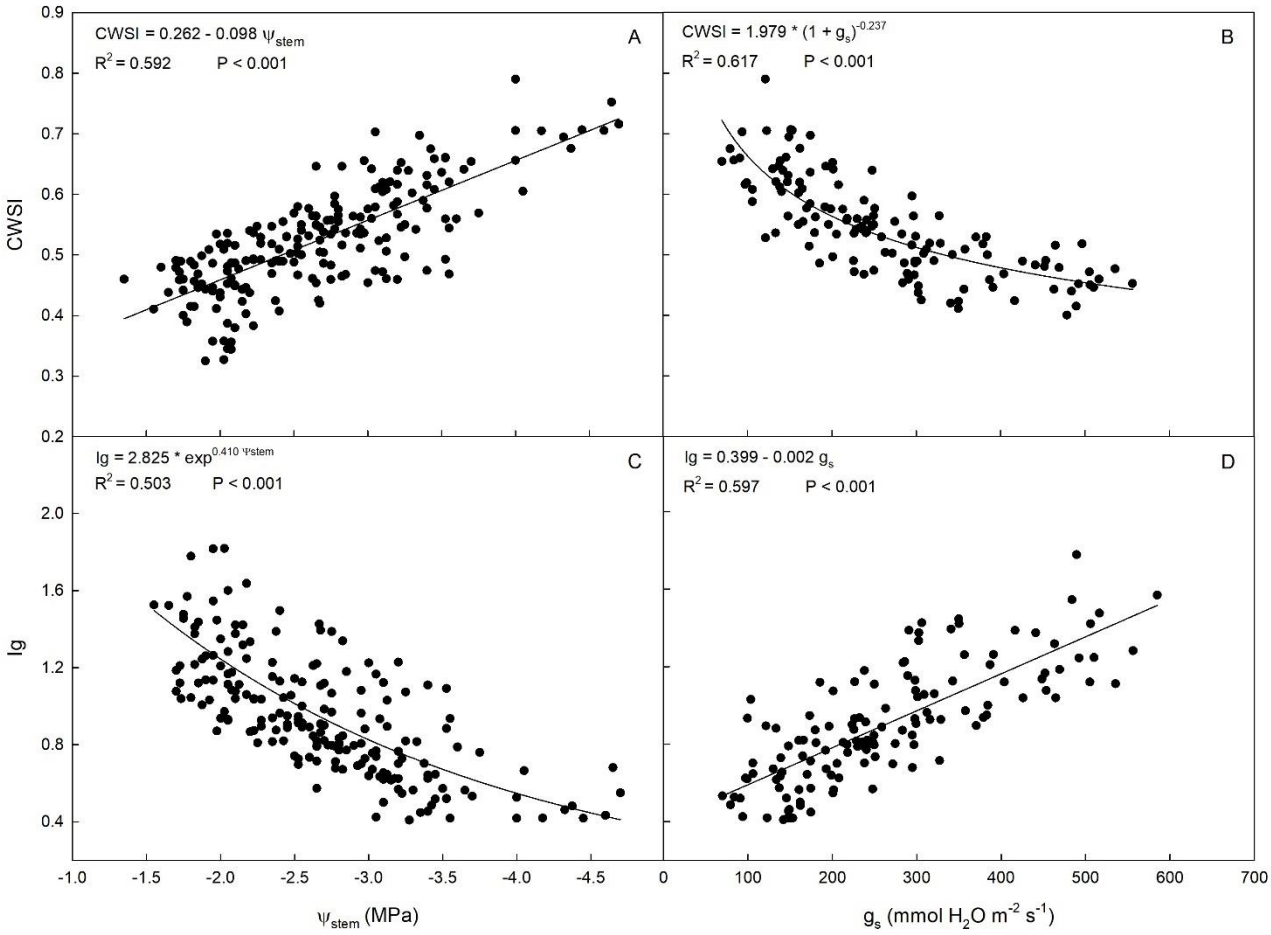

Fig. 6. Relationships between stem water potential (Ψ_{stem}) and crop water stress index (CWSI, A), stomatal conductance (g_s) and CWSI (B), Ψ_{stem} and stomatal conductance index (Ig, C), and g_s and Ig (D) in 'Calatina' olive trees from 1 August to 10 October 2023.

Fruit based-sensing

For associations with ΔW and RGR only the period of cell expansion was taken into account, as the fruit exhibits minimal response to changes in water status during the maturation stage. In fact, during maturation stage, internal and external changes in the fruit texture, flavor, and color prevail over water exchanges (Giovannoni 2001; Carella et al. 2021). On the other hand, when the fruit is in the stage of cell division, phloem and xylem contribution are similar (Morandi et al. 2007). During this phase, carbohydrate intake is essential. They are mainly sourced from actively photosynthesizing leaves and transported into the fruit through the phloem (Génard et al. 2008). On the contrary, during pit hardening stage, fruit water flows are very limited. At this stage, water deficit do not affect fruit growth (Goldhamer 1997; Moriana et al. 2003; Corell et al. 2022). At fruit cell expansion stage, a direct exponential relationship between ΔW and Ψ_{stem} was observed (Fig. 7A). Specifically, as Ψ_{stem} increased, fruit weight fluctuations become more and more pronounced, increasing its response sensitivity. At Ψ_{stem} values below -2.5 MPa, ΔW began to lose response sensitivity, suggesting that below this threshold fruit water flows tended to stabilize. This relationship between ΔW and Ψ_{stem} suggests that below this Ψ_{stem} value, the drupe may promptly respond to water stress by enhancing its water retention capacity. Specifically, a gradual fruit stomatal closure may be occurred, decreasing fruit transpiration rate and maintaining appropriate tissue hydration (Lescourret et al. 2001; Morandi et al. 2010). Secondly, a fruit osmotic adjustment may be occurred, leading to the accumulation of solutes capable of decreasing the osmotic potential and contributing to maintain tissues hydration. In olive, fruit osmotic adjustment was documented by Girón et al. in cv. Manzanillo. To date, few studies have correlated fruit ΔW and Ψ_{stem}. In 'Arbequina' olive, Fernandes et al. observed a linear relationship between the two parameters in full irrigated plants, while no relationship was observed in trees under water deficit. Furthermore, it is worth noting that

the 'Calatina' fruit maintained a high water exchange capacity even when the Ψ_{stem} ranged from about -3 to -2.5 Mpa (mild water stress condition).
A positive linear relationship was observed between ΔW and g_s (Fig. 7B). However, such relationship proved to be less tight than the relationship between Ψ_{stem} and ΔW. A direct exponential relationship was also observed between RGR and Ψ_{stem} (Fig. 7C). It is interesting to note that RGR is markedly higher at Ψ_{stem} levels between -2 and -1.5 Mpa, further suggesting that maintaining plants within that range ensures optimal fruit growth rates. Conversely, RGR began to approach zero at Ψ_{stem} of about -3 Mpa, losing sensitivity to further ecreases of Ψ_{stem}, and reaching slightly negative values at Ψ_{stem} below -3 Mpa. In other studies, mainly linear relationships between fruit growth rate and Ψ_{stem} were reported (Boini et al. 2019; Scalisi et al. 2020; Marino et al. 2021). However, the range of Ψ_{stem} examined was narrower than in this study.
No significant relationship was found between RGR and g_s, suggesting that fruit growth mainly responded to changes in Ψ_{stem} rather than g_s (Fig. 7D). In 'Gala' apple, Boini et al. (2019) studied the correlations between fruit growth parameters, Ψ_{stem} and gas exchanges. The Authors found that the fruit growth rate exhibited the strongest correlation with Ψ_{stem}. Interestingly, the fruit daily size fluctuations, in contrast to this study, showed a stronger relationship with g_s rather than with Ψ_{stem}. This discrepancy may stem from measurements taken during the late stages of apple cell expansion, where factors influencing fruit external and internal changes may differ from olive. As expected, no significant relationships between fruit growth parameters and Ψ_{stem} or g_s were identified after the cell expansion stage in our study.

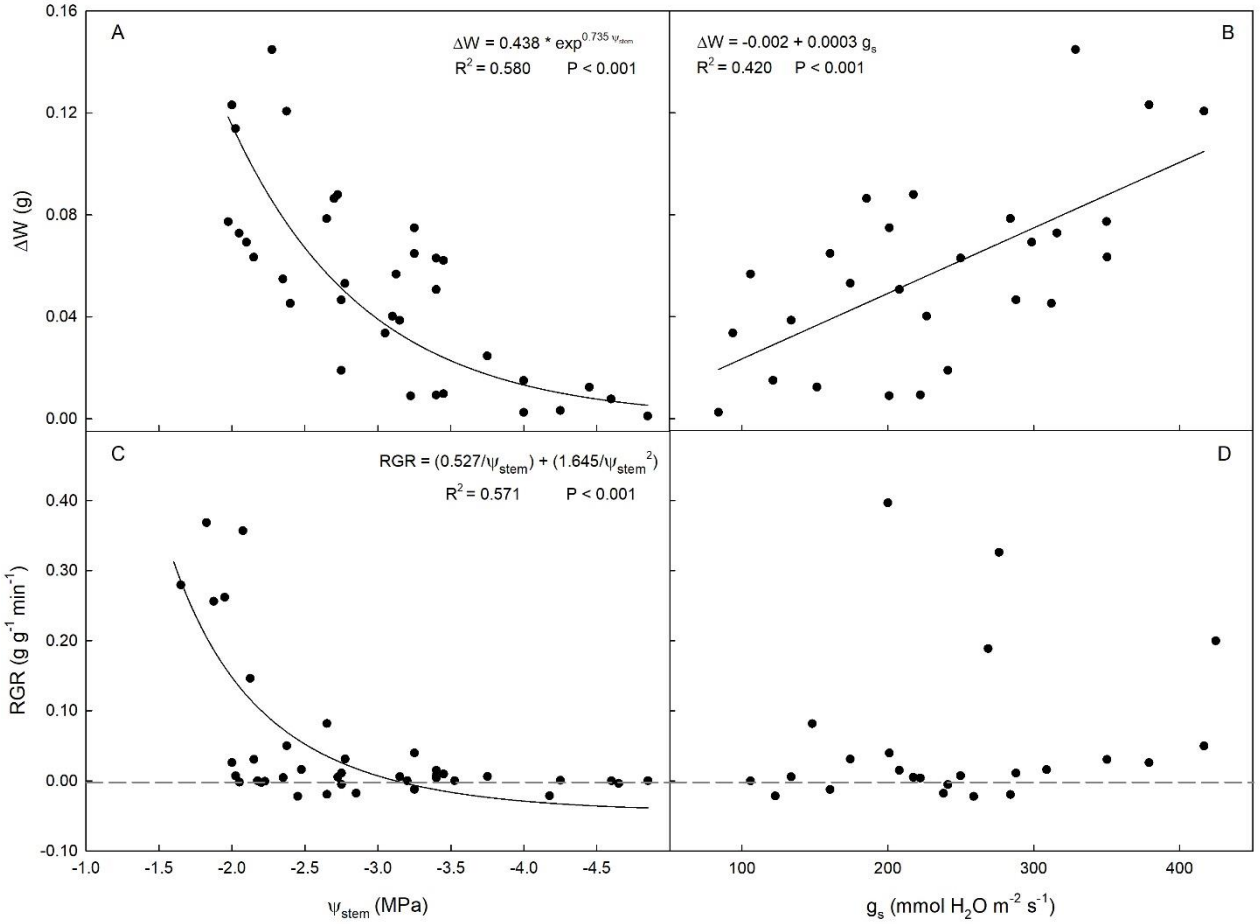

Fig. 7. Relationships between fruit fruit daily weight fluctuations (ΔW) and stem water potential (Ψ_{stem}, A), ΔW and stomatal conductance (g_s, B), fruit relative growth rate (RGR) and Ψ_{stem}, and RGR and g_s in 'Calatina' olive trees from 1 August to 26 September 2023.

Remote sensing

The experiments allowed the investigation of the spectral conditions of each plant as a function of Ψ_{stem}. Specifically, different behavior was observed in the different bands and consequently also in the vegetation indices (Fig. 7). In the VIS and NIR zones, the average reflectance of the vegetation showed the typical plant trend. Indeed, in the visible zone of the electromagnetic spectrum (400 – 700 nm), a higher reflectance of DS plants compared to FI plants was observed (Fig. 7A). In the NIR zone (700 – 900 nm), the opposite trend was observed. Specifically, the reflectance in the bands of blue,

green, red, RedEdge and NIR were 3.8% 8.4%, 5.6%, 25.3% and 38%, respectively in the FI trees, while they were 4.1%, 9.02%, 6.3%, 25.4% and 37% in the DS trees. Similar reflectance patterns have also been observed in other studies conducted on olive trees (Rallo et al., 2014) as well as other crops (Pôças et al., 2017). NDVI is considered the reference vegetation index for plant vigor and health. In this regard, the differences between FI and DS plants are evident, especially on September 19, where the Ψ_{stem} range was wider (Fig. 8B).

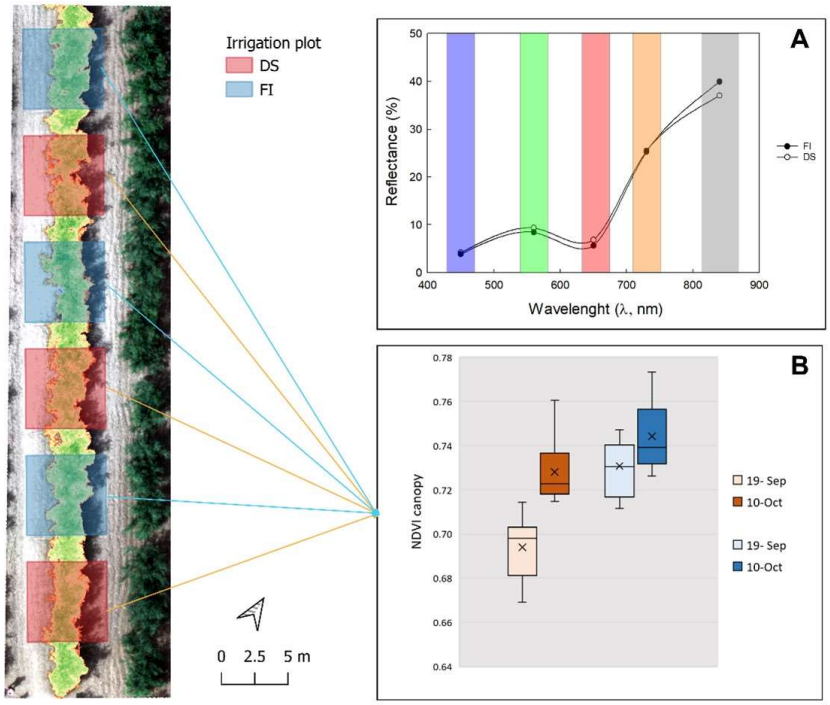

Fig. 8. Representation of canopy NDVI along a tree row for full irrigation (FI) and drought stress (DS) treatments. The frequency histogram (A) concerns the first acquisition date (19 September) while the box-plot (B) shows the NDVI values on 19 September and 10 October 2023 for both treatments.

All the indices were higher in FI than in DS plants, except for the WI (Table 2). Indeed, while all the other indices are used to estimate plant growth and health conditions (Noori and Panda, 2016; Jorge et al., 2019; Jurado et al., 2020; Stateras and Kalivas, 2020), the WI is an index directly related to water stress detection (Peñuelas et al., 1993; Pôças et al., 2017). Furthermore, an increase of all the indices is observed as the season progresses. All indices were able to differentiate between the two irrigation treatments at the time of greater water stress (19 September), lower Ψ_{stem}. Furthermore, only NDRE, GNDVI, WI, NDGI, and GI were able to differentiate the two treatments also in October.

Table 2. Vegetation indices for 'Calatina' olive trees on 19 September and 10 October. When present, letters denote significant differences between full irrigated (FI) and drought stressed (DS) trees ($P < 0.05$).

	NDVI [a]	NDRE	GNDVI	CVI	MSAVI	WI	NDGI	GI
19 September								
DS	0.692 ± 0.012	0.191 ± 0.005	0.613 ± 0.014	2.891 ± 0.088	0.495 ± 0.031	0.171 ± 0.011	0.184 ± 0.014	1.441 ± 0.022
FI	0.733 ± 0.014	0.201 ± 0.006	0.639 ± 0.014	3.038 ± 0.121	0.521 ± 0.022	0.149 ± 0.009	0.202 ± 0.011	1.488 ± 0.029
	*	**	**	*	*	**	*	**
10 October								
DS	0.733 ± 0.022	0.210 ± 0.007	0.639 ± 0.013	3.051 ± 0.140	0.505 ± 0.040	0.147 ± 0.009	0.190 ± 0.023	1.481 ± 0.038
FI	0.752 ± 0.019	0.233 ± 0.012	0.660 ± 0.020	3.131 ± 0.121	0.553 ± 0.038	0.129 ± 0.022	0.220 ± 0.034	1.564 ± 0.073
	n.s.	**	*	n.s.	n.s.	*	*	*

n.s., no significantly different; *, significantly different for $P < 0.05$; **, significantly different for $P < 0.01$; ***, significantly different for $P < 0.001$.
[a] NDVI = normalized difference vegetation index, NDRE = normalized difference RedEdge index, GNDVI = green normalized difference vegetation index, CVI = chlorophyll vegetation index, MSAVI = modified soil-adjusted vegetation index, WI = water index, NDGI = normalized difference greenness index, GI = green index.

The linear relationships between indices calculated from UAV multispectral camera and Ψ_{stem} on 19 September and 10 October were split by date because they showed significantly different slopes as a function of date (Table 3). In detail, significant differences between slopes were found in all the vegetation indices taken into account. This can be explained because on 10 October, trees were more hydrated, which reduced the measured range of Ψ_{stem}, making the changes in indices not easily appreciable. Indeed, on 10 October, the regressions slopes were less steep than those on 19 September.

Table 3. Comparison of the regression slopes for the relationships between vegetation indices and stem water potential (Ψ_{stem}) on 19 September and 10 October in 'Calatina' olive trees (t-test, $P < 0.05$).

	Slope		P-value
	19 September	10 October	
NDVI	0.018	0.106	0.008
MSAVI	0.016	0.126	0.004
NDRE	0.008	0.047	0.014
NDGI	0.01	0.107	0.005
GNDVI	0.017	0.088	0.007
WI	-0.012	-0.072	0.003
CVI	0.106	0.397	0.033
GI	0.031	0.348	0.005

A strong and significant positive linear relationship was found between NDVI and Ψ_{stem} on 19 September (Fig. 9A), while a weaker but significant linear relationship was observed on 10 October. NDVI is a vegetation index closely dependent on chlorophyll content and leaf cell structures. Specifically, chlorophyll has a strong absorption peak in the red region, while leaf mesophyll constituents and canopy structure are the factors that positively influence canopy NIR reflectance (Gitelson, 2004; Caruso et al., 2023). Indeed, increases in NIR reflectance correlate with increases in leaf thickness (Castro and Sanchez-Azofeifa, 2008). Thus NDVI is mainly used for the assessment of changes in canopy biophysical properties (leaf area index, fraction of absorbed photosynthetically active radiation, chlorophyll content, etc.) (Gitelson, 2004). These characteristics are closely related to the water status of the plant, as water is the main component of metabolic processes (e.g., photosynthesis) that determine chlorophyll content and canopy structure (Hailemichael et al., 2016). Since these parameters are closely related to plant water status, NDVI serves as a reliable indirect indicator of plant water status. Similar relationships in olive were found by Marino et al. (2014) and Rallo et al. (2014).

Also MSAVI was linearly related to Ψ_{stem} on both dates, but reported the lowest R^2 on 19 September and one of the highest R^2 on 10 October (Fig. 9B). To date, mixed results have been found in the literature on the effectiveness of the MSAVI and similar soil-adjusted indexes for assessing plant water status. In grapevine, Romero et al. (2018) reported a stronger correlation between MSAVI and Ψ_{stem} compared to NDVI. Conversely, Conesa et al. (2019) observed a weaker relationship in nectarine. Since this is an index that tends to remove the soil effect, the effectiveness of removing this effect may depend on different soil characteristics, as the spectral signature of the soil background varies with color, moisture, texture, etc. (Baumgardner et al., 1986). Ren and Feng compared MSAVI with two soil unadjusted vegetation indices (NDVI and simple ratio index, SR), finding that the performance of MSAVI for estimating above-ground vegetation is lower than NDVI and SR.

Relationships of Ψ_{stem} with NDRE were similar to those with NDVI (Fig. 9C). Since NDRE is calculated using the RedEdge band, it turns out to be a sensitive indicator of changes in chlorophyll content, thus indirectly related to plant water status (Boiarskii and Hasegawa, 2019; Roma et al., 2023). Similar relationships have been observed in the literature in other tree species such as sweet cherry (Blanco et al., 2020) and grapevine (Tang et al., 2022).

Relationships with NDGI showed relatively low R^2 values on both dates (Fig. 9D). This result partly disagrees with results found in other studies, which instead emphasize its reliability (Rallo et al., 2014; Pôças et al., 2015). However, since it is a greenness index, it may be influenced by factors like canopy exposure, e.g., paraheliotropism, as suggested by Rallo et al (2014).

A strong significant linear relationship was found between GNDVI and Ψ_{stem} on both 19 September and 10 October (Fig. 9E), suggesting that this vegetation index may be one of the most accurate in estimating 'Calatina' tree water status. GNDVI, taking into account the Green band, is positively correlated with anthocyanin content and negatively correlated with chlorophyll content, making it very sensitive to abiotic stresses (Viña and Gitelson, 2010). Since GNDVI is very sensitive to variations in chlorophyll content, the stronger correlation observed on 10 October compared to other indices can be attributed to the pronounced impact of light changes on chlorophyll content. Indeed, photosynthetically active radiation (PAR) on 10 October was 1633.55 ± 195.11 µmol m^{-2} s^{-1} (in contrast to 1121.15 ± 205.50 µmol m^{-2} s^{-1} recorded on 19 September). To date, there are not many studies on the assessment of olive tree water status using GNDVI. Rallo et al (2014) found a significant relationship between GNDVI and Ψ_{stem} in 'Nocellara del Belice' olive, however, the coefficient of determination ($R^2 = 0.41$) was lower than in this study. Contrarily, numerous studies on grapevines have

consistently demonstrated that GNDVI is one of the most reliable indirect predictors of Ψ_{stem} (Helman et al., 2018; Cogato et al., 2022; Caruso and Palai, 2023).

Finally, CVI and GI were indices that correlated weakly with $\Psi_{stem,}$ both on 19 September and 10 October (Fig. 9 G-H). Similarly to NDGI, they are closely related to greenness, so they can be easily affected by canopy exposure (Vincini et al., 2008; Rallo et al., 2014). Although CVI is a good indicator of chlorophyll status, it has been little used for plant water status assessment. Andrade Junior et al. (2022) found a significant linear relationship between CVI and Ψ_{stem} in soybean, but weaker than NDVI and optimized soil adjusted VI (OSAVI). GI, on the other hand, has been used in several experiments. In olive, Rallo et al. observed a relationship with similar coefficient of determination (R^2 = 0.45). In 'Cabernet Sauvignon' grapevine, the relationship between GI and Ψ_{stem} was weak (Romero et al., 2018), while in Grenache and Shiraz grapevines, it proved to be a good indicator of drought stress (Cogato et al., 2022).

WI was one of the indices that showed a strong, but negative relationship with Ψ_{stem} on both dates (Fig. 9F). This occurred since it is given by the ratio of the Red to NIR reflectance. Thus, as water stress increases, Red reflectance increased and NIR reflectance decreased. Since this is an index closely dependent on NIR reflectance, it is often correlated with leaf relative water content (RWC) (Peñuelas et al., 1994). The reflectance in NIR is associated with plant cell structures, particularly the cell wall. Consequently, alterations in plant water status involving changes in cell turgor affect cell wall structure and ultimately NIR reflectance (Peñuelas et al., 1993). However, it is important to note that under prolonged water stress conditions, plants may adjust osmotically, which can affect the correlation between WI and Ψ_{stem}. Similar results in olive were found by Asgari et al. (2023) and Marino et al. (2014). On the other hand, Rallo et al. (2014) observed a weaker relationship between WI and Ψ_{stem}. WI was also found to be a good predictor of Ψ_{stem} in grapevine (Serrano et al., 2010) and 'Satsuma' mandarin (Dzikiti et al., 2010). In summary, from highest to lowest R^2, NDVI, GNDVI, WI, and NDRE were the indices that correlated best with Ψ_{stem}, especially when the range of hydration considered was wide. In contrast, CVI, NDGI, GI and MSAVI were worse predictors of Ψ_{stem} than the aforementioned. Considering the higher reliability of Ψ_{stem} as the primary parameter for assessing plant water status, correlations between all the vegetation indices and g_s were not reported.

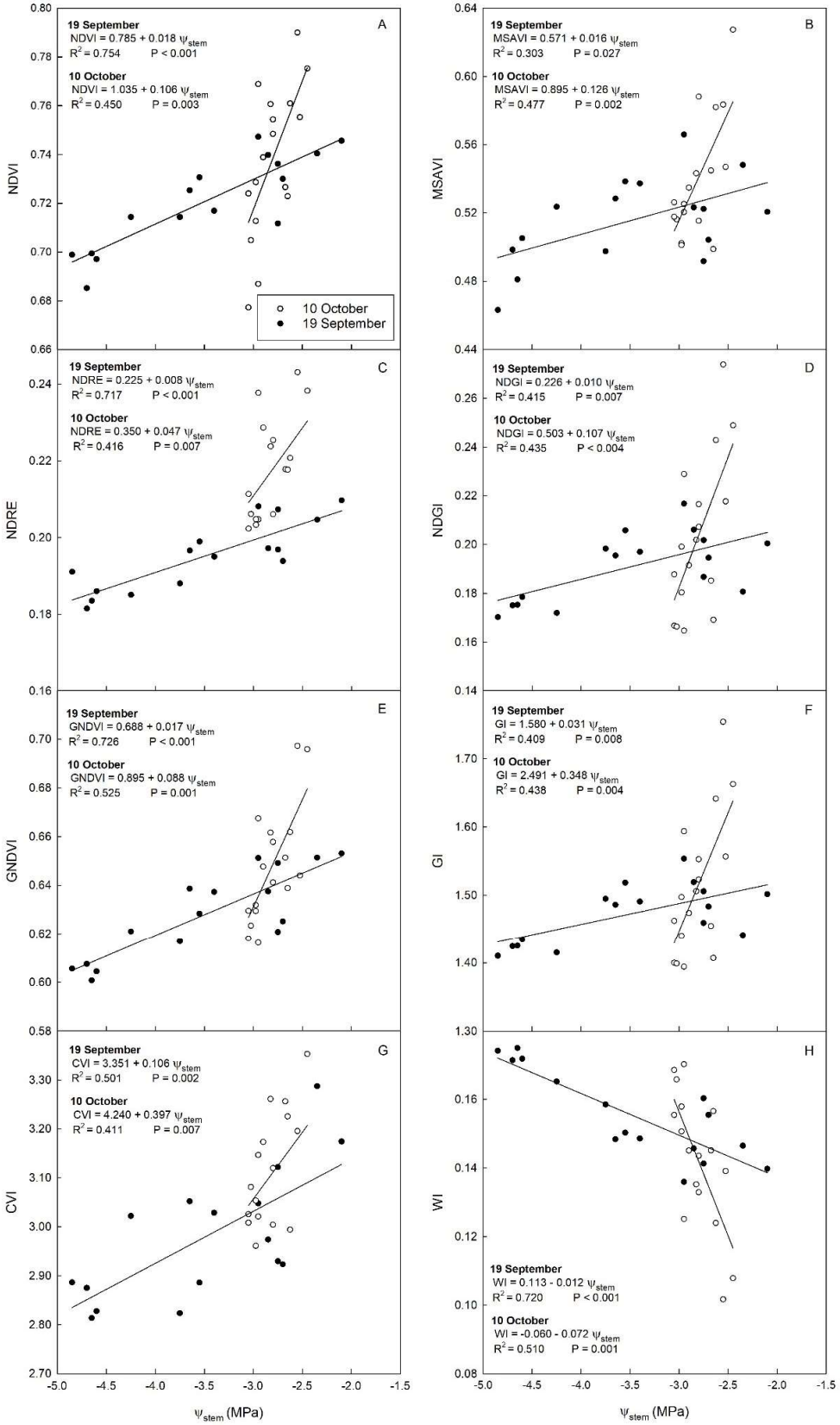

Fig. 9. Linear relationships between stem water potential (Ψ_{stem}) and normalized difference vegetation index (NDVI), normalized difference RedEdge index (NDRE), green normalized difference vegetation index (GNDVI), chlorophyll vegetation index (CVI), modified soil-adjusted vegetation index (MSAVI), water index (WI), normalized difference greenness index (NDGI), green index (GI) on 19 September (black dots) and 10 October (white dots) 2023.

Conclusions

The following trial aimed to integrate proximal and remote sensing techniques to show the benefits of using both monitoring methods, while simultaneously assessing the water status and response of 'Calatina' olive under two distinct irrigation regimes.
Indices obtained from thermal imaging, continuous fruit monitoring and remote sensing showed significant relationships in most cases. In detail, CWSI calculated using the direct method proved to be a reliable indicator of both ψ_{stem} and g_s. While Ig correlated better with g_s, thus proving to be a good indicator of stomatal conductance. As for the ΔW and RGR of the fruit, calculated by continuous monitoring of fruit gauges, both parameters increase exponentially as ψ_{stem} increases. In particular, ΔW was found to be the index that correlates most strongly with ψ_{stem} during the trial period. These data can provide valuable insights into the temporal dynamics of fruit growth, helping to identify the onset of water stress in the drupe. This could represent the exact time when to irrigate. Regarding vegetation indices obtained from multispectral data, NDVI, GNDVI, WI and NDRE were found to be the vegetation indices that correlate best with ψ_{stem}, achieving high levels of accuracy. Useful information on the spatial variability of the olive orchard related to plant water status can be obtained with these vegetation indices. This information can subsequently serve both for strategic placement of proximal sensors and for managing irrigation differently within the orchard considering the spatial variability. Further studies on integrating proximal and remote sensing data will be necessary to establish intervention thresholds. This should also include monitoring other plant organs (leaf, trunk) and providing quantitative indication on irrigation volume. Incorporating sensors to measure sap flow or leaf transpiration could offer valuable information about plant water usage.

Aknowledgements
We would like to thank Rosario Bono for hosting our trials.

Funding
The author(s) declare financial support was received for the research, authorship, and/or publication of this article. The present study was partly funded by the projects: Ecosistema dell'innovazione Sicilian MicronanoTech Research And Innovation Center -SAMOTHRACE. Fondo Finalizzato alla Ricerca di Ateneo FFR_D13_008811. European Project H2020-MSCA-RISE-2020 - ref. 101007702.

Data availability
The raw data of this article will be made available by the authors.

Conflict of interest
The authors declare that the research was carried out in the absence of any commercial or financial relationships that represent a potential conflict of interest.

Author information

Authors and Affiliations
Department of Agricultural, Food and Forest Sciences (SAAF), University of Palermo, 90128 Palermo, Italy
Alessandro Carella, Roberto Massenti, Francesco Paolo Marra, Pietro Catania, Eliseo Roma, & Riccardo Lo Bianco

Contributions
All authors contributed to the study conceptualization. Resources: Riccardo Lo Bianco, Francesco Paolo Marra, Roberto Massenti, Pietro Catania; Investigation: Alessandro Carella, Eliseo Roma, Roberto Massenti; Supervision: Riccardo Lo Bianco, Francesco Paolo Marra, Pietro Catania; Data curation and validation: Alessandro Carella, Eliseo Roma, Roberto Massenti; Formal analysis: Alessandro Carella, Eliseo Roma, Riccardo Lo Bianco; Visualization: Alessandro Carella, Eliseo Roma, Roberto Massenti; Writing – original draft: Alessandro Carella, Eliseo Roma, Roberto Massenti; Writing – review and editing: Riccardo Lo Bianco, Pietro Catania;. All authors read and approved the final manuscript.

Corresponding author
Correspondence to Alessandro Carella. Email: alessandro.carella@unipa.it

Ethic declarations

Competing interests

The authors declare no competing interests.

References

Abboud S, Vives-Peris V, Dbara S, Gómez-Cadenas A, Pérez-Clemente RM, Abidi W, Braham M (2021) Water status, biochemical and hormonal changes involved in the response of *Olea europaea* L. to water deficit induced by partial root-zone drying irrigation (PRD). Sci Hortic 276:109737. https://doi.org/10.1016/j.scienta.2020.109737

Ahumada-Orellana L, Ortega-Farías S, Poblete-Echeverría C, Searles PS (2019) Estimation of stomatal conductance and stem water potential threshold values for water stress in olive trees (cv. Arbequina). Irrig Sci 37:461–467

Alexopoulos A, Koutras K, Ali SB, Puccio S, Carella A, Ottaviano R, Kalogeras A (2023) Complementary Use of Ground-Based Proximal Sensing and Airborne/Spaceborne Remote Sensing Techniques in Precision Agriculture: A Systematic Review. Agronomy 13(7):1942. https://doi.org/10.3390/agronomy13071942

Andrade Junior AS de, Silva SP da, Setúbal IS, Souza HA de, Vieira PF (2022) Remote detection of water and nutritional status of soybeans using UAV-based images. Eng Agríc 42:e20210177

Asgari A, Hooshmand A, Broumand-Nasab S, Zivdar S (2023) Potential application of spectral indices for olive water status assessment in (semi-) arid regions: A case study in Khuzestan Province, Iran. Plant Direct 7(6):e494

Baumgardner MF, Silva LF, Biehl LL, Stoner ER (1986) Reflectance properties of soils. Adv Agron 38:1–44

Bazzi CL, Schenatto K, Upadhyaya S, Rojo F, Kizer E, Ko-Madden C (2019) Optimal placement of proximal sensors for precision irrigation in tree crops. Precis Agric 20(4):663–674. https://doi.org/10.1007/s11119-018-9604-3

Belfiore N, Vinti R, Lovat L, Chitarra W, Tomasi D, de Bei R, Meggio F, Gaiotti F (2019) Infrared thermography to estimate vine water status: Optimizing canopy measurements and thermal indices for the varieties Merlot and Moscato in northern Italy. Agronomy 9(12):821

Ben-Gal A, Agam N, Alchanatis V, Cohen Y, Yermiyahu U, Zipori I, Presnov E, Sprintsin M, Dag A (2009) Evaluating water stress in irrigated olives: correlation of soil water status, tree water status, and thermal imagery. Irrig Sci 27(5):367–376. https://doi.org/10.1007/s00271-009-0150-7

Berni J, Zarco-Tejada P, Sepulcre-Cantó G, Fereres E, Villalobos F (2009) Mapping canopy conductance and CWSI in olive orchards using high resolution thermal remote sensing imagery. Remote Sens Environ 113(11):2380–2388

Blanco V, Blaya-Ros PJ, Castillo C, Soto-Vallés F, Torres-Sánchez R, Domingo R (2020) Potential of UAS-based remote sensing for estimating tree water status and yield in sweet cherry trees. Remote Sens 12(15):2359

Blanco V, Willsea N, Campbell T, Howe O, Kalcsits L (2023) Combining thermal imaging and soil water content sensors to assess tree water status in pear trees. Front Plant Sci 14:1197437

Blaya-Ros PJ, Blanco V, Domingo R, Soto-Valles F, Torres-Sánchez R (2020) Feasibility of low-cost thermal imaging for monitoring water stress in young and mature sweet cherry trees. Appl Sci 10(16):5461

Boiarskii B, Hasegawa H (2019) Comparison of NDVI and NDRE indices to detect differences in vegetation and chlorophyll content. J Mech Contin Math Sci 4:20–29

Boini A, Manfrini L, Bortolotti G, Corelli-Grappadelli L, Morandi B (2019) Monitoring fruit daily growth indicates the onset of mild drought stress in apple. Sci Hortic 256:108520

Carella A, Gianguzzi G, Scalisi A, Farina V, Inglese P, Bianco RL (2021) Fruit growth stage transitions in two mango cultivars grown in a Mediterranean environment. Plants 10(7):1332

Carella A, Massenti R, Lo Bianco R (2023) Testing effects of vapor pressure deficit on fruit growth: a comparative approach using peach, mango, olive, orange, and loquat. Front Plant Sci 14

Carella A, Massenti R, Milazzo G, Caruso T, Lo Bianco R (2022) Fruiting, Morphology, and Architecture of 'Arbequina' and 'Calatina' Olive Branches. Horticulturae 8(2):109. https://doi.org/10.3390/horticulturae8020109

Caruso G, Palai G (2023) Assessing grapevine water status using Sentinel-2 images. Italus Hortus 30(3):70–79

Caruso G, Palai G, Gucci R, Priori S (2022a) Remote and Proximal Sensing Techniques for Site-Specific Irrigation Management in the Olive Orchard. Appl Sci 12(3):1309. https://doi.org/10.3390/app12031309

Caruso G, Palai G, Marra FP, Caruso T (2021) High-Resolution UAV Imagery for Field Olive (Olea europaea L.) Phenotyping. Horticulturae 7(8):258. https://doi.org/10.3390/horticulturae7080258

Caruso G, Palai G, Tozzini L, D'Onofrio C, Gucci R (2023) The role of LAI and leaf chlorophyll on NDVI estimated by UAV in grapevine canopies. Sci Hortic 322:112398

Caruso G, Palai G, Tozzini L, Gucci R (2022b) Using visible and thermal images by an unmanned aerial vehicle to monitor the plant water status, canopy growth and yield of olive trees (cvs. Frantoio and Leccino) under different irrigation regimes. Agronomy 12(8):1904

Castro KL, Sanchez-Azofeifa GA (2008) Changes in spectral properties, chlorophyll content and internal mesophyll structure of senescing Populus balsamifera and Populus tremuloides leaves. sensors 8(1):51–69

Cocozza C, Marino G, Giovannelli A, Cantini C, Centritto M, Tognetti R (2015) Simultaneous measurements of stem radius variation and sap flux density reveal synchronisation of water storage and transpiration dynamics in olive trees. Ecohydrology 8(1):33–45. https://doi.org/10.1002/eco.1483

Cogato A, Jewan SYY, Wu L, Marinello F, Meggio F, Sivilotti P, Sozzi M, Pagay V (2022) Water stress impacts on grapevines (Vitis vinifera L.) in hot environments: physiological and spectral responses. Agronomy 12(8):1819

Conesa MR, Conejero W, Vera J, Ramírez-Cuesta JM, Ruiz-Sánchez MC (2019) Terrestrial and remote indexes to assess moderate deficit irrigation in early-maturing nectarine trees. Agronomy 9(10):630

Connor DJ (2005) Adaptation of olive (Olea europaea L.) to water-limited environments. Aust J Agric Res 56(11):1181–1189

Corell M, Pérez-López D, Andreu L, Recena R, Centeno A, Galindo A, Moriana A, Martín-Palomo M (2022) Yield response of a mature hedgerow oil olive orchard to different levels of water stress during pit hardening. Agric Water Manag 261:107374

Costa JM, Ortuño MF, Lopes CM, Chaves MM (2012) Grapevine varieties exhibiting differences in stomatal response to water deficit. Funct Plant Biol 39(3):179–189

Dzikiti S, Verreynne J, Stuckens J, Strever A, Verstraeten W, Swennen R, Coppin P (2010) Determining the water status of Satsuma mandarin trees [Citrus Unshiu Marcovitch] using spectral indices and by combining hyperspectral and physiological data. Agric For Meteorol 150(3):369–379

Egea G, Padilla-Díaz CM, Martínez J, Fernández JE, Pérez-Ruiz M (2016) Use of aerial thermal imaging to assess water status variability in hedgerow olive orchards.

Fernandes RDM, Cuevas MV, Diaz-Espejo A, Hernandez-Santana V (2018) Effects of water stress on fruit growth and water relations between fruits and leaves in a hedgerow olive orchard. Agric Water Manag 210:32–40

Fernandez J-E (2014) Understanding olive adaptation to abiotic stresses as a tool to increase crop performance. Environ Exp Bot 103:158–179

Fuentes S, De Bei R, Pech J, Tyerman S (2012) Computational water stress indices obtained from thermal image analysis of grapevine canopies. Irrig Sci 30(6):523–536

García-Tejero I, Hernández A, Padilla-Díaz C, Diaz-Espejo A, Fernández J (2017) Assessing plant water status in a hedgerow olive orchard from thermography at plant level. Agric Water Manag 188:50–60

García-Tejero IF, Rubio AE, Viñuela I, Hernández A, Gutiérrez-Gordillo S, Rodríguez-Pleguezuelo CR, Durán-Zuazo VH (2018) Thermal imaging at plant level to assess the crop-water status in almond trees (*cv*. Guara) under deficit irrigation strategies. Agric Water Manag 208:176–186. https://doi.org/10.1016/j.agwat.2018.06.002

Génard M, Dauzat J, Franck N, Lescourret F, Moitrier N, Vaast P, Vercambre G (2008) Carbon allocation in fruit trees: from theory to modelling. Trees 22:269–282

Giovannini A, Venturi M, Gutiérrez-Gordillo S, Manfrini L, Corelli-Grappadelli L, Morandi B (2022) Vascular and Transpiration Flows Affecting Apricot (Prunus armeniaca L.) Fruit Growth. Agronomy 12(5):989

Giovannoni J (2001) Molecular biology of fruit maturation and ripening. Annu Rev Plant Biol 52(1):725–749

Girón I, Corell M, Galindo A, Torrecillas E, Morales D, Dell'Amico J, Torrecillas A, Moreno F, Moriana A (2015) Changes in the physiological response between leaves and fruits during a moderate water stress in table olive trees. Agric Water Manag 148:280–286

Gitelson AA (2004) Wide dynamic range vegetation index for remote quantification of biophysical characteristics of vegetation. J Plant Physiol 161(2):165–173

Goldhamer DA (1997) Regulated deficit irrigation for California canning olives. pp 369–372

Gómez-Bellot MJ, Parra A, Nortes P, Alarcón JJ, Ortuño MF (2024) Searching for a deficit irrigation strategy to save water and improve fruit quality without compromising pomegranate production. Sci Hortic 324:112631. https://doi.org/10.1016/j.scienta.2023.112631

Hailemichael G, Catalina A, González M, Martin P (2016) Relationships between water status, leaf chlorophyll content and photosynthetic performance in Tempranillo vineyards. South Afr J Enol Vitic 37(2):149–156

Helman D, Bahat I, Netzer Y, Ben-Gal A, Alchanatis V, Peeters A, Cohen Y (2018) Using time series of high-resolution planet satellite images to monitor grapevine stem water potential in commercial vineyards. Remote Sens 10(10):1615

Herrmann I, Karnieli A, Bonfil D, Cohen Y, Alchanatis V (2010) SWIR-based spectral indices for assessing nitrogen content in potato fields. Int J Remote Sens 31(19):5127–5143

Idso SB (1982) Non-water-stressed baselines: a key to measuring and interpreting plant water stress. Agric Meteorol 27(1–2):59–70

Jackson RD, Idso S, Reginato R, Pinter Jr P (1981) Canopy temperature as a crop water stress indicator. Water Resour Res 17(4):1133–1138

Jin J, Huang N, Huang Y, Yan Y, Zhao X, Wu M (2022) Proximal Remote Sensing-Based Vegetation Indices for Monitoring Mango Tree Stem Sap Flux Density. Remote Sens 14(6):1483. https://doi.org/10.3390/rs14061483

Jones HG, Stoll M, Santos T, Sousa C de, Chaves MM, Grant OM (2002) Use of infrared thermography for monitoring stomatal closure in the field: application to grapevine. J Exp Bot 53(378):2249–2260

Jorge J, Vallbé M, Soler JA (2019) Detection of irrigation inhomogeneities in an olive grove using the NDRE vegetation index obtained from UAV images. Eur J Remote Sens 52(1):169–177

Jurado JM, Ortega L, Cubillas JJ, Feito F (2020) Multispectral mapping on 3D models and multi-temporal monitoring for individual characterization of olive trees. Remote Sens 12(7):1106

Khosravi A, Zucchini M, Mancini A, Neri D (2022) Continuous Third Phase Fruit Monitoring in Olive with Regulated Deficit Irrigation to Set a Quantitative Index of Water Stress. Horticulturae 8(12):1221. https://doi.org/10.3390/horticulturae8121221

Konapala G, Mishra AK, Wada Y, Mann ME (2020) Climate change will affect global water availability through compounding changes in seasonal precipitation and evaporation. Nat Commun 11(1):3044. https://doi.org/10.1038/s41467-020-16757-w

Lawson T, Blatt MR (2014) Stomatal size, speed, and responsiveness impact on photosynthesis and water use efficiency. Plant Physiol 164(4):1556–1570

Lescourret F, Génard M, Habib R, Fishman S (2001) Variation in surface conductance to water vapor diffusion in peach fruit and its effects on fruit growth assessed by a simulation model. Tree Physiol 21(11):735–741

Lo Bianco R, Proietti P, Regni L, Caruso T (2021) Planting Systems for Modern Olive Growing: Strengths and Weaknesses. Agriculture 11(6):494. https://doi.org/10.3390/agriculture11060494

Maccioni A, Agati G, Mazzinghi P (2001) New vegetation indices for remote measurement of chlorophylls based on leaf directional reflectance spectra. J Photochem Photobiol B 61(1–2):52–61

Mairech H, López-Bernal Á, Moriondo M, Dibari C, Regni L, Proietti P, Villalobos FJ, Testi L (2021) Sustainability of olive growing in the Mediterranean area under future climate scenarios: Exploring the effects of intensification and deficit irrigation. Eur J Agron 129:126319. https://doi.org/10.1016/j.eja.2021.126319

Marino G, Caruso T, Ferguson L, Marra FP (2018) Gas exchanges and stem water potential define stress thresholds for efficient irrigation management in olive (Olea europea L.). Water 10(3):342

Marino G, Pallozzi E, Cocozza C, Tognetti R, Giovannelli A, Cantini C, Centritto M (2014) Assessing gas exchange, sap flow and water relations using tree canopy spectral reflectance indices in irrigated and rainfed Olea europaea L. Environ Exp Bot 99:43–52

Marino G, Scalisi A, Guzmán-Delgado P, Caruso T, Marra FP, Lo Bianco R (2021) Detecting Mild Water Stress in Olive with Multiple Plant-Based Continuous Sensors. Plants 10(1):131. https://doi.org/10.3390/plants10010131

Marques P, Pádua L, Sousa JJ, Fernandes-Silva A (2023) Assessing the Water Status and Leaf Pigment Content of Olive Trees: Evaluating the Potential and Feasibility of Unmanned Aerial Vehicle Multispectral and Thermal Data for Estimation Purposes. Remote Sens 15(19):4777

Marra F, Marino G, Marchese A, Caruso T (2016) Effects of different irrigation regimes on a super-high-density olive grove cv."Arbequina": Vegetative growth, productivity and polyphenol content of the oil. Irrig Sci 34:313–325

Massenti R, Ioppolo A, Veneziani G, Selvaggini R, Servili M, Lo Bianco R, Caruso T (2022a) Low Tree Vigor, Free Palmette Training Form, and High Planting Density Increase Olive and Oil Yield Efficiency in Dry, Sloping Areas of Mediterranean Regions. Horticulturae 8(9):817. https://doi.org/10.3390/horticulturae8090817

Massenti R, Scalisi A, Marra FP, Caruso T, Marino G, Lo Bianco R (2022b) Physiological and Structural Responses to Prolonged Water Deficit in Young Trees of Two Olive Cultivars. Plants 11(13):1695. https://doi.org/10.3390/plants11131695

Matese A, Baraldi R, Berton A, Cesaraccio C, Di Gennaro S, Duce P, Facini O, Mameli M, Piga A, Zaldei A (2018) Estimation of Water Stress in Grapevines Using Proximal and Remote Sensing Methods. Remote Sens 10(1):114. https://doi.org/10.3390/rs10010114

Melaouhi A, Baraza E, Escalona JM, El-AouOuad H, Mahjoub I, Bchir A, Braham M, Bota J (2021) Physiological and biochemical responses to water deficit and recovery of two olive cultivars (Olea europaea L., Arbequina and Empeltre cvs.) under Mediterranean conditions. Theor Exp Plant Physiol 33(4):369–383. https://doi.org/10.1007/s40626-021-00219-9

Mohamed AZ, Osroosh Y, Peters RT, Bates T, Campbell CS, Ferrer-Alegre F (2021) Monitoring water status in apple trees using a sensitive morning crop water stress index. Irrig Drain 70(1):27–41

Morandi B, Manfrini L, Losciale P, Zibordi M, Corelli-Grappadelli L (2010) The positive effect of skin transpiration in peach fruit growth. J Plant Physiol 167(13):1033–1037

Morandi B, Rieger M, Grappadelli LC (2007) Vascular flows and transpiration affect peach (Prunus persica Batsch.) fruit daily growth. J Exp Bot 58(14):3941–3947

Moriana A, Orgaz F, Pastor M, Fereres E (2003) Yield responses of a mature olive orchard to water deficits.

Moriana A, Pérez-López D, Prieto M, Ramírez-Santa-Pau M, Pérez-Rodriguez J (2012) Midday stem water potential as a useful tool for estimating irrigation requirements in olive trees. Agric Water Manag 112:43–54

Nikolaou G, Neocleous D, Christou A, Kitta E, Katsoulas N (2020) Implementing Sustainable Irrigation in Water-Scarce Regions under the Impact of Climate Change. Agronomy 10(8):1120. https://doi.org/10.3390/agronomy10081120

Noori O, Panda SS (2016) Site-specific management of common olive: Remote sensing, geospatial, and advanced image processing applications. Comput Electron Agric 127:680–689

Peñuelas J, Filella I, Biel C, Serrano L, Save R (1993) The reflectance at the 950–970 nm region as an indicator of plant water status. Int J Remote Sens 14(10):1887–1905

Peñuelas J, Gamon J, Fredeen A, Merino J, Field C (1994) Reflectance indices associated with physiological changes in nitrogen-and water-limited sunflower leaves. Remote Sens Environ 48(2):135–146

Pierantozzi P, Torres M, Tivani M, Contreras C, Gentili L, Parera C, Maestri D (2020) Spring deficit irrigation in olive (cv. Genovesa) growing under arid continental climate: Effects on vegetative growth and productive parameters. Agric Water Manag 238:106212. https://doi.org/10.1016/j.agwat.2020.106212

Pôças I, Gonçalves J, Costa PM, Gonçalves I, Pereira LS, Cunha M (2017) Hyperspectral-based predictive modelling of grapevine water status in the Portuguese Douro wine region. Int J Appl Earth Obs Geoinformation 58:177–190

Pôças I, Rodrigues A, Gonçalves S, Costa PM, Gonçalves I, Pereira LS, Cunha M (2015) Predicting grapevine water status based on hyperspectral reflectance vegetation indices. Remote Sens 7(12):16460–16479

Pokhrel Y, Felfelani F, Satoh Y, Boulange J, Burek P, Gädeke A, Gerten D, Gosling SN, Grillakis M, Gudmundsson L, Hanasaki N, Kim H, Koutroulis A, Liu J, Papadimitriou L, Schewe J, Müller Schmied H, Stacke T, Telteu C-E, Thiery W, Veldkamp T, Zhao F, Wada Y (2021) Global terrestrial water storage and drought severity under climate change. Nat Clim Change 11(3):226–233. https://doi.org/10.1038/s41558-020-00972-w

Pou A, Diago MP, Medrano H, Baluja J, Tardaguila J (2014) Validation of thermal indices for water status identification in grapevine. Agric Water Manag 134:60–72

Rallo G, Minacapilli M, Ciraolo G, Provenzano G (2014) Detecting crop water status in mature olive groves using vegetation spectral measurements. Biosyst Eng 128:52–68

Ramírez-Cuesta JM, Ortuño M, Gonzalez-Dugo V, Zarco-Tejada PJ, Parra M, Rubio-Asensio JS, Intrigliolo DS (2022) Assessment of peach trees water status and leaf gas exchange using on-the-ground versus airborne-based thermal imagery. Agric Water Manag 267:107628

Reinert S, Bögelein R, Thomas FM (2012) Use of thermal imaging to determine leaf conductance along a canopy gradient in European beech (Fagus sylvatica). Tree Physiol 32(3):294–302

Ren H, Feng G (2015) Are soil-adjusted vegetation indices better than soil-unadjusted vegetation indices for above-ground green biomass estimation in arid and semi-arid grasslands? Grass Forage Sci 70(4):611–619

Roma E, Catania P (2022) Precision Oliviculture: Research Topics, Challenges, and Opportunities—A Review. Remote Sens 14(7):1668

Roma E, Catania P, Vallone M, Orlando S (2023) Unmanned aerial vehicle and proximal sensing of vegetation indices in olive tree (*Olea europaea*). J Agric Eng 54(3). https://doi.org/10.4081/jae.2023.1536

Romero M, Luo Y, Su B, Fuentes S (2018) Vineyard water status estimation using multispectral imagery from an UAV platform and machine learning algorithms for irrigation scheduling management. Comput Electron Agric 147:109–117

Rouse JW, Haas RH, Schell JA, Deering DW, Harlan JC (1974) Monitoring the vernal advancement and retrogradation (green wave effect) of natural vegetation. NASAGSFC Type III Final Rep Greenbelt Md 371

Scalisi A, Marino G, Marra FP, Caruso T, Lo Bianco R (2020) A Cultivar-Sensitive Approach for the Continuous Monitoring of Olive (Olea europaea L.) Tree Water Status by Fruit and Leaf Sensing. Front Plant Sci 11:340

Serrano L, González-Flor C, Gorchs G (2010) Assessing vineyard water status using the reflectance based water index. Agric Ecosyst Environ 139(4):490–499

Stateras D, Kalivas D (2020) Assessment of Olive Tree Canopy Characteristics and Yield Forecast Model Using High Resolution UAV Imagery. Agriculture 10(9):385

Tang Z, Jin Y, Alsina MM, McElrone AJ, Bambach N, Kustas WP (2022) Vine water status mapping with multispectral UAV imagery and machine learning. Irrig Sci 40(4):715–730

Tong X, Wu P, Liu X, Zhang L, Zhou W, Wang Z (2022) A global meta-analysis of fruit tree yield and water use efficiency under deficit irrigation. Agric Water Manag 260:107321. https://doi.org/10.1016/j.agwat.2021.107321

Viña A, Gitelson AA (2010) Sensitivity to foliar anthocyanin content of vegetation indices using green reflectance. IEEE Geosci Remote Sens Lett 8(3):464–468

Vincini M, Frazzi E, D'Alessio P (2008) A broad-band leaf chlorophyll vegetation index at the canopy scale. Precis Agric 9:303–319

Wahab A, Abdi G, Saleem MH, Ali B, Ullah S, Shah W, Mumtaz S, Yasin G, Muresan CC, Marc RA (2022) Plants' Physio-Biochemical and Phyto-Hormonal Responses to Alleviate the Adverse Effects of Drought Stress: A Comprehensive Review. Plants 11(13):1620. https://doi.org/10.3390/plants11131620

Yu M-H, Ding G-D, Gao G-L, Zhao Y-Y, Yan L, Sai K (2015) Using plant temperature to evaluate the response of stomatal conductance to soil moisture deficit. Forests 6(10):3748–3762

GENERAL CONCLUSIONS

The combination of proximal and remote sensing techniques represents an efficient system for a comprehensive assessment of fruit tree water status. Specifically, this combination provides a more complete and precise evaluation of the plant's water status as proximal sensors offer continuous and real-time data for individual plants (time scale), while remote sensing systems expand information across the orchard (space scale). Thus, high-quality information considering both spatial and temporal variability is obtained. This could enable the development of irrigation systems that act punctually and efficiently in terms of water usage.

Thermography techniques have proven useful for assessing the olive trees water status under various growth conditions. Strong significant relationships between thermal indices (especially CWSI) and stem water potential were observed in both young plants under protected environment and adult plants in the open field, as described in chapters 2 and 4 of this thesis. Furthermore, as already well-known from the literature, these techniques adapt well to both remote and proximal sensing. However, the thermal indices thresholds need to be well-defined considering various aspects, including cultivar, environment, geographical area of cultivation, and plant age. Therefore, models that take these aspects into account will need to be developed.

Continuous sensors like fruit gauges, on the other hand, are capable of providing useful real-time information about fruit size changes. Having this type of data is important both in science for studying fruit growth dynamics under different water and environmental conditions and for producers to manage irrigation for best final outputs. These sensors can be useful for detecting the moment when the fruit begins to experience water stress, thus allowing for timely application of irrigation water. However, it is necessary to couple data from these sensors with others that show the response of other tree organs to changes in water status. Sensors like dendrometers for stem or leaf turgor probes can provide an initial alarm of tree water stress, while sensors like sap flow probes or leaf capacitance sensors can estimate the tree water usage. In chapter 3, the utility of fruit gauges was demonstrated both for studying the responses of the drupe to a wide range of water potentials and for studying the relationships between fruit growth rate and environment (vapor pressure deficit - VPD) in five different fruit tree species (peach, mango, olive, orange and loquat). Indeed, for more efficient irrigation management, it is crucial to understand the physiological responses of the fruit to temperature and relative humidity variations depending on its growth stage. In detail, based on the findings described in chapter 3, it can be asserted that VPD data is a fundamental indicator of fruit

growth, especially when the cell expansion process prevails, where fruit water flows are decisive. Furthermore, these results are important in the context of climate change with rising temperatures and drought phenomena becoming more frequent during summer days.

Multispectral data obtained from drone, on the other hand, proved to be useful for assessing the water status of olive trees in the field. In Chapter 4, certain indices derived from multispectral data (NDVI, GNDVI, NDRE, and WI) associated best to stem water potential. However, it was found that the relationships between vegetation indices may vary depending on the survey period and the plant water potential range. To better clarify this, further studies for the development of models assessing the water status of olive trees using multispectral data need to be conducted under different water conditions and at different times during the irrigation season.

Finally, the results obtained in this thesis can be useful for stimulating further research for the development of models and systems that jointly use data from remote and proximal sensing. Nowadays, models based on artificial intelligence and machine learning techniques appear to be very promising and can represent a new frontier for improving knowledge about the integration of precision farming techniques and for the development of efficient and sustainable precision irrigation systems.

ACKNOWLEDGEMENTS

Firstly, I am grateful to my PhD supervisor, Prof. Riccardo Lo Bianco, for continuously supporting me throughout my studies, starting from my master's degree thesis. He imparted knowledge and scientific rigor, consistently providing constructive criticism on my work for this dissertation and was always present during moments of difficulty.

Furthermore, I would like to thank my co-supervisor, Prof. Francesco Paolo Marra, for his useful advice in designing the experiments, for providing various tools, and for helping me in their use.

I would like to thank Dr. Roberto Massenti, who played a fundamental role in the realization of all the experiments presented, and for proving to be more of a friend than just a colleague, even sharing happy moments beyond the academic environment.

I thank my laboratory mates at the University of Palermo for their concrete help with field measurements, for the useful discussions, and for the fun moments that made this experience more enjoyable. In detail, I thank Valeria Imperiale, Pedro Tomas Bulacio Fischer, and Antonino Ioppolo. Additionally, I thank Stefano Puccio and Dario Scuderi, colleagues and faithful friends since our bachelor's degree thesis, for the stimulating scientific and non-scientific discussions, and for always being present even outside the academic world.

Further sincere thanks go to Dr. Umberto Michelucci and Prof. Francesca Venturini for welcoming me into their team in Winterthur, allowing me to participate in their research activities, and for providing me with the basics of data analysis with Python and with artificial intelligence and optical sensor techniques. These were useful for my experiments and certainly fundamental for my future work. I would also like to thank Arnaud Gucciardi for his valuable technical advice during my period of research in Switzerland and for the enjoyable times we shared outside of work.

A special thanks goes to Monica, for always being my rock, for cheering me up whenever I doubted myself, and for celebrating every one of my successes over the past three years and beyond.

Last but not least, I am grateful to my mother, father, and brother for their unconditional support throughout every step of my life, always believing in me, and for making me the person I am today.